# REPORT DOCUMENTATION PAGE

Form Approved
OMB No. 0704-0188



| 1. AGENCY USE ONLY (Leave blank) | 2. REPORT DATE | 3. REPORT TYPE AND DATES COVERED |
|---|---|---|
| | May 1996 | Final, 04/01/91 - 12/31/94 |

**4. TITLE AND SUBTITLE**

OEIC Transmitters Employing Ultra Low Threshold Three Terminal Lasers

**5. FUNDING NUMBERS**

N00014-91-J-1728

**6. AUTHOR(S)**

P. D. Dapkus

**7. PERFORMING ORGANIZATION NAME(S) AND ADDRESS(ES)**

University of Southern California
Department of EE-Electrophysics
502 Powell Hall of Engineering
University Park
Los Angeles, CA 90089-0271

**8. PERFORMING ORGANIZATION REPORT NUMBER**

**9. SPONSORING/MONITORING AGENCY NAMES(S) AND ADDRESS(ES)**

Dr. Yoon Soo Park
Code ONR 312
Office of Naval Research
800 N. Quincy Street
Arlington, VA 22217-5660

**10. SPONSORING/MONITORING AGENCY REPORT NUMBER**

**11. SUPPLEMENTARY NOTES**

**12a. DISTRIBUTION/AVAILABILITY STATEMENT**

Approved for public release: Distribution unlimited

**12b. DISTRIBUTION CODE**

**13. ABSTRACT (Maximum 200 words)**

A program of research to investigate the integration of optoelectronic and electronic devices for transmitters is described. The report describes research aimed at developing low threshold laser for using in these transmitters and describes three different types of lasers: a folded cavity surface emitting laser, an ultralow threshold intracavity contacted vertical cavity laser structure and an ultralow threshold, electrically isolated vertical cavity laser structure employing oxide semiconductor Bragg mirrors. In all cases the lasers utilized a buried oxide current and mode control layer to reduce the threshold. The individual accomplishments of the program are described in detail and directions for future research are listed.



**14. SUBJECT TERMS**

**NUMBER OF PAGES**

**16. PRICE CODE**

| 17. SECURITY CLASSIFICATION OF REPORT | 18. SECURITY CLASSIFICATION OF THIS PAGE | 19. SECURITY CLASSIFICATION OF ABSTRACT | 20. LIMITATION OF ABSTRACT |
|---|---|---|---|
| Unclassified | Unclassified | Unclassified | UL |

# DISCLAIMER NOTICE

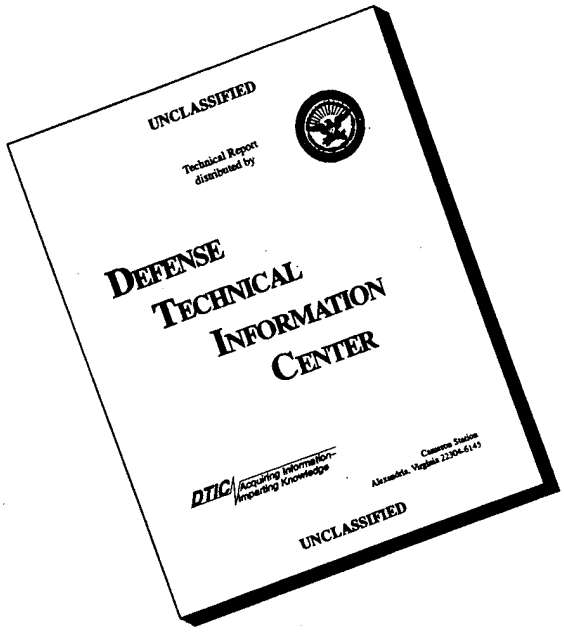


**THIS DOCUMENT IS BEST QUALITY AVAILABLE. THE COPY FURNISHED TO DTIC CONTAINED A SIGNIFICANT NUMBER OF PAGES WHICH DO NOT REPRODUCE LEGIBLY.**

# Final Report

## ONR Grant # N00014-91-J-1728

## OEIC Transmitters Employing Ultra Low Threshold Three Terminal Lasers

(Previously: "Optimization and Application of InP-Based Monolithic Integrated Photoreceivers")

P. D. Dapkus, Principal Investigator
Department of Electrical Engineering
University of Southern California
Los Angeles, CA 90089-0271

May 1996

## Table of Contents


**1.0 INTRODUCTION** ..... 1

**2.0 TECHNICAL RESULTS** ..... 4

**2.1 Folded Cavity Surface Emitting Lasers (FCSEL's)** ..... 5
2.1.1 Folded Cavity Surface-Emitting InGaAs/GaAs Lasers with Low Threshold Current Density and High Efficiency
2.1.2 Lasing Characteristics of High-Performance Narrow-Stripe InGaAs/GaAs Quantum Well Lasers Confined by AlAs Native-Oxide
2.1.3 Low-Threshold Native-Oxide Confined Narrow-Stripe Folded-Cavity Surface-Emitting InGaAs/GaAs Lasers
**2.2 Vertical Cavity Surface Emitting Lasers (VCSEL's)** ..... 46
2.2.1 Microcavity Effects on the Spontaneous Emission from InGaAs/GaAs Quantum Wells
2.2.2 Ultralow Threshold Current Vertical-Cavity Surface-Emitting Lasers Obtained with Selective Oxidation
2.2.3 Influence of Mirror Reflectivity on Laser Performance of Very Low Threshold Vertical-Cavity Surface-Emitting Lasers
**2.3 VCSEL's Employing Oxide Semiconductor Bragg Mirror** ..... 75
2.3.1 Wide Bandwidth Distributed Bragg Reflectors Using Oxide-GaAs Multilayers
2.3.2 Epitaxial (Al,Ga)InP/Oxide Distributed Bragg Reflectors for Use in Visible Wavelength Optical Devices
2.3.3 Ultralow Threshold Current Vertical-Cavity Surface-Emitting Lasers with AlAs Oxide/GaAs Distributed Bragg Reflectors

**3.0 SUMMARY OF ACCOMPLISHMENTS** ..... 104

**4.0 FUTURE RESEARCH** ..... 104

**APPENDIX – Reprints of published papers** ..... 106

# 1.0 INTRODUCTION

## 1.0 INTRODUCTION

This program was originally granted to Professor Stephen Forrest to investigate OEIC receivers. About half way through the program, the emphasis was changed to transmitters and when Professor Dapkus became PI the title was changed to its present one.

Optoelectronic integrated circuits are required for a variety of high performance systems to reduce part count, improve reliability and reduce cost. At present the development of OEIC's is proceeding at an uneven pace. OEIC receivers in the GaAs, InP and Si technologies are well ahead of the development of monolithic transmitters in any technology. The purpose of this research program is to investigate technologies that will advance the state of the art in OEIC transmitters by providing laser designs that are integrable and that have ultralow power requirements. Lasers that are designed for integration with electronics must share several common traits:
1.) low threshold current (< 1 mA),
2.) high differential quantum efficiency (>50%),
3.) high speed operation (> 5 GHz),
4.) integrable design,
5.) vertical light emission.
In addition, it is desirable if the devices can be operated using a third terminal with voltage control. The original concept of this program was to develop such a component. However when it was realized that the use of third terminal with the FCSEL design to be described below was not compatible with achieving ultralow current operation and when such operation was achieved with a VCSEL, the emphasis of the program was switched to the use of VCSEL's.

In this report we describe three laser designs which were investigated during the first phase of this program that share these common traits but vary in their ease of integration.

Folded cavity surface emitting lasers (FCSEL's) are in-plane lasers in which the beam is deflected towards by an in-cavity 45° mirror. The top surface of the device acts as one of the mirrors of the device. During this program we have developed the techniques for ion beam etching AlGaAs/GaAs/InGaAs laser structures to form highly perfect 45° and vertical mirrors. These have been demonstrated in Section 2.1.1 by the demonstration of state of the art broad area FCSEL's. This technology was combined with buried oxide confined laser stripes (Section 2.1.2 ) to demonstrate FCSEL's with state of the art threshold currents and efficiencies (Section 2.1.3). These devices are easily integrated with electronics. The major drawback of buried oxide stripe devices is that the threshold currents are limited to values of 2-3 mA by the out diffusion of carriers from the active region. For these reasons the majority of the program was effort was focused on VCSEL's in which the active area can be scaled to very small dimensions to reduce the current even further.

The vertical Cavity lasers that were developed in this program were based on a new perspective and design paradigm. Previous devices emphasized the electrical terminal characteristics with series resistance and forward voltage being the key driving factors in the device optimization. The intent was to improve the wall plug

efficiency of the devices by reducing the electrical power wasted in contact and interface voltage drops. However any doping in the mirror structure that is done to reduce the voltage drop through them also introduces optical loss. In our work, we decided to bypass the mirrors with the electrical path and to make direct contact to the active confining layers of the devices. By reducing the optical loss, the device can be re optimized for low threshold by increasing the mirror reflectivity and reducing the number of quantum wells. The path to this optimization was systematically pursued by optimizing the growth of quantum wells in resonant cavities and investigating the effects of the cavity resonance on the enhancement of the QW luminescence. (Section 2.2.1) Based on this optimization, fabrication of VCSEL device structures was begun. The concept of low loss which underlies this work was also being pursued simultaneously in other efforts to fabricate novel VCSEL's with oxide / semiconductor Bragg mirrors. In that work intracavity contacts were a necessity and the technology was well advanced. as a result intracavity contacts were also employed in the all semiconductor Bragg mirror devices. These devices yielded the lowest threshold current density ever achieved, 140 A/ $cm^2$, and the lowest threshold VCSEL ever made $I_{th}$ = 8.7 μA. (Section 2.2.2) A key feature of these devices was the use of a buried oxide current aperture to control the current flow and the optical mode. Subsequent characterization of these devices showed that the key attribute that led to the record low threshold was the low optical losses in the device. (Section 2.2.3)

VCSEL's require approximately 6 μm of epitaxial growth for the complete structure. The thickness of the device makes it difficult to grow and integrate with electronic devices which are much thinner. as a result we pursued an alternate technology to all semiconductor mirrors to reduce the number of layers and the overall thickness. Our approach was based on the used of the native oxide of AlAs as one of the mirror pairs. We first demonstrated the concept by fabricating Bragg mirrors in the IR (Section 2.3.1) and visible portions of the spectrum (Section 2.3.2) using AlAs oxide and the appropriate semiconductor. Very wide bandwidths exceeding the all semiconductor Bragg reflectors by a factor of five with a factor of three less epitaxial growth were demonstrated. These mirrors were then incorporated into a VCSEL as the top mirror (section 2.3.3 ) to assess the performance in a rigorous application. VCSEL's with threshold as low as 140 A/$cm^2$ and high efficiency were demonstrated. the remaining challenge for these devices is to devise the means to incorporate oxide DBR's for both mirrors and to provide low resistance contact to the device.

# 2.0 TECHNICAL RESULTS

## 2.1 FOLDED CAVITY SURFACE EMITTING LASERS (FCSEL's)

# Folded-Cavity Surface-Emitting InGaAs/GaAs Lasers with Low Threshold Current Density and High Efficiency

Yong Cheng, Gye Mo Yang, and P.Daniel Dapkus

National Center for Integrated Photonic Technology, Department of Electrical Engineering/ Electrophysics, University of Southern California, Los Angeles, CA 90089-0483

## ABSTRACT

Low threshold current and high efficiency folded-cavity surface-emitting InGaAs/GaAs lasers (FCSEL's) that employ high quality internal 45° deflectors are demonstrated. A simplified process involving a stop etch to position the surface emitting output mirror close to the waveguide and ion-beam-etching (IBE) to form the 45° deflecting mirror is presented. FCSEL's (cavity length 800μm) employing two 45° deflectors, are obtained with threshold current density as low as 112.5A/cm$^2$ and surface-emission external quantum efficiency as high as 65% (0.82W/A). The performance of these monolithic FCSEL's is very close to that of cleaved edge-emitting lasers. The additional loss due to the folded-cavity design is estimated as 4.2cm$^{-1}$.

High performance surface-emitting lasers are promising devices for applications to optoelectronic integrated circuits. Vertical-cavity surface-emitting lasers (VCSEL's) have been extensively studied. However, the electrical and thermal impedance of VCSEL's limit the maximum output power of the devices. As an alternate approach for surface emission, lasers with internal 45° total reflection mirrors (referred to as folded-cavity surface emitting lasers (FCSEL's)) or external 45° deflection mirrors are utilized to couple the light in the horizontal cavity towards the surface. Generally, the folded-cavity design with internal 45° total reflection mirrors is preferred over external 45° deflectors because more efficient deflection of the guided beam is expected. To date, threshold currents as low as 8mA for InGaAs/GaAs FCSELs incorporating high reflectivity epitaxial Bragg reflectors have been reported.[1-2] High power GaAs/AlGaAs narrow ridge waveguide[3] and broad area[4] FCSEL's have been demonstrated, as well as high power two-dimensional arrays of FCSEL's.[5-7] In a FCSEL, additional losses, such as diffraction loss in the folded unguided region, coupling loss owing to angular inaccuracy of the 45° mirror, scattering loss due to roughness of dry-etched facets, are introduced which may limit the performance. In this paper, we present a design and fabrication approach that minimize these losses and permit high efficiency operation.

A schematic diagram of the laser we present is shown in Fig.1. The laser positions the output mirror close to the waveguide to minimize the distance over which the deflected beam travels unguided.[8-9] Analysis predicts that this distance is the critical factor in determining the effective loss in the folded cavity.[8] Different dry-etching techniques such as chlorine assisted-ion-beam-etching (CAIBE),[3,6-7] angled ion-reactive-etching (RIE),[1] ion

milling,[2,4-5] etc., have been used to achieve 45° deflectors. A high quality 45° deflector requires that the facet angle be controlled within ±1° and the smoothness be <0.1μm RMS. The lasers we describe here employ 45° deflectors fabricated by ion-beam-etching (IBE). The lasers use a GaAs etch stop layer to permit the cladding layer to be etched to within 0.4μm from the cavity at the output mirror.[9] The FCSEL's (cavity length 800μm), with two 45° deflectors, are obtained with threshold current density as low as 112.5A/cm$^2$ and surface-emission external quantum efficiency as high as 65% (0.82W/A). The performance of these monolithic FCSEL's is very close to that of cleaved edge-emitting lasers. The additional loss due to the folded-cavity design is estimated as 4.2cm$^{-1}$.

The laser structure designed for FCSEL's is a single quantum well graded-index separate-confinement heterojunction (SQW-GRINSCH) grown by metalorganic chemical vapor deposition (MOCVD) with the following layers : a 1000Å n-GaAs buffer (2x10$^{18}$ cm$^{-3}$) layer, a 11000Å n-$Al_{0.6}Ga_{0.4}As$ bottom n-cladding (5x10$^{17}$cm$^{-3}$) layer, a 500Å GaAs etch-image layer, a 4000Å n-$Al_{0.6}Ga_{0.4}As$ bottom n-cladding (5x10$^{17}$cm$^{-3}$)layer, a 1500Å $Al_xGa_{1-x}As$ graded layer with x varying from 0.6 to 0.2, a 120Å GaAs layer, a 80Å $In_{0.24}Ga_{0.76}As$ quantum well layer, a 120Å GaAs layer, a top 1500Å $Al_xGa_{1-x}As$ graded layer, a 4000Å p-$Al_{0.6}Ga_{0.4}As$ layer, a 500Å GaAs etch-stop layer, a 11000Å p-$Al_{0.6}Ga_{0.4}As$ top p-cladding (5x10$^{17}$cm$^{-3}$) layer, and then a 1000Å GaAs cap layer.

Device processing starts with mesa etching to define broad area stripes. Mesas of 100μm wide and 0.6μm deep are etched in a solution of $H_2SO_4$:$H_2O_2$:$H_2O$ (1:8:160). A 1000Å $Si_3N_4$ layer is then deposited on the

sample using plasma enhanced chemical vapor deposition. Photoresist is applied to open a window on the mesa top for $CF_4$ etching $Si_3N_4$. Ti/Pt/Au is e-beam deposited on the top of the sample as the p-contact. The sample is now lithography patterned for the output mirror etching. First, GaAs cap layer is removed by a selective etchant ( Citric Acid : $H_2O_2$ / 4:1). Second, the top AlGaAs cladding layer is selectively etched in a HF solution down to the GaAs stop layer. The wafer is now ready to be patterned for IBE. A single layer of photoresist is chosen as mask for IBE of the 45° deflecting mirrors. The quality of the mask, in terms of profile and smoothness, is crucial to good results. A photoresist layer with a nearly-vertical side wall and smooth edges must be achieved in order to etch facets with high quality. Ion beam etching (IBE) is performed at $9x10^{-5}$Torr with an $Ar^+$ ion beam at 800eV on Technics 300 Series TLA 5.5 Ion Beam Milling System. For a 1μm deep 45° undercut, the sample is tilted by 70° for 180 minutes etching. The SEM pictures, shown in Fig.2a and 2b, indicate that smooth etched 45° deflectors have been obtained. An optimum separation must be achieved between the IBE window and the end of the p-contact to allow efficient mode coupling while at the same time allowing efficient pumping of the end of the active region. This separation is chosen to be 2-5μm. After the sample is lapped down to about 100μm, AuGe/Ni/Au is e-beam deposited on the bottom of the sample as n-contact. Then, the sample is alloyed at 400°C for 40 seconds.

The FCSEL design employed here positions the output mirror as close to the waveguide as possible to reduce the light path through unguided region to minimize the diffraction loss. The calculations reported by N.C.Frateschi *et al* [8] indicate an increase of the beam divergence and a strong reduction of the feedback as the unguided region path is increased. In our FCSEL structure,

the unguided region can be easily reduced by controlling output mirror position with the stop etch layer. At some point, further reduction in the waveguide will cause a large disturbance in the propagating cavity mode that may reduce the output coupling at 0.4μm. There is no apparent disturbance based on the measured far-field patterns.

The lasers are tested under pulsed operation (500ns pulse width, 10kHz repetition rate). The emission spectra exhibit multiple modes centered around ~990nm. Fig.3 shows a typical L-I curve for a FCSEL ( L = 640μm) consisting of one vertical output mirror and one cleaved facet. The threshold current density is 133A/cm$^2$ and the external quantum efficiencies are 41% (0.52W/A) and 38% (0.48W/A) for the light output from the top surface and the cleaved facet, respectively, which gives a total external quantum efficiency of 79%. For comparison, broad-area cleaved lasers (L = 650μm) made from this material have the threshold current density of 108A/cm$^2$ and the external quantum efficiency of 78%.

In Fig.4, a typical L-I curve for a broad area FCSEL ( L = 800μm), consisting of two vertical output mirrors and two internal 45° deflectors. The threshold current density is 112.5A/cm$^2$ and the external quantum efficiency is 65% (0.82W/A) for surface emission. The performance of these monolithic FCSELs is very close to that of cleaved edge-emitting lasers. Compared with cleaved edge-emitting lasers, additional losses such as diffraction loss ($\alpha_{diff}$), coupling loss ($\alpha_{coupl}$), and scattering loss ($\alpha_{scatt}$) are introduced in FCSEL's. These additional losses resulting from a folded-cavity can be written as

$$\alpha_{FC} = \alpha_{diff} + \alpha_{coupl} + \alpha_{scatt} \qquad (1)$$

The external quantum efficiency $\eta_d$ of a FCSEL is defined as

$$\eta_d = \eta_i \frac{\alpha_m}{\alpha_m + \alpha_{int} + \alpha_{FC}} \quad (2)$$

where $\eta_i$ is the internal quantum efficiency, $\alpha_m$, $\alpha_{int}$ are the mirror loss and the internal loss, respectively. The internal quantum efficiency and the internal loss for the edge-emitting lasers made from this material are 92% and 1.7cm$^{-1}$, respectively. Using the 65% for the total external quantum efficiency of the FCSEL, therefore, the additional loss due to the folded-cavity, $\alpha_{FC}$, is estimated as 4.2cm$^{-1}$ for the above devices.

The broad area GaAs/AlGaAs FCSEL's (L=500μm), reported by S.S.Ou *et al* [4], exhibited threshold current densities of 360A/cm$^2$ and surface-emission quantum efficiency of 22%. W.D Goodhue *et al* [7] demonstrated two-dimensional arrays of InGaAs/AlGaAs FCSEL's (L=1000μm) with threshold current density of 185A/cm$^2$ and surface-emission quantum efficiency of 28% per facet. Compare with these reported results, the FCSELs (L=800μm) we report here, to our best knowledge, have the lowest threshold current density of 112.5A/cm$^2$ and the highest differential quantum efficiency of 32.5% per facet.

The surface emission far-field patterns are measured at 40mW output power level under cw operation. Fig.5 shows the far-field profiles for surface emission perpendicular and parallel to the junction. It can be seen that the full width at half maximum (FWHM) of the far-field perpendicular ($\theta_\perp$) and parallel ($\theta_{//}$) to the junction are 39.8° and 9.4°, respectively. These FWHM values are comparable to those of edge-emitting broad area lasers.

In conclusion, we report the fabrication of high quality 45° deflectors using ion-beam-etching (IBE) techniques and the characteristics of simply designed InGaAs/GaAs FCSEL's with high performance. FCSEL's (cavity length 800μm), consisting of two internal 45° deflectors, are obtained with The threshold current density of 112.5A/cm$^2$ and the external quantum efficiency of 65% (0.82W/A) for surface emission. The additional loss due to the folded-cavity is estimated as 4.2cm$^{-1}$. The performance of the FCSEL's presented here can be further improved. For example, the 0.4μm distance between the horizontal output mirror and the top waveguide layer of the FCSEL may not be optimum. It may be further reduced to decrease the diffraction loss. Second, optimized facet coatings may be applied to the output mirrors so that more single ended surface-emitting power can be achieved. The high quality 45° deflectors and high performance InGaAs/GaAs FCSEL's presented here, based on well-calibrated ion-beam-etching (IBE) technique and simply designed junction-up device structure, suggest the potential fabrication of high performance monolithic two-dimensional arrays of FCSEL's.

# ACKNOWLEDGMENT

The authors wish to thank S. S. Ou for help on IBE technique, F.Fang, M.Jansen, K.Walker, J.J.Yang for testing assistance, H.Zhao, M.H. MacDougal, K.Uppal for useful discussions. This work is supported by ARPA through the Ultra program, and by the Office of Naval Research.

# References


1. C.P.Chao, K.K.Law, J.L.Merz, "Design and Fabrication of Ridge Waveguide Folded-Cavity In-Plane Surface-Emitting Lasers". *IEEE Photon. Technol. Lett.*, vol.4, p.223, 1992.

2. N.C.Frateschi, P.D.Dapkus, S.S.Ou, J.J.Yang, M.Jansen, "Low Threshold InGaAs/GaAs 45° Folded-Cavity Surface-Emitting Lasers Grown on Structured Substrates". *IEEE Photon. Technol. Lett.*, vol.5, p.741, 1993.

3. F.R.Gfleller, P.Buchmann, K.Dätwyler, J.P.Reithmaier, P.Vettiger, D.J.Webb, "50mW CW Operated Single-Mode Surface-Emitting AlGaAs lasers with 45° Total Reflection Mirrors", *IEEE Photon. Technol. Lett.*, vol.4, p.698,1992.

4. S.S.Ou, M.Jansen, J.J.Yang, M. Sergant, "High-power cw operation of GaAs/AlGaAs surface-emitting lasers mounted in the junction-up configuration". *Appl. Phys. Lett.*, 59, p.1037 (1991).

5. D.W.Nam, R.G.Waarts, D.F.Welch, D.R.Scifres, "Operating Characteristics of High Continuous Power (50W) Two-Dimensional Surface-Emitting Laser Arrays", *IEEE Photon. Technol. Lett.*, vol.5, p.281,1993.

6. J.P.Donnelly, W.D.Goodhue, C.A.Wang, R.J.Bailey, G.A.Lincoln, G.D.Johnson, L.J.Missaggia, J.N.Walpole, "CW Operation of Monolithic Arrays of Surface-Emitting Folded-Cavity InGaAs/AlGaAs Diode Lasers". *IEEE Photon. Technol. Lett.*, vol.5, p.747,1993.

7 W.D.Goodhue J.P.Donnelly, C.A.Wang, G.A.Lincoln, K.Rauschenbach, R.J.Bailey, G.D.Johnson, "Monolithic two-dimensional surface-emitting strained-layer InGaAs/AlGaAs and AlInGaAs/AlGaAs diode laser arrays with over 50% differential quantum efficiencies", *Appl. Phys. Lett.*, 59, p.632 (1991).

8. N.C.Frateschi, P.D.Dapkus, S.S.Ou, J.J.Yang, M.Jansen, "Analysis of Nonplanar Wave Propagation Through Multilayer Bragg Reflectors for Folded Cavity and Vertical Cavity Surface Emitting Laser Structures", *IEEE J. Quantum Electron.*, vol31, no.4, April (1995).

9. C.P.Chao, G.J.Shiau, S.R.Forrest, "1.3μm Wavelength, InGaAsP-InP Folded-Cavity Surface-Emitting Lasers Grown by Gas-Source Molecular-Beam Epitaxy". *IEEE Photon. Technol. Lett.*, vol.6, p.1406, 1994.

# Figure Captions

Fig. 1, The schematic diagram of a FCSEL structure.

Fig. 2a, A SEM picture showing the cross-section of an ion-beam-etched 45° deflector.

Fig. 2b, A SEM picture showing the smoothness of an ion-beam-etched 45° deflector.

Fig. 3, Typical L-I curves of emission from surface and edge for a FCSEL ( L = 640μm), consisting of a horizontal output mirror, an internal 45° deflectors and a cleaved mirror, under pulsed operation at room temperature.

Fig. 4, A typical L-I curve of surface emission for the FCSELs ( L = 800μm), consisting of two horizontal output mirror and two internal 45° deflectors, under pulsed operation at room temperature.

Fig. 5, The far-field profiles for the surface emission (a) perpendicular to the junction and (b) parallel to the junction.

Fig. 1

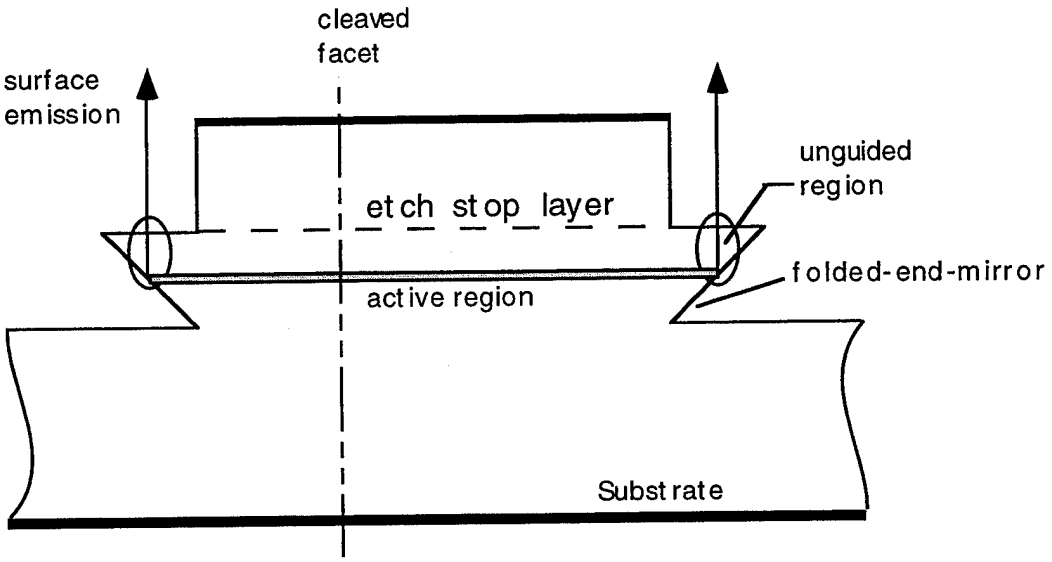
cleaved
facet
surface
emission
unguided
region
etch stop layer
folded-end-mirror
active region
Substrate

Fig. 2a

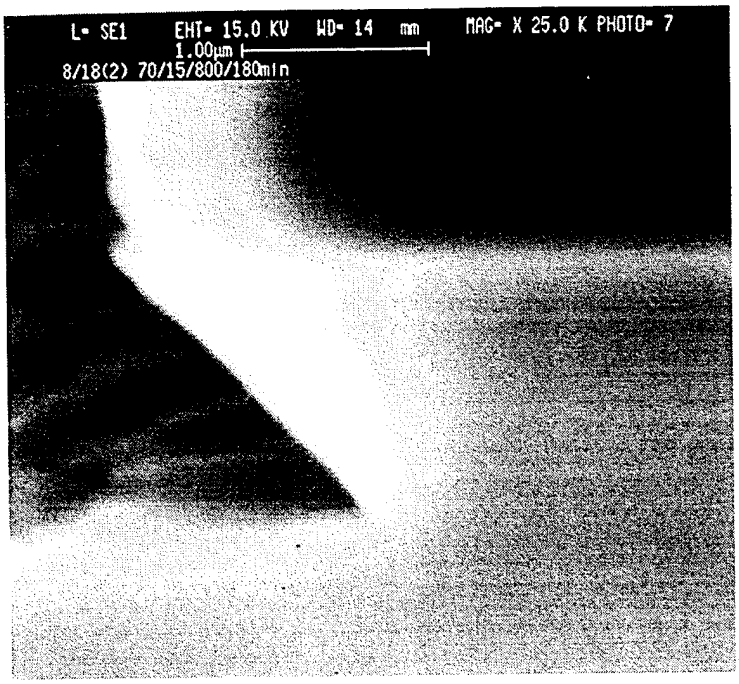
L= SE1 EHT= 15.0 KV WD= 14 mm MAG= X 25.0 K PHOTO= 7
1.00µm
8/18(2) 70/15/800/180min

Fig. 2b

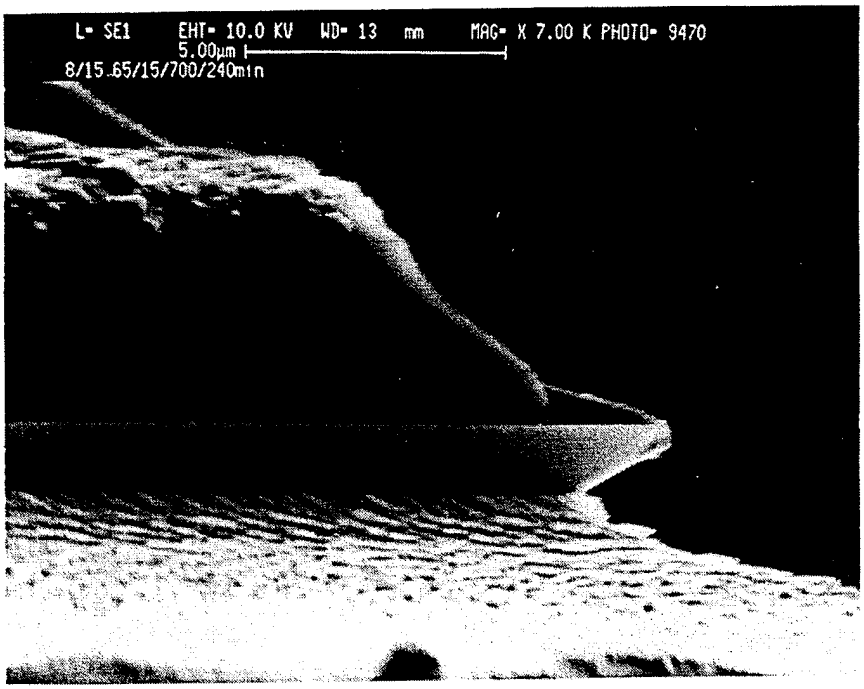
L= SE1 EHT= 10.0 KV WD= 13 mm MAG= X 7.00 K PHOTO= 9470
5.00µm
8/15.65/15/700/240min

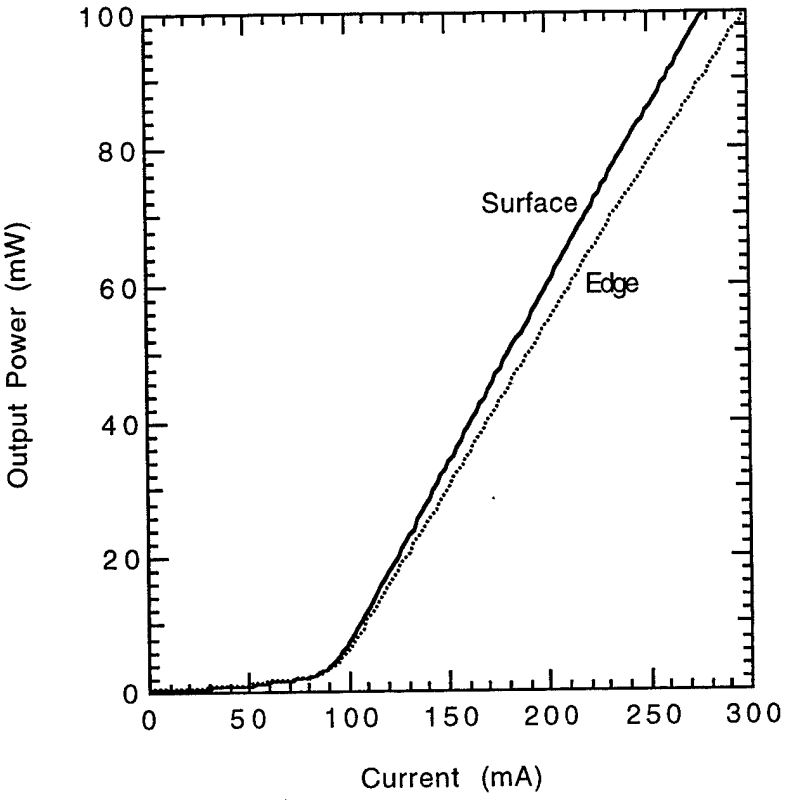
100
80
60
40
20
0
Output Power (mW)
Surface
Edge
0
50
100
150
200
250
300
Current (mA)

Fig. 3

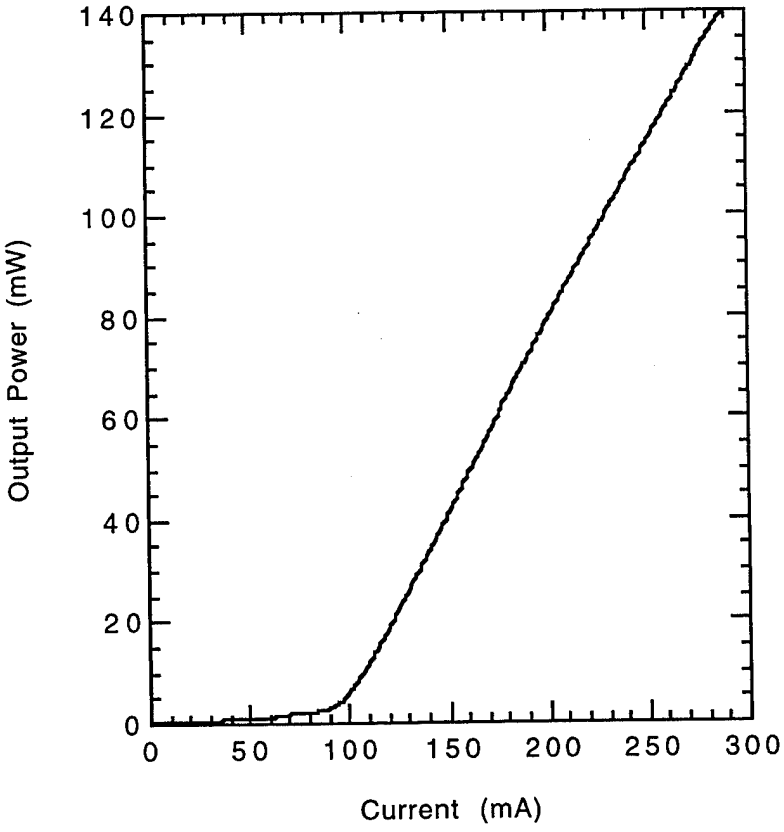
140
120
100
80
60
40
20
0
Output Power (mW)
0
50
100
150
200
250
300
Current (mA)

Fig. 4

Fig. 5

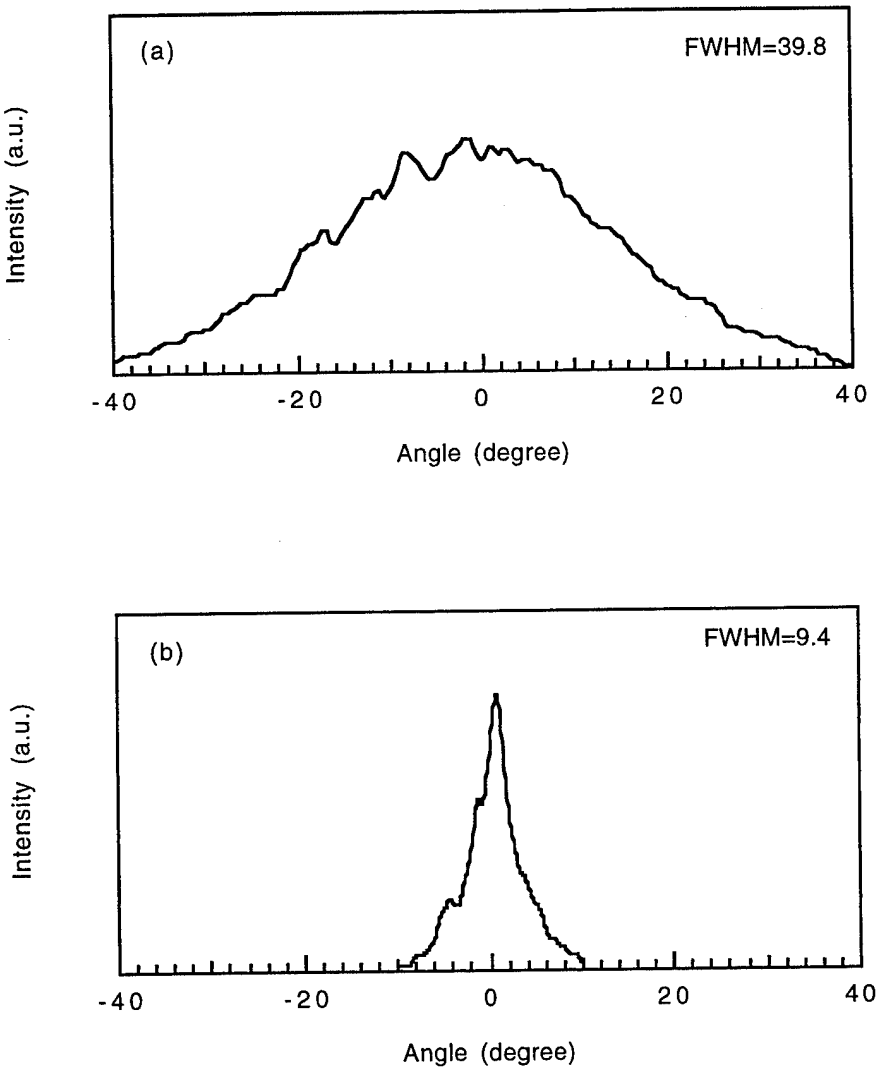
(a)
FWHM=39.8
Intensity (a.u.)
-40
-20
0
20
40
Angle (degree)
(b)
FWHM=9.4
Intensity (a.u.)
-40
-20
0
20
40
Angle (degree)

# Lasing Characteristics of High-Performance Narrow-Stripe InGaAs/GaAs Quantum Well Lasers Confined by AlAs Native-Oxide

Yong Cheng, P.Daniel Dapkus, Michael H. MacDougal, and Gye Mo Yang

National Center for Integrated Photonic Technology, Department of Electrical Engineering/ Electrophysics, University of Southern California, Los Angeles, CA 90089-0483

## ABSTRACT

High-performance narrow-stripe InGaAs/GaAs quantum well lasers with integral buried AlAs native-oxide layers have been fabricated. AlAs native-oxide layers above and below waveguide region were employed for current and optical confinement to form narrow-stripe lasers. A low temperature (400°C) anisotropic wet oxidation technique was used to selectively oxidize AlAs layers in the epitaxial structure. The devices demonstrated continuous wave threshold currents of 3.5mA, external quantum efficiencies of 82%, and a characteristic temperature of 133K for 1.8μm-wide aperture, 400μm-long devices. Threshold currents of 1.7mA were obtained by applying HR/HR coatings.

# I. Introduction

Semiconductor laser diodes with near mA threshold currents and high quantum efficiencies are needed for application to optoelectronic integrated circuits (OEIC's) and in optical interconnects. High-performance index-guided lasers have been reported by several groups.[1-3] These devices usually require more complex processing than, for example, ridge waveguide or oxide stripe lasers, which although simpler to fabricate are affected by current spreading and lateral carrier diffusion in the active layer that limit the practical applications of these devices.[4]

There has been interest in recent years to apply buried layers of a native oxide to optoelectronic devices because it is an insulator and has a low refractive index (n~1.55). The native-oxide of AlGaAs provides both electronic and optical confinement making it possible to fabricate low threshold, high efficiency quantum well lasers. In addition, its use simplifies processing of lasers. For semiconductor edge-emitting lasers, the native-oxide of AlGaAs has been utilized to fabricate stripe-geometry lasers[5], and index-guided lasers[6]. For vertical-cavity surface-emitting lasers, the native-oxide of AlAs has been employed in DBR structures,[7] and for current constriction[8,9] to achieve low threshold devices. S.A.Maranowski *et al* [5] demonstrated a stripe-geometry structure in which the laser stripe is defined by both top and bottom native-oxide layers. AlGaAs native-oxide confined InGaAs/GaAs narrow-stripe lasers (~2.5μm-wide aperture, 305μm-long cavity) were reported with threshold currents of 8mA and quantum efficiency of 61%. This paper explores further the design and properties of these lasers with the goal of optimizing their performance, quantifying the degree of optical and carrier confinement and

comparing their properties to state of the art buried heterostructure lasers. The devices we report exhibit continuous wave threshold currents of 3.5mA, external quantum efficiencies of 82%, and characteristic temperatures of 133K for 1.8μm-wide aperture, 400μm-long cavity devices. Threshold currents of 1.7mA are obtained by applying HR coatings.

## II. Device Design and Fabrication

The device design is schematically shown in Fig.1. The AlAs layers above and below the waveguide region are oxidized from the edge of an etched mesa to form a narrow-stripe structure. Since the native-oxide of AlAs is a transparent insulator and has a small refractive index, both electronic and optical confinement can be expected. The oxidation rate of AlGaAs depends strongly on Al composition.[10] AlAs is chosen in our devices to the minimize effects of compositional nonuniformity and to increase reproducibility. Its use instead of the ternary, AlGaAs, relaxes the compositional uniformity requriements to obtain the desired oxide profile and also decreases the oxidation time. Ultimately, an alloy would be used in the oxide layer to ensure reliability. Since the top native-oxide layer forms a current constriction aperture, it is necessary to put the top AlAs layer close to the waveguide in order to minimize current spreading effects.

The laser structure in this work is a single quantum well graded-index separate-confinement heterojunction (SQW-GRINSCH) grown by metalorganic chemical vapor deposition (MOCVD). The waveguide region includes: a 1000Å n-type AlAs layer, a 500Å n-$Al_xGa_{1-x}As$ graded layer with x varying from 1.0 to

0.6, a 500Å n-$Al_{0.6}Ga_{0.4}As$, a 1500Å n-$Al_xGa_{1-x}As$ graded layer with x varying from 0.6 to 0.2, a 120Å GaAs layer, a 80Å $In_{0.24}Ga_{0.76}As$ quantum well layer, a 120Å GaAs layer, a top 1500Å $Al_xGa_{1-x}As$ graded layer, a 500Å p-$Al_{0.6}Ga_{0.4}As$, a 500Å p-$Al_xGa_{1-x}As$ graded layer with x varying from 0.6 to 1.0, a 1000Å p-type AlAs layer. The top AlAs layer is about 2500Å above the active region.

The mesas to expose the edge of the AlAs layers for oxidation are formed by wet chemical etching using an $H_2O / H_2O_2/H_2SO_4$ (160:8:1) solution. The oxidation is performed at 400°C in $H_2O$-vapor-saturated $N_2$. A SEM picture of the oxidized mesa cross-section is shown in Fig.2. The aperture defined by top AlAs oxide layer is about 1.8μm after 8.5min oxidation. The lower oxide aperture is wider owing to the doping dependence of the oxidation process.[11] After oxidation, the sample is fully covered by $Si_3N_4$ using PECVD and 10μm-wide stripes are opened on the mesa top using a $CF_4$ plasma etching. Ti/Pt/Au is e-beam deposited on the mesa top as the p-contact. In this way, we minimize the possible negative effects on laser performance from the trapezoidal shape of the diode and charge trapping [5]. After the sample is lapped down to about 100μm, AuGe/Ni/Au is e-beam deposited on the bottom of the sample as the n-contact. Finally, the sample is alloyed at 400°C for 40 seconds. The wafer is then cleaved into laser bars for testing.

## III. Device Characteristics

The devices are probe-tested under continuous wave (CW) operation at room temperature without a heat sink. A typical light output vs current (L-I) curve for

device with 1.8μm-wide aperture, 400μm-long cavity is shown in Fig.3. A threshold current of 3.5mA ($J_{th}$~490A/cm$^2$) is obtained with external quantum efficiency of 82%. The pulsed (500ns width, 10kHz repetition rate) threshold current density of broad area lasers (100μm-wide stripes) made from the same material is 70A/cm$^2$ for a 1500μm cavity length. Thermal effects influence the output power when the pumping current is 25mA or more in these unbonded devices. By applying high-reflection (HR) dielectric ($SiO_2$/Si) coating on one facet, a threshold current of 2.6mA is obtained. The threshold current is 1.7mA with both facets HR coated. The inset in Fig.3 shows the spectra for the uncoated device at different pumping levels. From 3mA to 4mA, the spectrum narrows down considerably. In the above-threshold regime, particularly when I>5mA, single longitudinal mode operation becomes dominant as the power in side modes saturates. This suggests that good current and optical confinement exist in these narrow-stripe structures.

The near-field and far-field patterns are measured under CW operation at room temperature, as shown in Fig.4. The near-field pattern measured at drive current of 6mA indicates a round shape with the full width at half power (FWHP) of ~2μm due to the narrow active region. The far-field patterns are measured at different pumping levels from 6mA to 12mA. The full width at half maximum (FWHM) of the far-field perpendicular and parallel to the junction plane are 35° and 15°, respectively. The measurement of the temperature dependence of threshold current indicates that the CW threshold currents vary from 3mA to 4.7mA in the temperature range of 0°C-50°C. A characteristic temperature of 133K is obtained.

Fig.5 shows the cavity length dependence of the threshold current and the reciprocal external quantum efficiency ($\eta_d^{-1}$). Low threshold currents can be expected for laser cavity lengths in the range of 300-500μm. From the cavity length dependence of $\eta_d^{-1}$, the internal quantum efficiency and the internal losses for such narrow-stripe lasers are estimated as 90.2% and 4.1cm$^{-1}$, respectively.

In Fig.6, the threshold currents for the devices with different current aperture widths are plotted. Compared with the device reported by S.A.Maranowski *et al* [5], the lasers in this work have lower threshold and higher efficiency. The data reported by H. Zhao *et al* [1] for buried-heterostructure lasers grown on the non-planar substrates are also shown in Fig.6 for comparison. Those devices exhibit lower threshold current at comparable width, presumably due to better lateral confinement of the carriers and the optical fields.

In Fig.7, the threshold currents and quantum efficiencies for 25 devices (400μm-long cavity) on a laser bar are plotted. It can be seen that the threshold currents and the quantum efficiencies are (3.8±0.3)mA and (79±3)%, respectively, for the devices along the bar. Such good uniformity of high performance lasers suggests potential application of this technology to laser arrays.

## IV. SUMMARY

In conclusion, we report the fabrication and characteristics of the low threshold current and high efficiency narrow-stripe InGaAs/GaAs quantum well lasers confined by AlAs native-oxide layers. AlAs native-oxide layers above and

below waveguide region are employed for current and optical confinement. The low temperature (400°C) selective wet oxidation technique is used to achieve native oxide layers. The devices demonstrate continuous wave threshold currents of 3.5mA, external quantum efficiencies of 82%, and characteristic temperature of 133K for 1.8μm-wide aperture, 400μm-long cavity. The threshold currents of 1.7mA are obtained by applying HR coatings.

## ACKNOWLEDGMENT

The authors wish to thank F. Fang, K. Walker, M. Jansen, J.J. Yang for testing assistance, K.Uppal for useful discussions. This work is supported by ARPA through the Ultra program and by the Office of Naval Research.

## REFERENCES

1. H. Zhao, M.H. MacDougal, P.D.Dapkus, K. Uppal, Y. Cheng, and G.M. Yang, "Submilliampere threshold current InGaAs/GaAs/AlGaAs lasers and laser arrays grown on nonplanar substrates," *Journal of Selected Topics in Quantum Electronics*, Vol.1, No.2, pp196-202, June 1995.

2. Y.K. Sin, H. Horikawa, Y. Matsui, and T. Kamijoh, "Ultralow laser threshold and high speed InGaAs-GaAs-InGaP buried heterostructure strained quantum well lasers for optical interconnects", *Electron. Lett.*, vol.29, pp.873-874 (1993).

3. T.R. Chen, L.E. Eng, B. Zhao, Y.H. Zhuang, and A. Yariv, "Strained single quantum well InGaAs laser with a threshold of 0.25mA", *Appl. Phys. Lett.*, 63, pp2621-2623 (1993).

4. H.C. Casey, Jr., and M.B. Panish, *Heterostructure Lasers* (Academic, New York, 1978), Part B, pp217-224.

5. S.A.Maranowski, A.R.Sugg, E.I.Chen, and N.Holonyak,Jr., "Native oxide top- and bottom-confined narrow stripe p-n $Al_yGa_{1-y}As$-GaAs-$In_xGa_{1-x}As$ quantum well heterostructure laser", *Appl. Phys. Lett.*, 63, pp1660-1662(1993).

6. S.J.Caracci, F.A.Kish, N.Holonyak,Jr., S.A.Maranowski, S.C.Smith, and R.D.Burnham, "High-performance planar native-oxide buried-mesa index-guided AlGaAs-GaAs quantum well heterostructure lasers", *Appl. Phys. Lett.*, 61, pp321-323(1992).

7. M.H.MacDougal, P.D.Dapkus, V.Pudikov, H.Zhao, and G.M. Yang, "Ultralow threshold current vertical-cavity surface-emitting lasers with AlAs oxide-GaAs distributed Bragg reflectors", *IEEE, Photon. Technol. Lett.*, 7, 229(1995).

8. D.L. Huffaker, D.G. Deppe, and K. Kumar, "Native-oxide defined ring contact for low threshold vertical-cavity lasers", *Appl. Phys. Lett.*, 65, pp97-99(1994).

9. G.M. Yang, M.H. MacDougal, and P.D. Dapkus, "Ultralow threshold current vertical-cavity surface-emitting lasers obtained with selective oxidation", *Electron. Lett.*, Vol.31, No.11, pp886-888, (1995).

10. K.D. Choquette, R.P. Schneider Jr., K.L. Lear, and K.M. Geib, "Low threshold voltage vertical-cavity lasers fabricated by selective oxidation", *Electron. Lett.*, vol.30, pp.2043-2044 (1994).

11. F.A.Kish, S.A.Maranowski, G.E.Höfler, N.Holonyak,Jr., S.J.Caracci, J.M.Dallesasse, and K.C.Hsieh, "Dependence on doping type (p/n) of the water vapor oxidation of high-gap $Al_xGa_{1-x}As$", *Appl. Phys. Lett.*, 60,pp3165-3167(1994).

# FIGURE CAPTIONS

Fig.1, The schematic of narrow-stripe InGaAs/GaAs quantum well laser confined by native oxide layers above and below the waveguide region.

Fig.2, A SEM picture of the oxidized mesa cross-section. The aperture of 1.8μm-wide for current through is defined by top native-oxide.

Fig.3, A typical L-I curve for device with 1.8μm-wide aperture, 400μm-long cavity under CW operation at room temperature. The inset shows the spectra for the device at different pumping levels.

Fig.4, The near-field and far-field patterns of the device.

Fig.5 The cavity length dependence of the threshold current and the reciprocal external quantum efficiency ($\eta_d^{-1}$).

Fig.6, Threshold currents for the devices with different width of current aperture. Data from refs. [1] and [5] are also shown for comparison.

Fig.7, The distribution of threshold current and quantum efficiency for 25 devices (400μm-long cavity) on a laser bar.

Fig.1

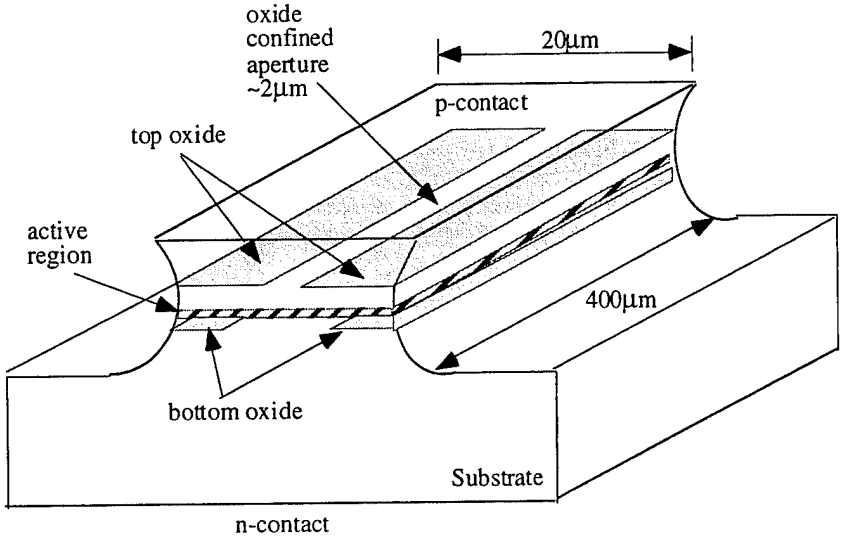
oxide
confined
aperture
~2μm
20μm
p-contact
top oxide
active
region
400μm
bottom oxide
Substrate
n-contact

Fig.2

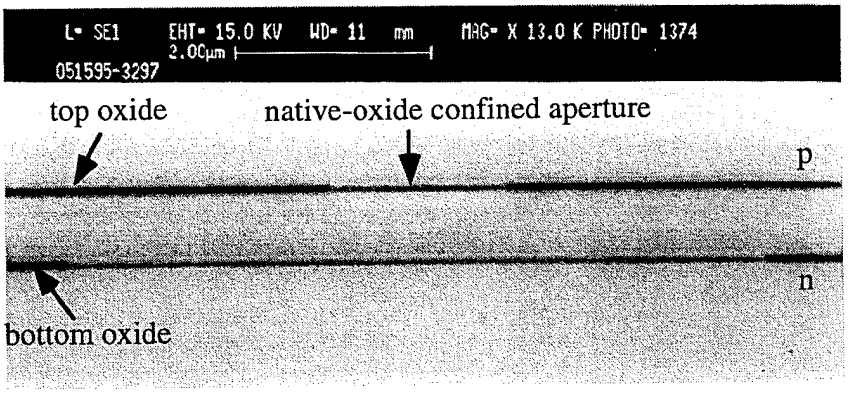
L= SE1 EHT= 15.0 KV WD= 11 mm MAG= X 13.0 K PHOTO= 1374
2.00μm
051595-3297
top oxide
native-oxide confined aperture
p
n
bottom oxide

Fig.3

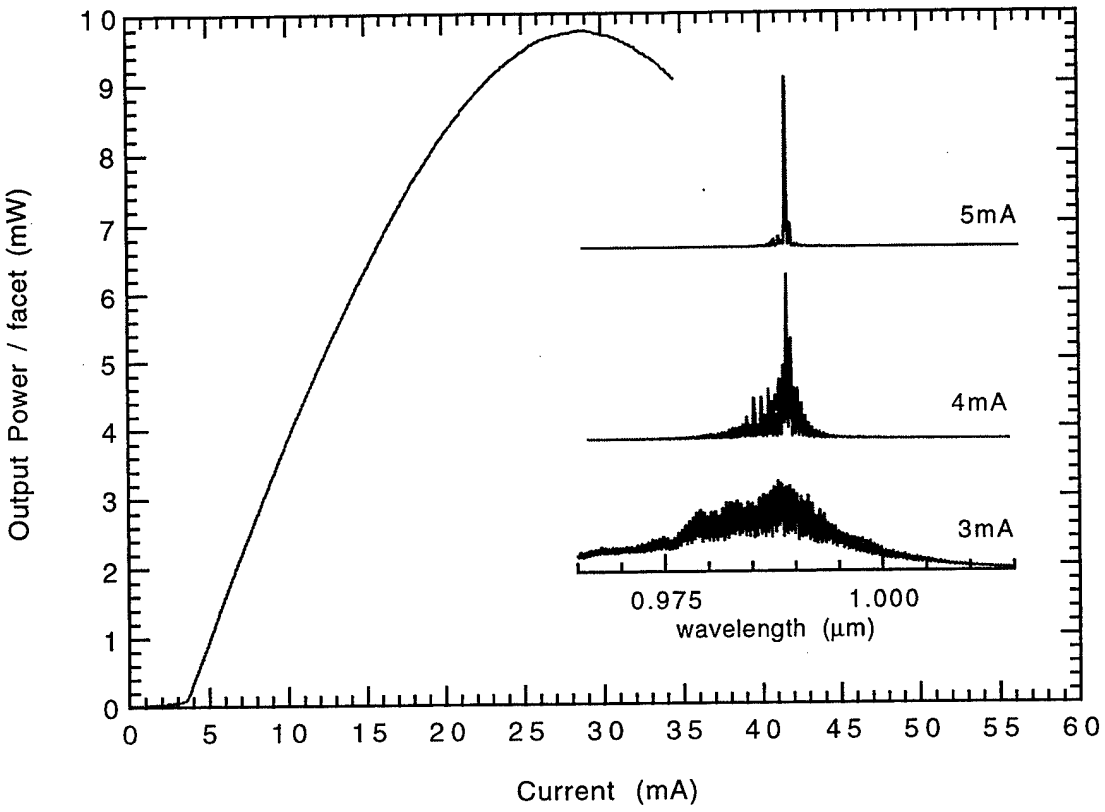
Output Power / facet (mW)
Current (mA)
5mA
4mA
3mA
0.975
1.000
wavelength (μm)

Fig.5

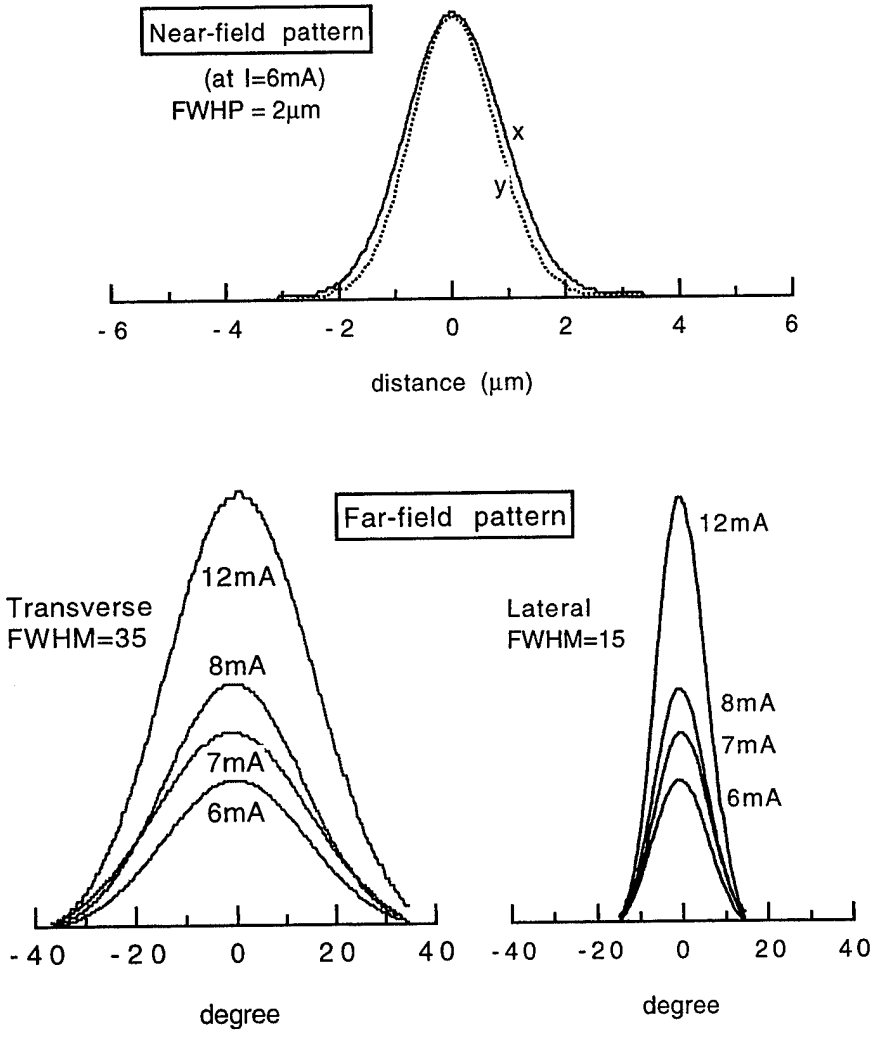
Near-field pattern
(at I=6mA)
FWHP = 2μm
x
y
-6
-4
-2
0
2
4
6
distance (μm)
Far-field pattern
Transverse
FWHM=35
12mA
8mA
7mA
6mA
-40
-20
0
20
40
degree
Lateral
FWHM=15
12mA
8mA
7mA
6mA
-40
-20
0
20
40
degree

Fig. 5

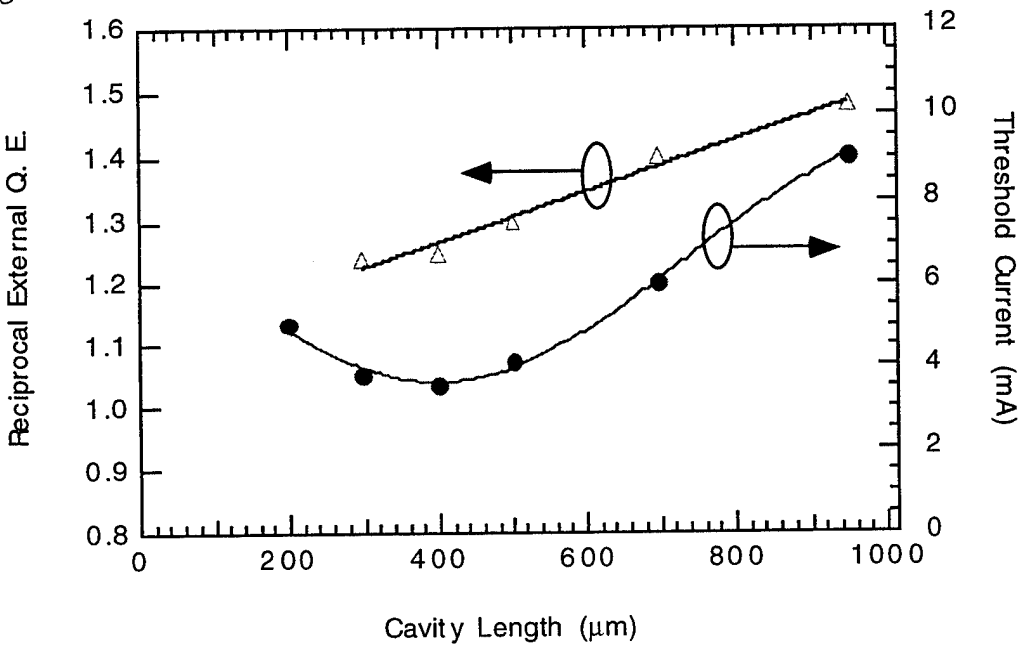
Reciprocal External Q. E.
Threshold Current (mA)
Cavity Length (μm)
1.6
1.5
1.4
1.3
1.2
1.1
1.0
0.9
0.8
12
10
8
6
4
2
0
0
200
400
600
800
1000

Fig. 6

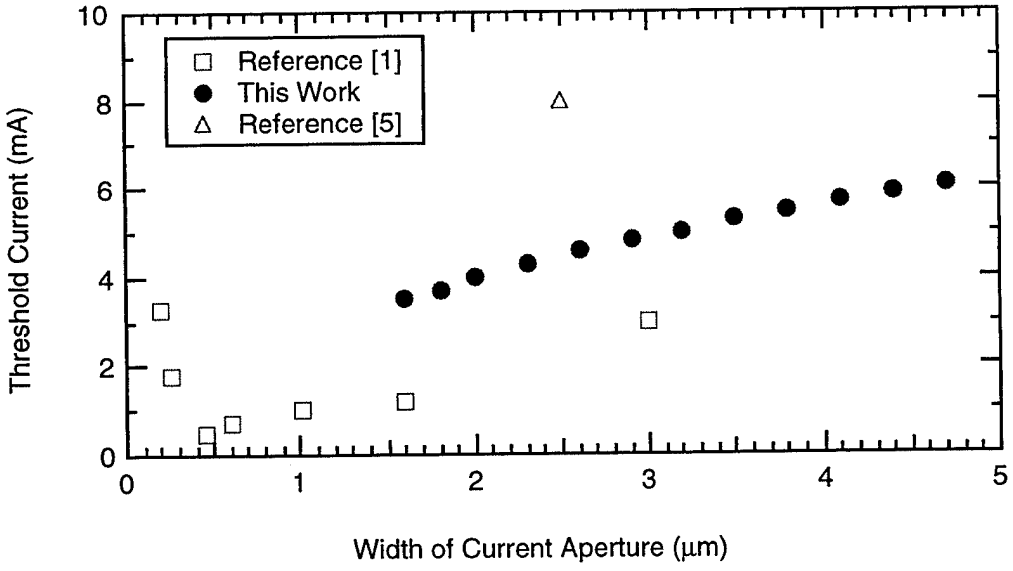
Reference [1]
This Work
Reference [5]
Threshold Current (mA)
Width of Current Aperture (μm)
10
8
6
4
2
0
0
1
2
3
4
5

Fig.7

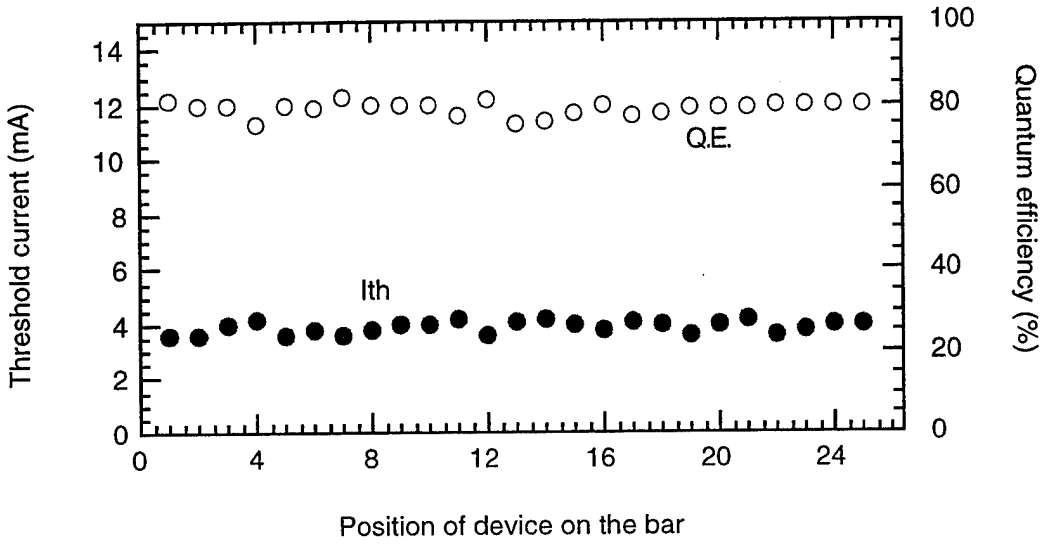
Threshold current (mA)
Quantum efficiency (%)
Q.E.
Ith
Position of device on the bar
0
2
4
6
8
10
12
14
0
20
40
60
80
100
0
4
8
12
16
20
24

# Low-Threshold Native-Oxide Confined Narrow-Stripe Folded-Cavity Surface-Emitting InGaAs/GaAs Lasers

Yong Cheng, Gye Mo Yang, Michael H. MacDougal, and P.Daniel Dapkus

National Center for Integrated Photonic Technology, Department of Electrical Engineering/ Electrophysics, University of Southern California, Los Angeles, CA 90089-0483

## ABSTRACT

Narrow-stripe folded-cavity surface-emitting InGaAs/GaAs lasers are demonstrated. AlAs native-oxide layers above and below waveguide region are employed for current and optical confinement to form narrow-stripe InGaAs/GaAs quantum well lasers. A low temperature (400°C) selective wet oxidation technique and ion-beam-etching technique are used to fabricate native-oxide confined narrow-stripes and internal 45° deflectors, respectively. Continuous wave threshold currents as low as 4.5mA and 59% surface-emitting quantum efficiencies are achieved on the devices with 2μm-wide aperture, 420μm-long cavity.

Low threshold and high efficiency folded-cavity surface-emitting lasers (FCSEL's) are of great interest for application to optoelectronic integrated circuits (OEIC's) and free space optical interconnects. FCSEL's employing dry-etched internal 45° deflectors to couple the light in the horizontal cavity towards the surface have the advantage of a much longer gain path. These devices are suitable for incorporation into three-terminal voltage controlled device designs that are useful in OEIC's[1]. High power GaAs/AlGaAs narrow ridge waveguide[2] and broad area[3] FCSEL's as well as high power two-dimensional arrays of FCSEL's[4-5] have been demonstrated. Threshold currents of 8mA for InGaAs/GaAs FCSEL's incorporating high reflectivity epitaxial Bragg reflectors, based on ridge waveguide structure[6] or non-planar substrate structure,[7] have been reported. Recently, we have demonstrated high performance broad area InGaAs/GaAs FCSEL's by using a novel folded-cavity design and a well-developed ion-beam-etching (IBE) technique.[8] In our FCSEL's design, the diffraction loss is reduced to result in low threshold, high efficiency lasers without employing Bragg reflectors.[8-9] As a result, much less stringent requirements for growth control is obtained.

A novel form of $Al_yGa_{1-y}As/GaAs/In_xGa_{1-x}As$ quantum well laser that is confined above and below the active region by an insulating low refractive index native oxide was first demonstrated by S.A.Maranowski *et al* [10]. The laser diodes are defined from a mesa edge by the selective lateral oxidation and anisotropic oxidation of high Al composition layers located above and below the waveguide region. This laser structure of narrow-stripe geometry provides excellent current and optical confinement.[10] In this letter, we report the fabrication and characteristics of native-oxide confined narrow-stripe folded-cavity surface-emitting InGaAs/GaAs lasers. Low temperature (400°C) selective

wet oxidation and ion-beam-etching techniques are used to fabricate native-oxide confined narrow-stripes and internal 45° deflectors, respectively. Continuous wave threshold currents as low as 4.5mA and 59% surface-emitting quantum efficiencies are achieved on devices with 2μm-wide aperture, 420μm-long cavity.

The laser structure, as shown in Fig.1, is a single quantum well graded-index separate-confinement heterojunction (SQW-GRINSCH) grown by metalorganic chemical vapor deposition (MOCVD) with the following layers : a 10000Å n-GaAs buffer ($2x10^{18}$ $cm^{-3}$) layer, a 10000Å n-$Al_{0.6}Ga_{0.4}As$ bottom n-cladding ($5x10^{17}cm^{-3}$) layer, a 500Å n-$Al_xGa_{1-x}As$ graded layer with x varying from 0.6 to 1.0, a 1000Å n-type AlAs layer, a 500Å n-$Al_xGa_{1-x}As$ graded layer with x varying from 1.0 to 0.6, a 500Å n-$Al_{0.6}Ga_{0.4}As$, a 1500Å n-$Al_xGa_{1-x}As$ graded layer with x varying from 0.6 to 0.2, a 120Å GaAs layer, a 80Å $In_{0.24}Ga_{0.76}As$ quantum well layer, a 120Å GaAs layer, a top 1500Å $Al_xGa_{1-x}As$ graded layer, a 500Å p-$Al_{0.6}Ga_{0.4}As$, a 500Å GaAs etch-stop layer, a 500Å p-$Al_{0.6}Ga_{0.4}As$, a 500Å p-$Al_xGa_{1-x}As$ graded layer with x varying from 0.6 to 1.0, a 1000Å p-type AlAs layer, a 500Å p-$Al_xGa_{1-x}As$ graded layer with x varying from 1.0 to 0.6, a 10000Å p-$Al_{0.6}Ga_{0.4}As$ top p-cladding ($5x10^{17}cm^{-3}$) layer, and then a 1000Å GaAs cap layer. The AlAs layers above and below waveguide and active region are designed to form current constriction after oxidation.

Device processing starts with lithographic patterning of 50μm wide stripes to define and etch the output mirrors. The GaAs cap layer is removed by a selective etchant ( Citric Acid : $H_2O_2$ / 4:1), and the top AlGaAs cladding layer and AlAs layer are selectively etched in a HF solution down to the GaAs stop layer. The sample is then coated with 1000Å of PECVD $Si_3N_4$ and patterned with 20μm-wide mesa stripes oriented perpendicular to the output mirror stripes. The

sample is then etched in a solution of $H_2SO_4$:$H_2O_2$:$H_2O$ (1:8:160) to expose both top and bottom AlAs layers for oxidation. The oxidation is performed in a furnace at 400°C in which a $H_2O$-vapor-saturated $N_2$ is flowing. Normally, the oxidation rate of p-type AlAs is faster than that of n-type AlAs.[11] An SEM picture of the oxidized mesa cross-section is shown in Fig.2a. The aperture defined by top AlAs oxide layer is about 2μm after 8minutes oxidation. This is also shown in Fig.2b which is the top view of the mesa under optical microscope. After oxidation, the sample is fully covered by $Si_3N_4$ using PECVD, and 10μm-wide stripes are opened on the mesa top. Then, the sample is patterned with 500μmX100μm windows on the mesa top where Ti/Pt/Au is e-beam deposited as p-contact. Now, the sample is ready to be patterned for dry etching. A single layer of photoresist is chosen as mask for IBE of the 45° deflecting mirrors. The processing of IBE technique was described somewhere else.[8] After the sample is lapped down to about 100μm, AuGe/Ni/Au is e-beam deposited on the bottom of the sample as n-contact. Finally, the sample is alloyed at 400°C for 40 seconds.

FCSEL's, consisting of a horizontal output mirror, an internal 45° deflector, and a cleaved mirror, are schematically shown in Fig.3a. An SEM picture in Fig.3b shows a wet etched output mirror and an ion beam etched 45° deflector.

The devices are tested under continuous wave (CW) operation at room temperature without a heat sink. The typical L-I and V-I curves for devices with 2μm-wide aperture, 420μm-long cavity are shown in Fig.4. Threshold currents of 6mA are obtained with external quantum efficiencies of 44% (0.55W/A) and 31% (0.38W/A) for edge emission and surface emission, respectively, which result in total quantum efficiency of 75%. A laser spectrum at 9mA pumping current, as shown in the inset of Fig.4, exhibits single mode operation of the native-oxide

confined narrow-stripe lasers. For comparison, the native-oxide confined narrow-stripe edge-emitting lasers with both-side cleaved mirrors made from the same material have the cw threshold currents of 6mA and total quantum efficiencies of 82%. The pulsed (500ns width, 10kHz repetition rate) threshold current density of broad area lasers (100μm-wide stripes) made from the same material is 70A/cm$^2$ for a 1500μm cavity length. As shown in Fig.4, the quantum efficiency for edge emission is higher than that for surface emission, which suggests that the effective reflectivity at the folded-cavity end is higher than that of cleaved facet (R=0.32). This may result from an uncontrolled change in the reflectivity of the output mirror or from an interference effect between the oxide layer and the top surface at the folded cavity end of the structure. The characteristic temperature ($T_0$) of FCSEL's is about 136K in the temperature range from 0°C to 50°C at CW operation.

To date, 8mA is the best reported threshold current for InGaAs/GaAs FCSEL's by C.P.Chao *et al*[6] on ridge waveguide structure, and N.Frateschi *et al*[7] in a buried structure on a non-planar substrate, with surface-emitting quantum efficiencies of 22% and 10%, respectively. These two structures are essentially HR/AR or HR/HR coated devices owing to utilization of high reflectivity epitaxial Bragg reflectors. The FCSEL's without Bragg reflectors we present here demonstrate threshold current of 6mA with surface-emitting quantum efficiency of 31%. By applying 90% HR dielectric coating on the cleaved facet of the above devices, a threshold current of 4.5mA with 59% surface-emitting quantum efficiency is obtained, as shown in Fig.5. To our best knowledge, this is the lowest threshold current reported to date for FCSEL's.

In conclusion, we report here the fabrication and characteristics of the lowest threshold current folded-cavity surface-emitting InGaAs/GaAs lasers. The devices are fabricated into narrow-stripes confined by AlAs native-oxide. Low temperature (400°C) selective wet oxidation and ion-beam-etching techniques are used to fabricate the native-oxide confined narrow-stripes and the internal 45° deflectors, respectively. Continuous wave threshold currents as low as 6mA and 31% surface-emitting quantum efficiencies are achieved on the devices with 2μm-wide aperture, 420μm-long cavity. The characteristic temperature of 136K is obtained for this kind of structure. With HR coated on the cleaved facet, the threshold current of 4.5mA and 59% surface-emitting quantum efficiency are achieved.

# ACKNOWLEDGMENT

This work is supported by ARPA through the Ultra program, and by the Office of Naval Research.

# References


1. N.C.Frateschi, H.Zhao, J.Elliot, S.Siala, M.Govindarajan, R.N.Nottenburg, and P.D.Dapkus, "Three-terminal bistable low-threshold strained InGaAs/GaAs laser grown on structured substrates for digital modulation", *IEEE Photon. Technol. Lett.*, vol.5, p.275,1993.

2. F.R.Gfleller, P.Buchmann, K.Dätwyler, J.P.Reithmaier, P.Vettiger, D.J.Webb, "50mW CW operated single-mode surface-emitting AlGaAs lasers with 45° total reflection mirrors", *IEEE Photon. Technol. Lett.*, vol.4, p.698,1992.

3. S.S.Ou, M.Jansen, J.J.Yang, M. Sergant, "High-power cw operation of GaAs/AlGaAs surface-emitting lasers mounted in the junction-up configuration". *Appl. Phys. Lett.*, 59, p.1037 (1991).

4. D.W.Nam, R.G.Waarts, D.F.Welch, D.R.Scifres, "Operating characteristics of High continuous power (50W) two-dimensional surface-emitting laser arrays", *IEEE Photon. Technol. Lett.*, vol.5, p.281,1993.

5. J.P.Donnelly, W.D.Goodhue, C.A.Wang, R.J.Bailey, G.A.Lincoln, G.D.Johnson, L.J.Missaggia, J.N.Walpole, "CW operation of monolithic arrays of surface-emitting folded-cavity InGaAs/AlGaAs diode lasers". *IEEE Photon. Technol. Lett.*, vol.5, p.747,1993.

6. C.P.Chao, K.K.Law, J.L.Merz, "Design and fabrication of ridge waveguide folded-cavity in-plane surface-emitting lasers". *IEEE Photon. Technol. Lett.*, vol.4, p.223, 1992.

7. N.C.Frateschi, P.D.Dapkus, S.S.Ou, J.J.Yang, M.Jansen, "Low threshold InGaAs/GaAs 45° folded-cavity surface-emitting lasers grown on structured substrates". *IEEE Photon. Technol. Lett.*, vol.5, p.741, 1993.

8 Y.Cheng, G.M.Yang, P.D.Dapkus, "Folded-Cavity Surface-Emitting InGaAs/GaAs Lasers with Low Threshold Current Density and High Efficiency". accepted for publication on *IEEE Photon. Technol. Lett.*.

9. C.P.Chao, G.J.Shiau, S.R.Forrest, "1.3μm Wavelength, InGaAsP-InP Folded-Cavity Surface-Emitting Lasers Grown by Gas-Source Molecular-Beam Epitaxy". *IEEE Photon. Technol. Lett.*, vol.6, p.1406, 1994.

10 S.A.Maranowski, A.R.Sugg, E.I.Chen, N.Holonyak,Jr., "Native oxide top- and bottom-confined narrow stripe p-n AlGaAs/GaAs/InGaAs quantum well heterostructure laser", *Appl. Phys. Lett.*, 63, p.1660 (1993).

11. F.A.Kish, S.A.Maranowski, G.E.Höfler, N.Holonyak,Jr., S.J.Caracci, J.M.Dallesasse, and K.C.Hsieh, "Dependence on doping type (p/n) of the water vapor oxidation of high-gap $Al_xGa_{1-x}As$", *Appl. Phys. Lett.*, 60, 3165(1994).

# Figure Captions

Fig. 1, The schematic of the conduction band of laser structure with AlAs layers above and below the waveguide region for oxidation.

Fig. 2a, An SEM picture of the oxidized mesa cross-section. The aperture defined by top AlAs oxide layer is about 2μm.

Fig.2b, The top view of the oxidized mesa under optical microscope.

Fig.3a, The schematic of a device for folded-cavity surface-emitting lasers.

Fig.3b, An SEM picture of a FCSEL with wet etched output mirror and ion beam etched 45° deflector.

Fig.4, The typical L-I and V-I curves for devices with 2μm-wide aperture, 420μm-long cavity. The inset shows a laser spectrum at 9mA.

Fig.5, The L-I curves for the FCSEL's with cleaved facet HR coated.

Fig.1

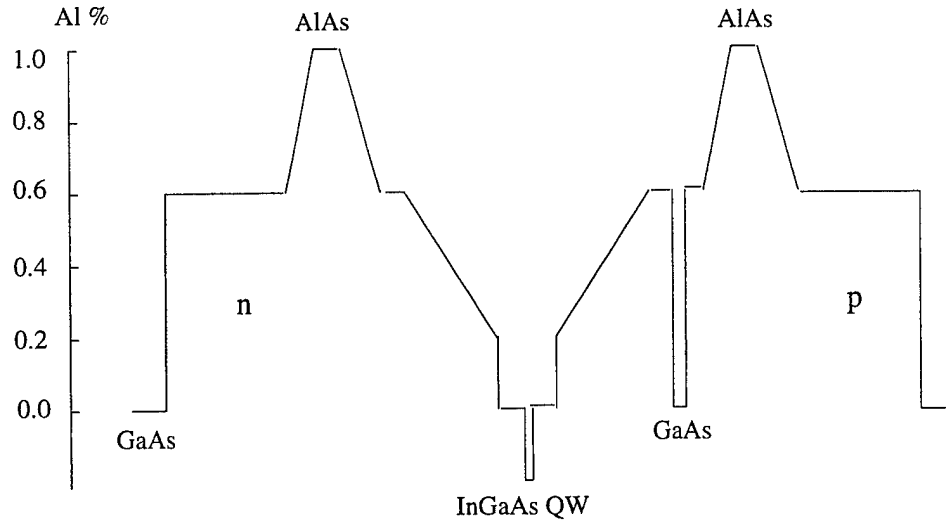


Fig.2a

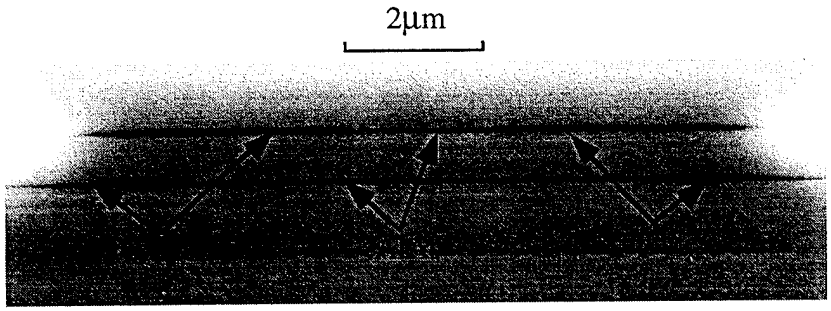


Fig.2b

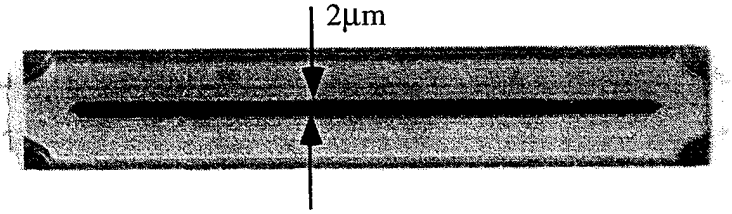

Fig.3a

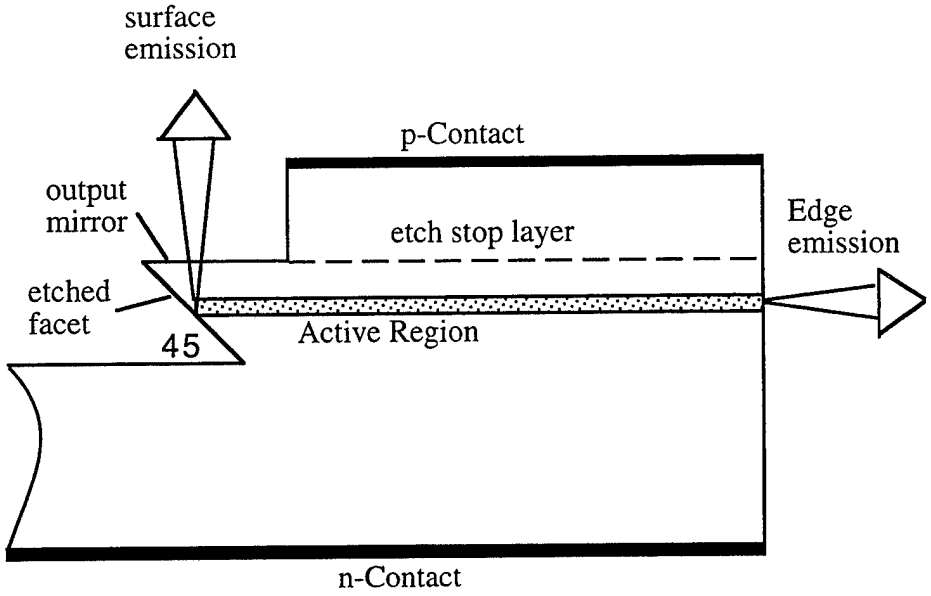
surface
emission
p-Contact
output
mirror
etch stop layer
Edge
emission
etched
facet
45
Active Region
n-Contact

Fig. 3b

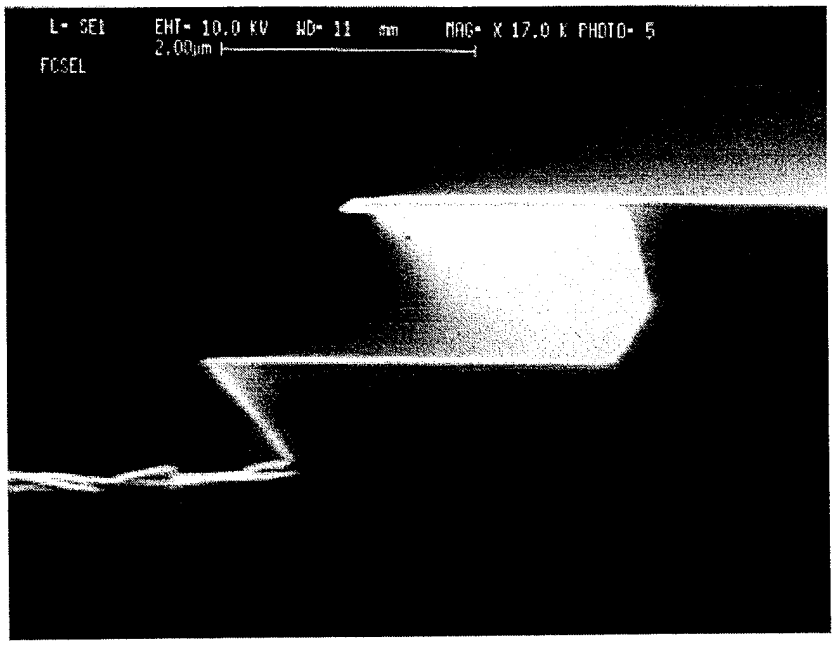
L= SEI
EHT= 10.0 KV
WD= 11 mm
MAG= X 17.0 K PHOTO= 5
2.00µm
FOSEL

Fig.4

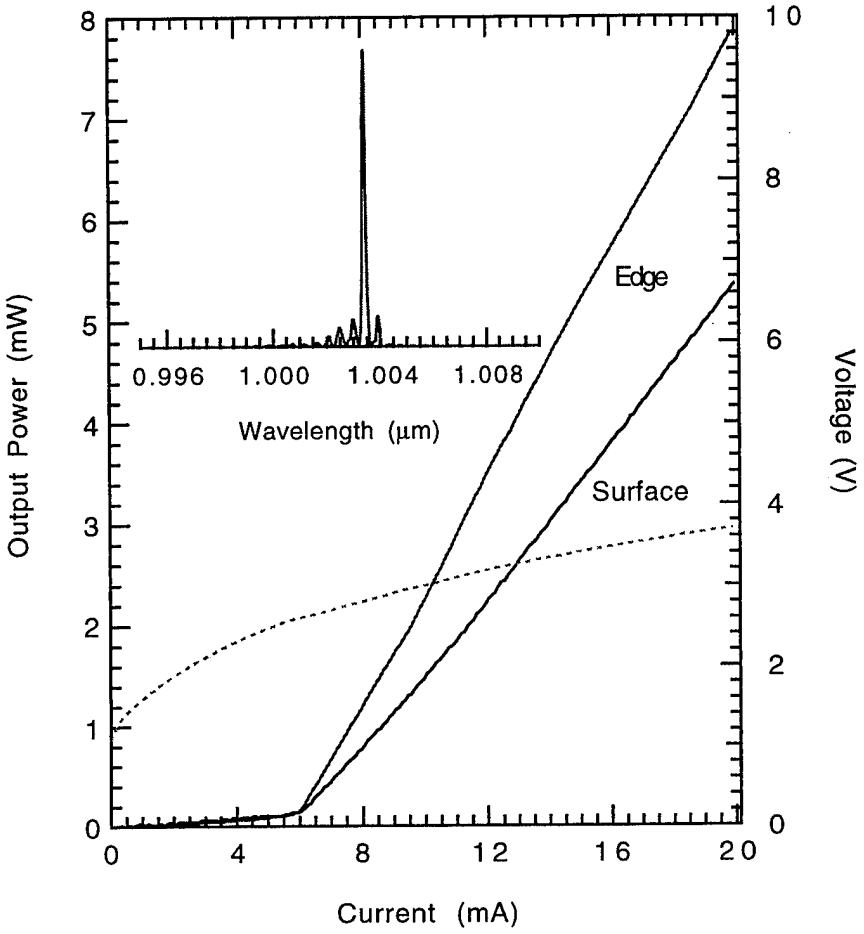
Output Power (mW)
Voltage (V)
Current (mA)
Edge
Surface
Wavelength (μm)
0.996
1.000
1.004
1.008
0
1
2
3
4
5
6
7
8
0
2
4
6
8
10
0
4
8
12
16
20

Fig.5

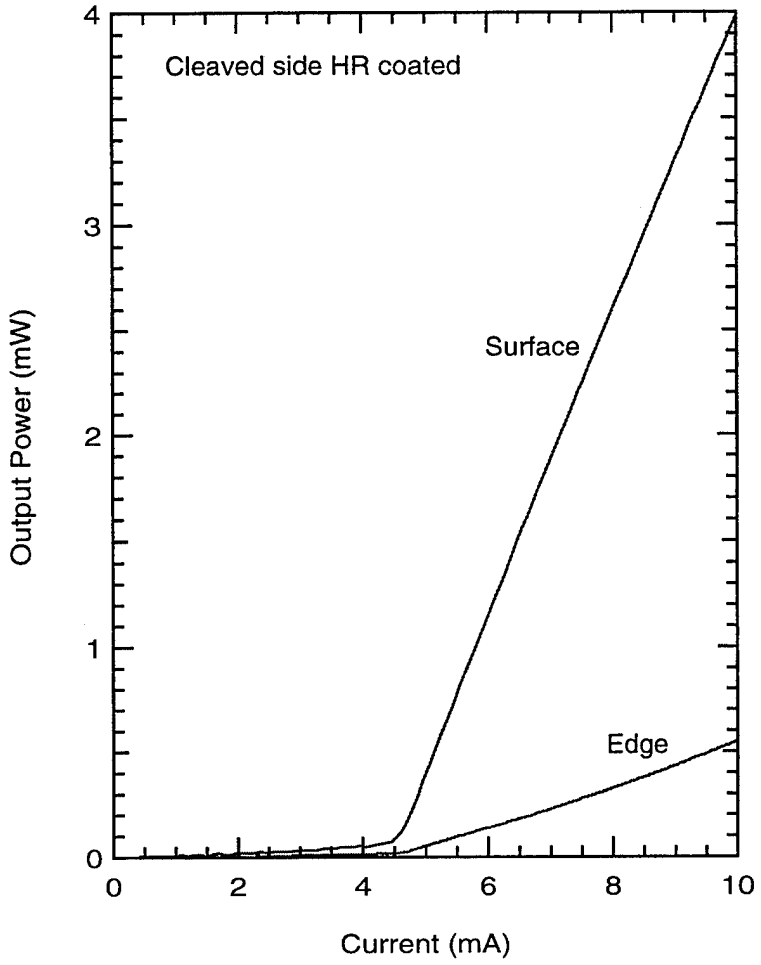
Cleaved side HR coated
Surface
Edge
Output Power (mW)
Current (mA)
0
1
2
3
4
0
2
4
6
8
10

Fig.7

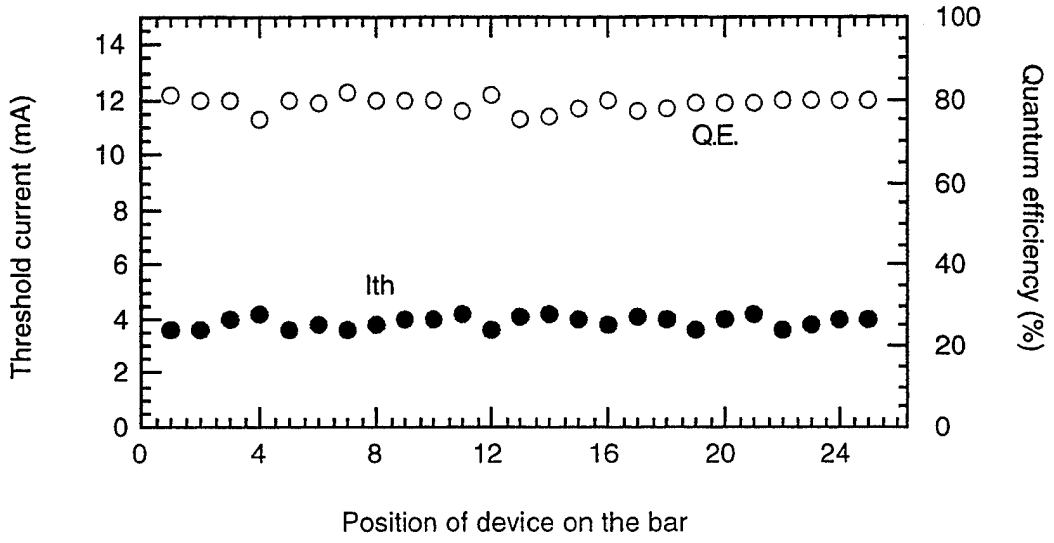
Threshold current (mA)
Quantum efficiency (%)
Q.E.
Ith
Position of device on the bar
0
2
4
6
8
10
12
14
0
20
40
60
80
100
0
4
8
12
16
20
24

## 2.2 VERTICAL CAVITY SURFACE EMITTING LASERS (VCSEL's)

# Microcavity effects on the spontaneous emission from InGaAs/GaAs quantum wells

G. M. Yang, M. H. MacDougal, H. Zhao,[a] and P. D. Dapkus[b]
*Department of Electrical Engineering/Electrophysics, University of Southern California, Los Angeles, California 90089-0483*

(Received 1 November 1994; accepted for publication 13 June 1994)

The spontaneous emission from an InGaAs/GaAs single-quantum well surrounded by AlAs/GaAs distributed Bragg reflectors (DBR) under the near-resonance condition between the exciton level and the confined optical mode is investigated. Under such conditions, on-axis spontaneous emission enhancement at the cavity resonant wavelength is clearly identified. The strength and character of the interaction of the exciton with the confined optical mode is determined by the dependence of photoluminescence spectra on the reflectivity of the DBR. Temperature dependence of the enhanced spontaneous emission shows the cavity resonant wavelength shifts at 0.85 Å/°C around room temperature. An increase of emission intensity at the cavity resonant wavelength with increasing temperature is also observed, which can be related to the increase of the interaction between excitonic emission and cavity mode. 

## I. INTRODUCTION

Quantum wells (QWs) embedded in microcavities have recently been employed to investigate both fundamental and applied aspects of photonics.[1–6] In a semiconductor microcavity, a high intensity optical field is confined by distributed Bragg reflectors (DBRs) composed of λ/4 multilayers. Reduction in the available photon modes in a direction perpendicular to the cavity results in an increase in the emission into allowed cavity modes. Experimental studies on the alteration of spontaneous emission characteristics in various systems have been carried out.[7–13] Much attention has been concentrated on making use of the microcavity effect in semiconductor optical devices to improve device performance in several respects, such as an extreme reduction of a threshold current for the onset of lasing, the suppression of noise, and low divergence of output beams. However, little attention has been given to the reflectivity dependence of spontaneous emission.

The thermal characteristics of vertical-cavity surface-emitting lasers (VCSELs) are uniquely determined by the relative spectral positions of the cavity resonance and laser gain. The lasing wavelength for a VCSEL is determined by the optical properties of the mirrors and the cavity. Both the gain spectrum and the cavity resonance shift to longer wavelengths, but at different rates with increasing temperature.[14–17] The temperature dependence of the cavity resonance is determined by the temperature dependence of the refractive indices, while the gain spectrum has the temperature dependence of the energy band gap. An understanding of the relationship between the gain spectrum and the cavity resonance is important in order to achieve low room-temperature thresholds, to minimize thermal quenching, and to improve high-temperature performance.

In this work, we report systematic experimental results on the reflectivity dependence of the spontaneous emission enhancement through the continuous tuning of the reflectivity, under a near resonance condition between the exciton level and the confined optical mode. This is similar to the detuning condition of a VCSEL taking into account the difference of the temperature dependence of the cavity mode and QW exciton level.[3] We also detune the interaction between the excitonic emission and cavity resonance mode by changing the temperature, which makes the emission intensity of the cavity resonance mode increase with increasing temperature. The thermal changes of the cavity resonant wavelength and the QW wavelength are determined at the same time by observing the peaks in the photoluminescence (PL) spectra.

## II. EXPERIMENTS

The vertical microcavity structure is grown by metalorganic chemical vapor deposition. The top and bottom DBRs consist of 15 pairs and 16 pairs of λ/4 AlAs/GaAs alternating layers, respectively. The 1-λ cavity consists of GaAs spacers and an 80 Å $In_{0.17}Ga_{0.83}As$ single QW at the center of the cavity. *In situ* laser reflectometry is used for thickness control of the AlAs and GaAs layers used in this structure.[18] The calculated reflectivities of bottom and top DBRs seen from the QW side are 99.1% and 99.4%, respectively. The wavelength of cavity mode is about 100 Å longer than the QW wavelength at room temperature. Because the wavelengths are distinguishable from each other, this system is ideal for measuring the temperature dependence of the QW wavelength and cavity resonant wavelength simultaneously.

In order to study DBR effects on the QW spontaneous emission clearly, the reflectivity of top DBR is continuously tuned using the selective etching of the quarter-wave stacks

[a]Present address: SDL, Inc., 80 Rose Orchard Way, San Jose, CA 95134-1365.
[b]Electronic mail: dapkus@mizar.usc.edu

 0021-8979/95/78(6)/3605/5/$6.00  

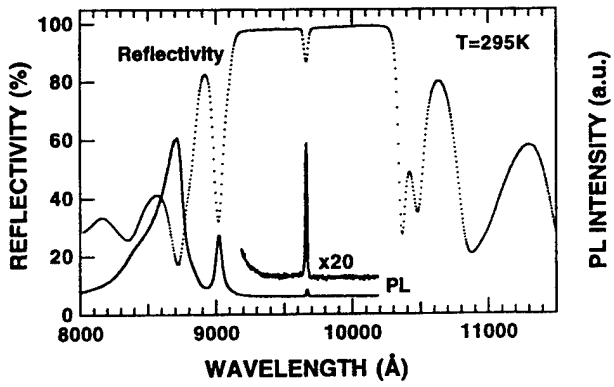


FIG. 1. Reflectivity and spontaneous emission spectra of the as-grown sample measured at room temperature. Photoluminescence was recorded with a solid angle of $\sim 3\times10^{-2}\ \pi$ measured from the normal to the epitaxial surface.

of the upper DBR. The GaAs and AlAs in DBR stacks are selectively etched using a 4:1 solution of citric acid/$H_2O_2$ and a buffered oxide etchant, respectively. After each pair is etched, the structure is characterized using PL and reflectivity measurements. Reflectivity measurements are performed using a Cary 2300 spectrophotometer in the reflection mode. The PL perpendicular to the sample surface is recorded with an acceptance solid angle of $\sim 3\times10^{-2}\pi$. The PL spectra are excited with $Ar^+$ laser through the top mirror. Since the high-reflectivity zone is away from the wavelength of the incident light, the pump laser is only slightly reflected by the top DBR mirror.

## III. RESULTS AND DISCUSSION

### A. Reflectivity-dependent spontaneous emission

Figure 1 shows the measured reflectivity and the spontaneous emission spectra of the as-grown sample at room temperature. A strong influence of the DBR reflectivity on the PL is observed. At a wavelength of 9666 Å, a dip in the reflectivity is observed, indicating the resonance mode of the cavity. $\delta$-functionlike emission spectra with a linewidth of 15 Å occurs at the cavity resonant wavelength, with the spontaneous linewidth determined by a cavity quality factor, $Q$, of about 280. It is also interesting to note the influence of the cavity resonances on the spontaneous emission of carriers excited in the GaAs layers. The PL spectrum shows peaks which coincide with the cavity transmission peaks.

The measured PL spectra at room temperature corresponding to different numbers of top DBR pairs are shown in Fig. 2. Since GaAs layers in the DBR absorb the excitation light, the spectral intensities for each condition cannot be compared with one another in an absolute sense. The spectral shapes do not change when the excitation intensity is varied from 50 (the detection limit) to 350 W/cm$^2$. The PL intensity increased linearly with the excitation intensity in this range, indicating that spontaneous emission is the dominant recombination process and stimulated emission is negligibly small. In the case of a top DBR with 15 pairs, a very sharp PL peak at 9666 Å is observed. As the number of top DBR pairs is decreased, another broad PL peak at a wavelength of 9565 Å

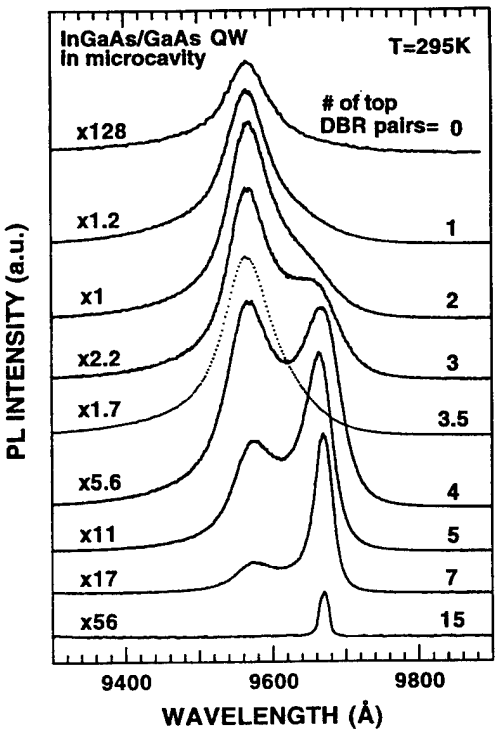


FIG. 2. Photoluminescence spectra measured at room temperature of microcavity corresponding to different numbers of top DBR pairs. The QW emission peak at 9565 Å and cavity resonance peak at 9666 Å are observed. In the case of 3.5 pairs DBR, AlAs is the topmost layer and phase matching condition is destroyed.

appears and becomes dominant. Finally, only the 9565 Å peak is seen in the structure without a cavity. This broad peak is the PL spontaneous emission of the InGaAs QW active layer without cavity resonance effects. The 9666 Å peak is related to the enhancement of the spontaneous emission of the InGaAs QW at the resonant wavelength of the cavity.

Figure 3 shows the measured reflectivity at room temperature corresponding to different numbers of top DBR pairs. Besides the resonance mode at 9666 Å, we observed an absorption-induced reflectance dip at 9565 Å due to the InGaAs QW, whose position is the same as that of its emission (see Fig. 2).[19] In particular, two dips occur in the reflectivity curve at room temperature in the structure with four pairs in the top DBR. In the structures with two or three pairs in the top DBR, the two dips cannot be resolved. However, with one pair in the top DBR, the broad and shallow dip centered at the resonant wavelength of the cavity is distinct from the QW absorption-related dip at 9565 Å. The dip at 9565 Å is still dominant in the structure without any top DBR, which consists of a bottom DBR and an active region. As the number of top DBR pairs decreases, the absorption-induced dip increases in strength in the reflectivity curve in the range of 7–3 pairs, and then weakens in the range of 2–0 pairs due to the decrease of cavity effect on QW absorption. Although the InGaAs active region is thin, optical absorption is enhanced, because of multiple reflection caused by the two DBR mirrors forming the vertical cavity. The cavity resonance dip becomes weak and broad as the number of top

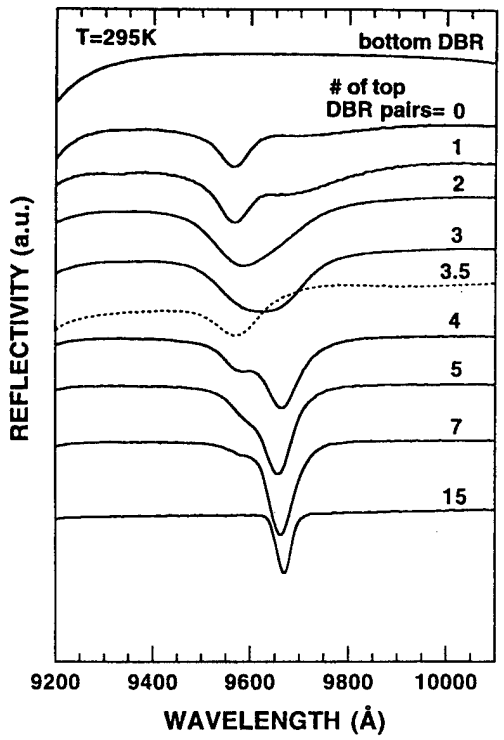


FIG. 3. Measured reflectivity spectra at room temperature of microcavity with different numbers of top DBR pairs when the wavelength detuning between QW wavelength and cavity mode wavelength is about 100 Å. In the case of 3.5 pairs DBR, AlAs is the topmost layer and phase matching condition is destroyed. The spectra are offset for clarity.

DBR pairs decreases, which is in a good agreement with theoretical results. This effect signifies that the 9565 Å dip is related to the interaction between the excitonic emission of InGaAs QW and cavity mode. Finally, the typical reflectivity curve of a DBR is observed after removing the cavity region below the top DBR.

To remove the cavity effects on InGaAs QW emission, the phase matching condition is intentionally destroyed by selective etching the GaAs layer on the top DBR. Thus, the topmost layer is AlAs. For proper phase matching, the phase of the final reflection should be equal to the phase of the previous reflection at the AlAs/GaAs interface (modulo $2\pi$). The dotted curves in Fig. 2 and Fig. 3 show the results of the structure with 3.5 pairs top DBR. In this structure, the photons reflected from the AlAs topmost layer/air interface and from the previous GaAs/AlAs interface are not phase-matched (modulo $\sim\pi/2$). Being exposed to $H_2O$ and air, the top AlAs layer is oxidized. Taking into account its refractive index of 1.55,[20] the oxidized AlAs has an optical thickness of $\sim\lambda/8$. The effect of the cavity has disappeared in PL spectrum as well as the reflectance spectrum. Only the QW spontaneous emission and absorption are observed in these curves.

In Fig. 4, we plot the experimentally determined enhancement factor in PL at the resonant wavelength as a function of the number of top DBR pairs, together with theoretical results. The modified vacuum field intensity $E^2$ in the resonance antinode position is calculated by simply assuming two lumped reflectors with a one wavelength thickness separation based on Ref. 21 and 22

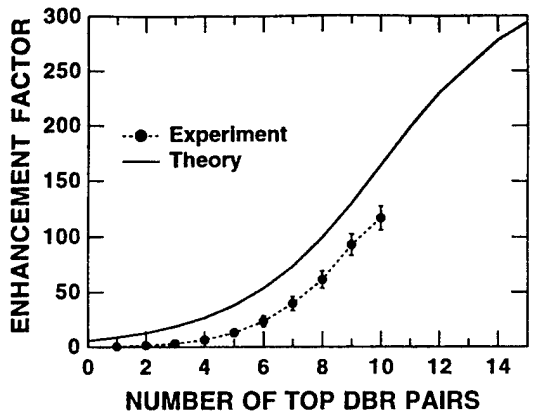


FIG. 4. Experimentally and theoretically determined spontaneous emission enhancement factor at the cavity resonant wavelength as a function of the number of top DBR pairs. The solid line is the theoretical fit and the dotted line is used as a guide for eyes.

$$\frac{E^2}{E_0^2}(\theta)=\frac{(1-R)[1+R+2\sqrt{R}\cos(2\pi\cos\theta)]}{(1-R)^2+4R\sin^2(2\pi\cos\theta)}, \tag{1}$$

$$\frac{E^2}{E_0^2}(\theta=0)=\frac{[1+\sqrt{R}]^2}{1-R}, \tag{2}$$

where it is assumed that the emission wavelength is coincident with the cavity resonant wavelength. $E_0^2$ is vacuum field intensity, $\theta$ is the angle in the cavity measured from the normal direction, and $R$ is the power reflectivity of DBRs. The on-axis emission ($\theta\approx 0$) is expected to exhibit a strong enhancement as $R\rightarrow 1$. The theoretically calculated curve is obtained by spatially integrating the spontaneous emission over the solid angle in the microcavity relative to free-space emission for each value of $R$. The variation of emission lifetime due to the cavity is not taken into account. The experimentally obtained enhancement factor is determined by fitting the line shape of QW emission and subtracting it from the measured on-axis PL spectrum to obtain the spectrum of cavity resonance emission. All spectra are first normalized to give the same QW emission intensity. Then, the ratio of resonance emission intensity to the QW emission intensity at the cavity resonant wavelength is plotted. Since most of excitation power is absorbed in the top mirror, QW emission cannot be detected in the structure when more than ten pairs are present in the top DBR, and the enhancement factor cannot be determined. The experimental data show that the resonant coupling of the excitonic emission with the cavity mode results in an enhancement of the oscillator strength of the spontaneous emission at the resonant wavelength by more than a factor of 100 when the top mirror has ten AlAs/GaAs pairs (which has an calculated reflectivity of $R\sim 96.7\%$). The expected enhancement with additional pairs results from a significant reduction in the number of available cavity modes and an increasing tendency to emit spontaneous emission into these modes. The experimental enhancement factor is

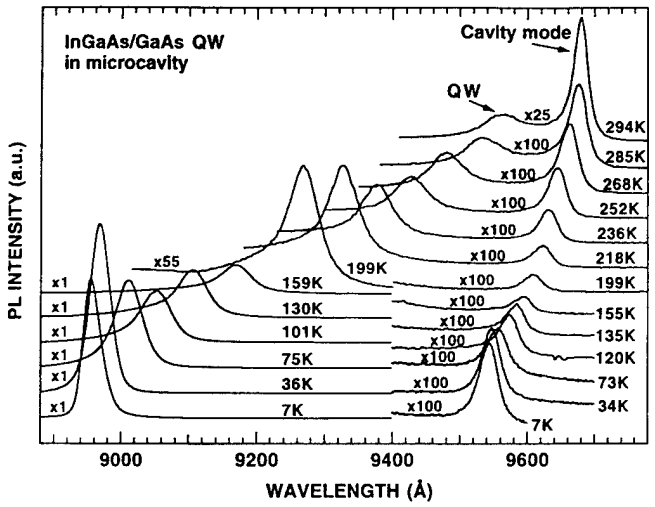


FIG. 5. Photoluminescence spectra of the cavity structure with 7 pairs in the top DBR as a function of temperature. Both the QW peak and the cavity mode peak are observed.

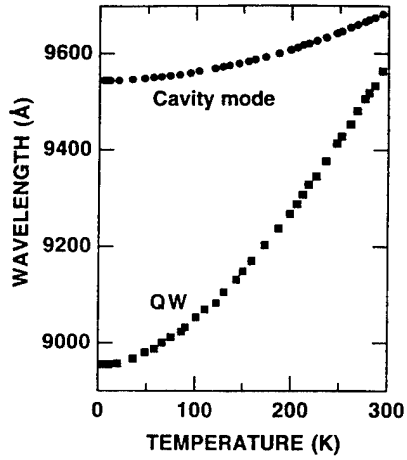


FIG. 6. Peak wavelengths of two photoluminescence emissions are plotted as a function of temperature. In the case of the QW peak, the exciton binding energy is not considered.

smaller than the calculated one, possibly due to the detuning of the emission wavelength from the cavity wavelength.[11]

### B. Influence of temperature on the enhanced spontaneous emission

Figure 5 shows the PL spectra of the cavity structure with seven pairs in the top DBR as a function of temperature. Both the QW peak and the cavity mode peak are observed. Both peaks shift to longer wavelengths with increasing temperature. However, the QW peak shifts faster than the cavity mode peak and, in fact, approaches the cavity mode peak. The QW peak broadens, and its intensity decreases abruptly with increasing temperature, which is due to the well-known phenomena of thermal broadening and thermal quenching. Meanwhile, the PL intensity of the cavity mode peak increases with increasing temperature above 150 K. This emission enhancement at the resonant wavelength is due to increased interaction between the excitonic emission and the cavity mode, which, in turn, is caused by the differing wavelength shifts with temperature. In the temperature range of 7–150 K, however, the PL intensity of the cavity mode peak decreases with increasing temperature. This phenomenon is not understood at present. The possibility of QW emission enhancement is low in this temperature range, since the QW peak wavelength is over 500 Å from the cavity mode wavelength on the shorter wavelength side.

In Fig. 6, the peak wavelengths of two PL emissions are plotted as a function of temperature. In the case of the QW peak, the exciton binding energy is not considered. The thermal variation of QW wavelength is ~3.3 Å/°C around room temperature, which is in good agreement with that of the lasing wavelength of edge-emitting lasers.[16] Meanwhile, the cavity mode wavelength shifts at 0.85 Å/°C around room temperature, which is in good agreement with the result determined using a thermally controlled reflectivity measurement in the cavity structure with a central layer of GaAs.[23] Also, this value agrees with the 0.84 Å/°C temperature coefficient measured from the temperature dependence of the lasing wavelength of InGaAs VCSEL with carrier confinement layers of $Al_{0.2}Ga_{0.8}As$.[24] But this shift is about 30% larger than the reported data of 0.6~0.65 Å/°C measured from the temperature dependence of the lasing wavelengths of GaAs VCSELs[15–17] and of InGaAs VCSELs with carrier confinement layers of $Al_{0.5}Ga_{0.5}As$.[3]

The difference in thermal variation of the cavity wavelength may originate from the different thermal variations of the refractive indices of the constituents in each structure. As well, the measurement of laser wavelength versus temperature is affected by local heating in the device.[15–17] There is inevitable error in measuring the device temperature by measuring the temperature of the device holder because excessive heating is produced in VCSELs by the high series resistance of the heterostructure DBRs and by the higher current densities at which VCSELs operate. The heat density is high and causes a large temperature gradient to build up. Lasing also occurs at high densities ($\sigma > 10^{12}$ cm$^{-2}$) of carriers in the QWs leading to enhanced many-body effects. The many-body effects can assist the lasing process by aligning spectral gain with longitudinal mode energy. As a consequence, the lasing threshold and wavelength are influenced by the many-body exchange correlation.[25] In this study, many-body effects and the temperature variation of sample due to the PL excitation light are negligible since the excitation intensity for PL is low (~100 W/cm$^2$ on the surface of sample).

## IV. CONCLUSIONS

We have studied microcavity effects on the spontaneous emission enhancement through the continuous tuning of the reflectivity. Quantum well absorption modulates PL emission and reflectivity even in the case of near resonance between the QW luminescence and mode energy (wavelength detuning $\Delta\lambda \approx 100$ Å from the cavity resonant wavelength at room temperature). The spontaneous emission enhancement factor is determined systematically by PL measurements. The room-temperature PL intensity of the on axis emission is 1–2 orders of magnitude higher for phase-matched cavity structure as compared to the structure without phase matching.

We also detune the interaction between the excitonic emission and cavity resonance mode by changing the temperature, which makes the emission intensity of the cavity resonance mode increase with increasing temperature. The optical mode shift with temperature was determined of 0.85 Å/°C by observing the temperature-dependence enhanced spontaneous emission at the cavity resonant wavelength instead of thermally controlled reflectivity measurement.

The work presented here quantifies the effects of a resonant cavity on the emission from a quantum well. The data clearly show that as the $Q$ of the cavity increases, the spontaneous emission normal to the surface is preferentially emitted in the allowed cavity mode. These data support the concepts that lead to the possibility of the "thresholdless" laser.[2]

## ACKNOWLEDGMENTS

One of the authors (G.M. Yang) is grateful for project sponsorship by Professor Byung-Doo Choe, Professor Hyung Jae Lee, and Professor Weon Guk Jeong. This work was partly supported by the Ministry of Science and Technology of Korea through SPRC at Jeonbuk National University and by the U. S. Office of Naval Research.

[1] C. Weisbuch, M. Nishioka, A. Ishikawa, and Y. Arakawa, Phys. Rev. Lett. **69**, 3314 (1992).
[2] Y. Yamamoto, F. Matinaga, S. Machida, A. Karlsson, J. Jacobson, G. Björk, and T. Mukai, J. Physique IV **3**, 39 (1993).
[3] D. B. Young, J. W. Scott, F. H. Peters, M. G. Peters, M. L. Majewski, B. J. Thibeault, S. W. Corzine, and L. A. Coldren, IEEE J. Quantum Electron. **29**, 2013 (1993).
[4] G. Shtengel, H. Temkin, T. Uchida, M. Kim, P. Brusenbach, and C. Parsons, Appl. Phys. Lett. **64**, 1062 (1994).
[5] D. G. Deppe and C. Lei, J. Appl. Phys. **70**, 3443 (1991).
[6] T. Baba, T. Hamano, F. Koyama, and K. Iga, IEEE J. Quantum Electron. **27**, 1347 (1991).
[7] K. Nishioka, K. Tanaka, T. Nakamura, Y. Lee, and M. Yamanishi, Appl. Phys. Lett. **63**, 2944 (1993).
[8] T. Yamauchi, Y. Arakawa, and M. Nishioka, Appl. Phys. Lett. **58**, 2339 (1991).
[9] E. F. Schubert, A. M. Vredenberg, N. E. J. Hunt, Y. H. Wong, P. C. Becker, J. M. Poate, D. C. Jacobson, L. C. Feldman, and G. J. Zydzik, Appl. Phys. Lett. **61**, 1381 (1992).
[10] A. M. Vredenberg, N. E. J. Hunt, E. F. Schubert, D. C. Jacobson, J. M. Poate, and G. J. Zydzik, Phys. Rev. Lett. **71**, 517 (1993).
[11] Y. Yamanoto, S. Machida, Y. Horikoshi, K. Igeta, and G. Björk, Opt. Commun. **80**, 337 (1991).
[12] N. E. Hunt, E. F Schubert, R. F. Kopf, D. L. Sivco, A. Y. Cho, and G. J. Zydzik, Appl. Phys. Lett. **63**, 2600 (1993).
[13] H. Cao, J. Jacobson, G. Björk, S. Pau, and Y. Yamamoto, Appl. Phys. Lett. **66**, 1107 (1995).
[14] B. Lu, P. Zhou, J. Cheng, K. J. Malloy, and J. C. Zolper, Appl. Phys. Lett. **65**, 1337 (1994).
[15] B. Tell, K. F. Brown-Goebeler, and R. E. Leibenguth, IEEE Photon. Tech. Lett. **5**, 637 (1993).
[16] B. Tell, K. F. Brown-Goebeler, R. E. Leibenguth, F. M. Baez, and Y. H. Lee, Appl. Phys. Lett. **60**, 683 (1992).
[17] G. Hasnain, K. Tai, L. Yang, Y. H. Wang, G. J. Fischer, J. D. Wynn, B. Weir, N. K. Dutta, and A. Y. Cho, IEEE J Quantum Electron. **27**, 1377 (1991).
[18] N. Frateschi, S. G. Hummel, and P. D. Dapkus, Electron. Lett. **27**, 155 (1991).
[19] A. Frey, G. Junk, and R. Hey, Appl. Phys. Lett. **64**, 2214 (1994).
[20] M. H. MacDougal, H. Zhao, P. D. Dapkus, M. Ziari, and W. H. Steier, Electron. Lett. **30**, 1147 (1994).
[21] K. H. Drexhage, in *Progress in Optics*, edited by E. Wolf (North-Holland, New York, 1974), Vol. 12, Chap. 4, p. 163.
[22] R. R. Chance, A. Prock, and R. Silbey, in *Advances in Chemical Physics*, edited by I. Prigogine and S. A. Rice (Wiley, New York, 1978), Vol. 37, Chap. 1, p. 1.
[23] J. Talgahader and J. S. Smith, Appl. Phys. Lett. **66**, 335 (1995).
[24] R. S. Geels, B. J. Thibeault, S. W. Corzine, J. W. Scott, and L. A. Coldren, IEEE J. Quantum Electron. **29**, 2977 (1993).
[25] P. L. Gourley, S. K. Lyo, T. M. Brennan, B. E. Hammons, C. F. Schaus, and S. Sun, Appl. Phys. Lett. **55**, 2698 (1989).

# Ultralow threshold current vertical-cavity surface-emitting lasers obtained with selective oxidation

Gye Mo Yang, Michael H. MacDougal, and P. Daniel Dapkus
Department of Electrical Engineering/Electrophysics,
University of Southern California,
Los Angeles, CA 90089-0483

*Indexing terms: Vertical cavity surface emitting lasers, Lasers*

## Abstract

We report InGaAs single quantum well vertical-cavity surface-emitting lasers with an intracavity p-contact fabricated by selective oxidation of AlAs and distributed Bragg reflectors composed of binary materials (AlAs/GaAs). A record low threshold current of 8.7 μA in ~3 μm square devices and of 140 μA in 10 μm square devices with maximum output powers over 1.2 mW are achieved.

Vertical-cavity surface-emitting lasers (VCSEL's) are promising for various applications in optical systems. VCSEL's fabricated by selective oxidation [1, 2] are attractive to achieve ultralow threshold currents [2-6]. Oxidized Al(Ga)As has been used as a current aperture under a top distributed Bragg reflector (DBR) mirror rather than proton implantation or pillar etching. The low refractive index (~1.55 [7]) of the wet thermal oxide films has also motivated their use in high refractive index contrast multilayer mirrors [7] and surface-emitting lasers based on such mirrors [4, 8]. Continuous-wave (CW) room-temperature threshold currents as low as 91 μA have been reported using the oxidized AlAs as a current aperture under a top dielectric DBR mirror [3]. However, low maximum output power and short lifetime of the order of minutes were observed in these structures due to the stress induced by the native-oxide layer [3]. Also, there are demonstrations of VCSEL's with oxidized AlGaAs as a buried current aperture within all-semiconductor monolithic structures [5, 6], which exhibit thresholds as low as 350 μA with very high power conversion efficiency [6]. In this letter, we report ultralow threshold single quantum-well (QW) VCSEL's fabricated by selective oxidation from an all epitaxial structure with intracavity p-contact layers grown by metalorganic chemical vapor deposition. 10 μm square devices show threshold currents of 140 μA with maximum output powers over 1.2 mW. Approximately 3 μm square devices show a threshold current of 8.7 μA and a corresponding threshold current density of ~97 A/cm$^2$. This threshold is the lowest reported to date for a semiconductor laser.

The design of this structure is optimized for low thermal resistance by using DBR's composed completely of binary materials. Since the top DBR would produce a very high resistance and substantial Joule heating due to the abrupt interfaces, it is bypassed by using an intracavity p-contact. Fig.1 shows a schematic cross-section of the fabricated VCSEL's. The epitaxial structure is grown on a n$^+$-GaAs (100) substrate and consists of a 30-pair n-doped AlAs/GaAs quarter-wave DBR, an

AlGaAs/GaAs/InGaAs resonant cavity, p-doped contact layers, and a 22-pair undoped AlAs/GaAs quarter-wave DBR. The active region contains a single $In_{0.2}Ga_{0.8}As$ QW of thickness 80 Å with adjacent GaAs barriers of thickness 150 Å. The cladding layers are $Al_{0.22}Ga_{0.78}As$ whose thickness are adjusted to bring the total cavity thickness to one wavelength. The p-doped contact layers are formed from a 0.25 λ AlAs current constriction layer and a 0.75 λ GaAs intracavity contact layer. Two intermediate layers of heavily p-doped 150 Å $Al_{0.7}Ga_{0.3}As$ / 150 Å $Al_{0.22}Ga_{0.78}As$ are used between them, which is effective in reducing the electrical series resistance and the stress induced by oxidized AlAs current constriction layer.

After growth, the top DBR is selectively wet etched into both 14 μm and 5 μm square mesas down to the p-type GaAs contact layer. Then, 50 μm square mesas, whose centers coincide with the centers of the 14 and 5 μm mesas, are formed by wet chemical etching, stopping just below the active region to expose the AlAs so that it may be oxidized. Thick $SiN_x$ is deposited on the top DBR sidewalls to protect the AlAs layers in the top mirror during oxidation of the current apertures. Current flow apertures of 10 and ~3 μm squares are formed below the 14 and 5 μm square top mirrors, respectively, by selective oxidation as described previously [1, 2, 4, 7]. The refractive index is 1.55 in the oxidized region of the current constriction layer and 2.96 in the unoxidized region of the current constriction layer, and this lateral index step provides index guiding in the cavity. Ti/Au is the p-type contact, and AuSn is the n-type contact.

The characteristics of all VCSEL's were constant, showing no burn-in effects during testing. The CW room-temperature laser characteristics in Fig. 2 and 3 show extremely low threshold currents of 140 μA and 8.7 μA for 10 μm and ~3 μm square devices, respectively, measured without a heatsink. The threshold current density of <100 $A/cm^2$ for the 3 μm square device is slightly lower than of 140 $A/cm^2$ for the 10 μm square device, since the lasing wavelength of 980.37 nm for the 3 μm square

device (see inset in Fig. 3) is closer to the QW photoluminescence wavelength (977.5 nm) than that of 992.34 nm for the 10 μm square device (see inset in Fig. 2). This variation of the cavity resonant wavelength is caused by nonuniformity of deposition rates in our growth chamber. The device with 10 μm square active region shows a maximum output power over 1.2 mW, a slope efficiency of 25 %, and a maximum power conversion efficiency of 10 % at 0.5 mA. The threshold voltages are 1.75 and 6.2 V for 10 and 3 μm square devices, respectively. We expect improvements in device performance with further processing optimization. The 10 μm square laser operates in a single mode with 20 dB of transverse mode suppression up to 3 times threshold.

The yield of the 3 μm square devices was low but a few of these devices produced threshold currents below 18 μA. The lowest threshold observed is 8.7 μA (see Fig. 3). This device operates with a slope efficiency of 10 % and produces a maximum output power of 160 μW. The spectral emission from this device shows a continuous increase in the side mode suppression ratio. At 160 μW output power, the side mode suppression ratio is 18 dB. The continuous variation of characteristics is characteristic of the behavior expected for microcavity lasers in which there is efficient coupling of the spontaneous emission into the cavity mode [9-11].

In conclusion, we have demonstrated record low threshold current of 8.7 μA VCSEL's fabricated from an all epitaxial structure based on selective oxidation. In addition, we have obtained output power greater than 1 mW in devices with threshold currents as low as 140 μA.

*Acknowledgments:* One of us (G.M.Yang) is grateful to Dr. Byung-Doo Choe, Dr. Hyung Jae Lee, and Dr. Weon Guk Jeong for their continuous encouragements. This work was supported by the Office of Naval Research and the Ministry of Science and Technology of Korea through SPRC at Jeonbuk National University.

## References


1 DALLESASSE, J. M., HOLONYAK, JR., N., SUGG, A. R., RICHARD, T. A., and El-ZEIN, N.: 'Hydrolyzation oxidation of $Al_XGa_{1-X}As$-AlAs-GaAs quantum well heterostructures and superlattices', *Appl. Phys. Lett.*, 1990, **57**, (26), pp. 2844-2846

2 HUFFAKER, D. L., DEPPE, D. G., and KUMAR, K.: 'Native-oxide defined ring contact for low threshold vertical-cavity lasers', *Appl. Phys. Lett.*, 1994, **65**, (1), pp. 97-99

3 HUFFAKER, D. L., SHIN, J., and DEPPE, D. G.: 'Low threshold half-wave vertical-cavity lasers', *Electron. Lett.*, 1994, **30**, (23), pp. 1946-1947

4 MACDOUGAL, M. H., DAPKUS, P. D., PUDIKOV, V., ZHAO, H., and YANG, G. M.: 'Ultralow threshold current vertical-cavity surface-emitting lasers with AlAs oxide/GaAs distributed Bragg reflectors', *IEEE Photonics Technol. Lett.*, 1995, **7**, (3), pp. 229-231

5 CHOQUETTE, K. D., SCHNEIDER, JR., R. P., LEAR, K. L., and GEIB, K. M.: 'Low threshold voltage vertical-cavity lasers fabricated by selective oxidation', *Electron. Lett.*, 1994, **30**, (24), pp. 2043-2044

6 LEAR, K. L., CHOQUETTE, K. D., SCHNEIDER, JR., R. P., KILCOYNE, S. P., and GEIB, K. M.: 'Selectively oxidised vertical cavity surface emitting lasers with 50 % power conversion efficiency', *Electron. Lett.*, 1995, **31**, (3), pp. 208-209

7 MACDOUGAL, M. H., ZHAO, H., DAPKUS, P. D., ZIARI M., and STEIER, W. H.: 'Wide-bandwidth distributed Bragg reflectors using oxide/GaAs multilayers', *Electron. Lett.*, 1994, **30**, (14), pp. 1147-1149

8 RIES, M. J., RICHARD, T. A., MARANOWSKI, S. A., HOLONYAK, JR., N., and CHEN, E. I.: 'Photopumped room-temperature edge- and vertical-cavity operation of AlGaAs-GaAs-InGaAs quantum-well heterostructure lasers utilizing native oxide mirrors', *Appl. Phys. Lett.*, 1994, **65**, (6), pp. 740-742

9 YAMAMOTO, Y., MACHIDA, S., and BJÖRK, G.: 'Micro-cavity semiconductor lasers with controlled spontaneous emission', *Opt. Quantum Electron.*, 1992, **24**, pp. S215-S243

10 YOKOYAMA, H., NISHI, K., ANAN, T. NAMBU, Y., BRORSON, S. D., IPPEN, E. P., and SUZUKI, M.: 'Controlling spontaneous emission and threshold-less laser oscillation with optical microcavities' *Opt. Quantum Electron.*, 1992, **24**, pp. S245-S272

11 SHTENGEL, G., TEMKIN, H., UCHIDA, T., KIM, M., BRUSENBACH, P., and PARSONS, C.: 'Spontaneous emission factor and its scaling in vertical cavity surface emitting lasers', *Appl. Phys. Lett.*, 1994, **64**, (9), pp. 1062-1064

## Figure Captions

Fig. 1 Schematic cross section of VCSEL with a native-oxide constriction layer and binary material DBRs.

Fig. 2 Light output and voltage against current characteristics for 10 μm square VCSEL. The inset shows lasing spectra at 280 μA and 700 μA.

Fig. 3 Light output against current characteristic for approximately 3 μm square VCSEL. Lasing spectra are shown at 15 μA, 500 μA and 1.5 mA.

Fig.1

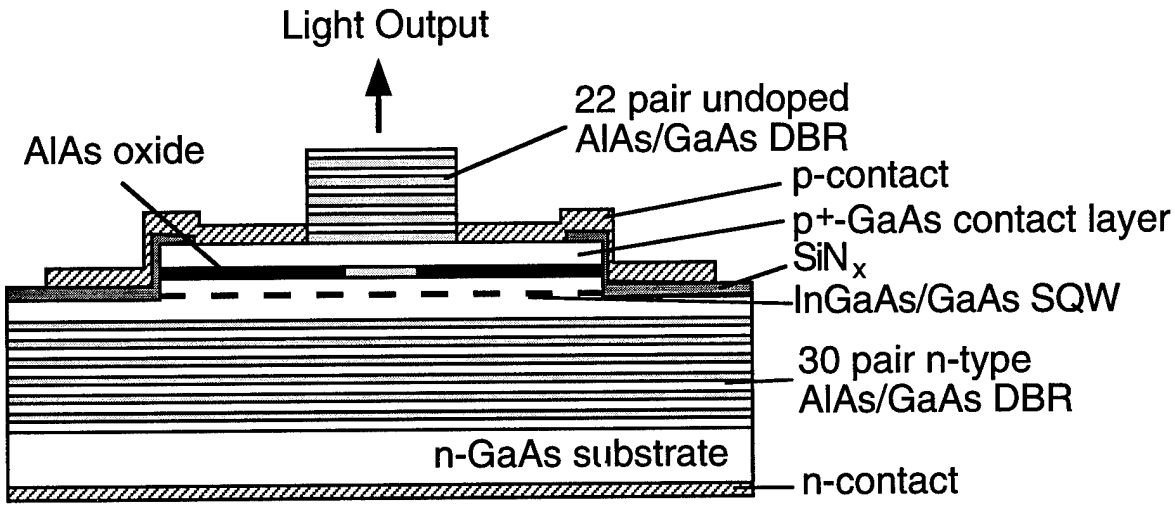
Light Output
22 pair undoped
AlAs/GaAs DBR
AlAs oxide
p-contact
p+-GaAs contact layer
$SiN_x$
InGaAs/GaAs SQW
30 pair n-type
AlAs/GaAs DBR
n-GaAs substrate
n-contact

Fig.2

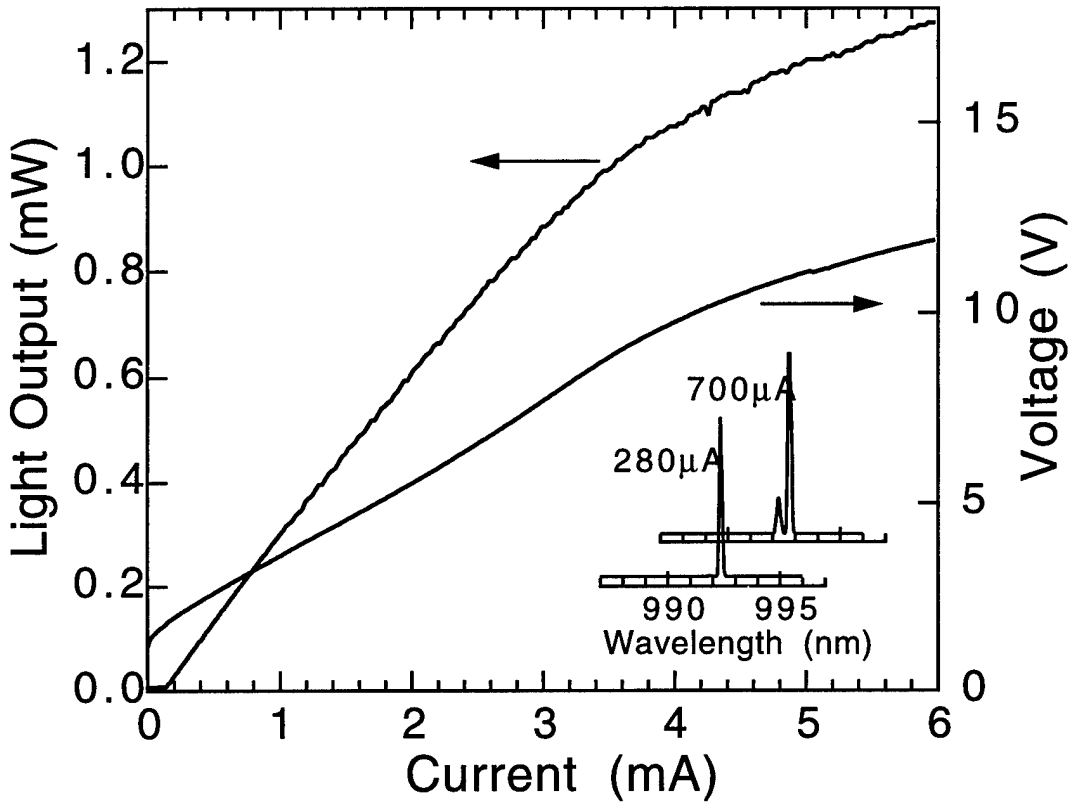
Light Output (mW)
1.2
1.0
0.8
0.6
0.4
0.2
0.0
0
1
2
3
4
5
6
Current (mA)
15
10
5
0
Voltage (V)
700μA
280μA
990
995
Wavelength (nm)

Fig.3

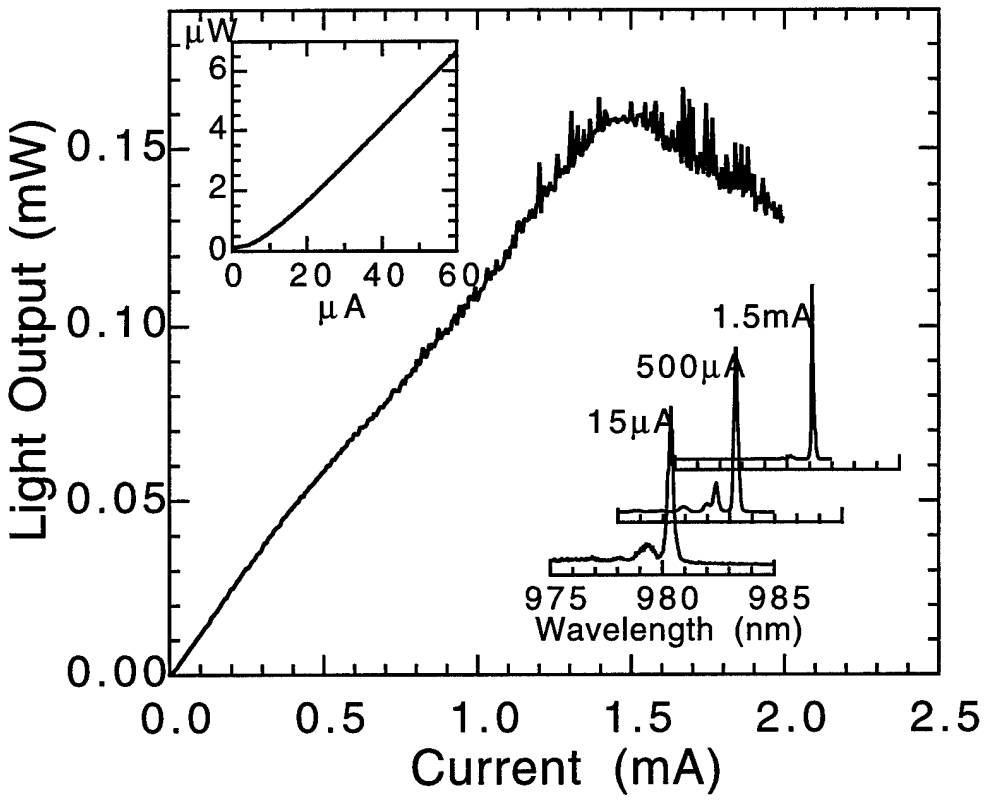
Light Output (mW)
0.00
0.05
0.10
0.15
0.0
0.5
1.0
1.5
2.0
2.5
Current (mA)
μW
6
4
2
0
0
20
40
60
μA
1.5mA
500μA
15μA
975
980
985
Wavelength (nm)

*Revised PTL MS #3849*

# Influence of mirror reflectivity on laser performance of very low threshold vertical-cavity surface-emitting lasers

Gye Mo Yang, Michael H. MacDougal, Vasily Pudikov, and P. Daniel Dapkus

*Department of Electrical Engineering/Electrophysics,*

*University of Southern California,*

*Los Angeles, CA 90089-0483*

## Abstract

The influence of mirror reflectivity on laser performance of InGaAs/GaAs vertical-cavity surface-emitting lasers fabricated by selective oxidation is investigated by the stepwise change of the number of pairs in top mirror stack after device fabrication. Devices with 18-pair stacks in the top mirror, which is the optimized number of pairs in this structure, show an output power over 1.9 mW and a slope efficiency of 55 % while maintaining a low threshold current of 212 μA. The analysis of the threshold current and differential efficiency related to mirror reflectivity shows an internal quantum efficiency of 95 %, an internal round-trip loss of 0.07 %, and a transparency current density of 71 A/cm$^2$.

Vertical-cavity surface-emitting lasers (VCSEL's) fabricated by selective oxidation are attractive to achieve ultralow threshold current and/or high external efficiency [1-4]. Oxidized Al(Ga)As has been used as a current aperture under a top DBR mirror or as a component of high refractive index contrast multilayers mirrors. Recently, there has also been an interest in measurements of some of the basic laser parameters needed for realistic modeling of VCSEL's [5, 6]. It is, thus, useful to vary the reflectivity of at least one mirror in order to determine the internal parameters of VCSEL [6]. In this paper, we report experimental results on the reflectivity dependence of the laser light-current characteristics for InGaAs single quantum well (SQW) VCSEL fabricated by selective oxidation from all epitaxial structure. By employing an intracavity contact to the p-layer, we are able to vary mirror losses by directly changing the number of pairs in distributed Bragg reflector (DBR) mirror in a low threshold VCSEL.

A schematic cross-section of the fabricated VCSEL's is shown in Fig. 1. The epitaxial structure grown by metalorganic chemical vapor deposition (MOCVD) consists of a 30-pair n-doped AlAs/GaAs quarter-wave DBR, an $Al_{0.22}Ga_{0.78}As/GaAs/In_{0.2}Ga_{0.8}As$ resonant $\lambda$-cavity, p-doped contact layers, and a 22-pair undoped AlAs/GaAs quarter-wave DBR. The p-doped contact layers are formed from a 0.25 $\lambda$ AlAs current constriction layer and a 0.75 $\lambda$ GaAs intracavity contact layer. After growth, the top DBR is selectively wet etched into 14 μm square mesas down to the p-type GaAs contact layer. Then, 50 μm square mesas, whose centers coincide with the centers of the 14 μm mesas, are formed by wet chemical etching. Current flow apertures of 10x10 $\mu m^2$ are formed below the 14 μm square top mirrors by selective oxidation [1-3].

This is a good device structure for studying the reflectivity-dependent laser characteristics because the top DBR is composed of binary materials (AlAs/GaAs) with abrupt interfaces and can be selectively removed one pair at a time. There are

also no changes in the current-voltage characteristics caused by reducing the number of top pairs owing to the use an intra-cavity p-contact. After photoresist is applied to open a window on the top mirror, the GaAs and AlAs in DBR stack are selectively etched using 4 : 1 solution of citric acid/$H_2O_2$ and 1 : 7 Buffered HF, respectively. After each pair is etched, the continuous-wave light-current curves of VCSEL are taken at room temperature. The threshold current and the light output slope efficiency through the top mirror are obtained for each value of the reflectivity of top mirror.

Fig. 2 shows the light-current curves for different numbers of pairs in the top DBR. The threshold current for 22-pair DBR is as low as 143 μA and corresponding threshold current density of 143 A/cm$^2$. As the mirror reflectivity is reduced, the output coupling from the cavity is increased, resulting in a higher external quantum efficiency. However, reducing the reflectivity also increases the total loss in the cavity tending to increase the threshold current. For very high mirror reflectivities, when the number of pairs in the top DBR is in the range of 18-22, the internal loss is dominant, so a decrease in mirror reflectivity results in very little change in the threshold current. The device with 18-pair stacks in the mirror shows an output power over 1.9 mW while maintaining a low threshold current of 212 μA. A slope efficiency of 55 % and a maximum power conversion efficiency of 16 % are achieved in this device. A further decrease in reflectivity (in the case of 16 and 15 pairs) results in an increase in threshold current and a decrease in differential efficiency. Increased drive current causes a temperature rise that shifts the gain peak causing a mismatch between the gain peak and the cavity mode. The temperature rise also lowers the carrier confinement in the QW. Finally, the device no longer lases because the mirror loss is too high and the gain at the cavity mode is too low to support laser operation.

We have measured the effect of temperature change on the threshold in a device with 22 pairs in the top DBR and found that a minimum threshold occurs around

room temperature where the cavity mode matches the gain peak. Also the emission wavelength increases quadratically with injection current. The change of wavelength up to 500 μA is approximately 0.04 nm, indicating that the thermal effects due to electrical resistance are quite small in this range.

In Fig. 3, we plot the inverse external efficiency as a function of $1/\ln(1/R)$, where $R=(R_tR_b)^{1/2}$ is the mean power reflectivity. $R_t$ and $R_b$ is the top and bottom mirror reflectivities, respectively. The external quantum efficiency for light coming out the top mirror, $\eta_d^t$, is measured just above the threshold current in each curve shown in Fig. 2 and the reflectivity for each structure is calculated using the transfer matrix method [7]. To obtain the external efficiency for total emission, $\eta_d$, $\eta_d^t$ is corrected by the power emitted through the bottom Bragg mirror using the following relation;

$$\eta_d^t = \eta_d \frac{(1-R_t)}{(1-R_t)+(1-R_b)\sqrt{\frac{R_t}{R_b}}} \qquad (1)$$

The reflectivity of the bottom mirror including 30 pairs DBR and calibration layers is about 99.986 % in the presence of the bottom metal contact. Layer thicknesses are determined to an accuracy of better than 2 % using in-situ laser reflectometry as a growth monitoring tool in our MOCVD reactor [8]. This error in layer thicknesses results in a very small change of DBR reflectivity of approximately 0.02 % at the lasing wavelength. For each mirror reflectivity, the threshold gain, $g_{th}$, is determined via [5]

$$\Gamma L_g g_{th} \xi = L + \ln(1/R) \qquad (2)$$

where Γ is the lateral confinement factor, $L_g$ is the total gain thickness, ξ is the gain enhancement factor due to the presence of the electric field standing wave in the cavity [9], and L is the round-trip loss. In the VCSEL, the light wave is traveling in an anisotropic region containing many different layers with various doping concentrations and penetrates a finite length into the DBR mirror region where

further scattering losses, diffraction losses, and absorption losses may occur. Therefore, the total loss is bundled into the term L. Then, the external quantum efficiency can be calculated using

$$\eta_d = \eta_i \frac{\ln(1/R)}{L + \ln(1/R)} \qquad (3)$$

where $\eta_i$ is the internal quantum efficiency.

We fit the data in Fig. 3 with $\eta_i$=0.95 and L=0.0007 in the range of 18-22 pairs in the top DBR to eliminate thermal effects on the efficiency, as discussed above. Approximately, we can write L as $L_{eff}\alpha_i$, where $L_{eff}$ is the effective cavity length, equal to the physical length of resonant cavity plus penetration depth into bottom and top mirrors and $\alpha_i$ is the internal loss. Using the relations obtained in Ref. 10, we calculate $L_{eff}$=1.294 μm for our device. Thus, $L_{eff}$ is nearly independent of the number of pairs in the top mirror in this range. It should be noted that $\alpha_i$ as determined here includes the usual intracavity losses and also losses in the DBR mirrors. The low value of $\alpha_i$~5.5 $cm^{-1}$ obtained here results, we believe, from the use of the oxide current constriction to reduce edge scattering losses and the use of an undoped p - mirror to reduce free carrier losses .

Threshold current densities, $J_{th}$, of the VCSEL's with various reflectivities are shown in Fig. 4. Here, a plot of log($J_{th}$) versus ln(1/R) is presented. When $J_{th}$ is low enough that laser operation on the second quantized state does not occur, the gain and current density can be related by a semilogarithic function $g = g_o \ln(\eta_i J / n_w J_{tr})$, where $g_o$ is the gain parameter, $J_{tr}$ is the transparency current density, and $n_w$ is the number of wells [11]. This relation does not take into account variation of gain with wavelength, which can have a large effect in VCSEL's. Thus, to be correct for VCSEL's, the gain peak and cavity resonance must be in perfect alignment for this equation to adequately describe the relationship of threshold

current and threshold gain in VCSEL's, as we have achieved in the structure described here. Then, we can relate the reflectivity and loss to the threshold current:

$$J_{th} = \frac{n_w J_{tr}}{\eta_i} \exp\left[\frac{L + \ln\left(\frac{1}{R}\right)}{\Gamma L_g g_o \xi}\right] \tag{4}$$

$$\ln(J_{th}) = \ln\left(\frac{n_w J_{tr}}{\eta_i}\right) + \frac{L}{\Gamma L_g g_o \xi} + \frac{1}{\Gamma L_g g_o \xi} \ln\left(\frac{1}{R}\right) \tag{5}$$

Eq. (5) says that $\ln(J_{th})$ is linearly depends on $\ln(1/R)$, which is confirmed in Fig. 4 in the range of R for which thermal effects are negligible. At high values of $\ln(1/R)$, a deviation of the data in Fig. 4 from linear dependence likely results from a shift of the gain peak caused by thermal effects. We fit the data in Fig. 4 with Eq. (5) using the measured values of $\eta_i$ and L to determine the values of $J_{tr}$ and $g_o$. We obtain $J_{tr}$ = 71 A/cm$^2$ and $1/(\Gamma L_g g_o \xi)$ = 558. If $\Gamma$ = 1, $\xi$ = 2, and $L_g$ =8 nm, then we obtain $g_o$=1120 cm$^{-1}$. Earlier experiments on InGaAs edge-emitting ultralow threshold lasers in our research group [14] have produced comparable material parameters for comparable structures ($J_{tr}$=44.5 A/cm$^2$, $g_o$=1132 cm$^{-1}$ , and $\eta_i$ = 0.98). Thus, the parameters of our VCSEL are consistent with these high quality structures.

In conclusion, we have fabricated VCSEL's by using oxide current constriction, intracavity p-contact, and binary semiconductor DBR structures. The cavity reflectivity is tuned by changing the number of pairs in the top DBR, which is useful to determine the internal parameters of VCSEL's. The device with an 18-pair stack in the top mirror, which gives the highest output power in this structure, shows an output power over 1.9 mW and a high slope efficiency of 55 % while maintaining a very low threshold current of 212 μA.

*Acknowledgments:* One of us (G.M.Yang) is grateful to Dr. Byung-Doo Choe, Dr. Hyung Jae Lee, and Dr. Weon Guk Jeong for their continuous encouragement. This work was supported by the Office of Naval Research, the Advanced Projects Research Agency through the National Center for Integrated Photonic Technology, and the Ministry of Science and Technology of Korea through SPRC at Jeonbuk National University.

## References

[1] D. L. Huffaker, J. Shin, and D. G. Deppe, "Low threshold half-wave vertical-cavity lasers", *Electron. Lett.*, **vol. 30**, no. 23, pp. 1946-1947, 1994.

[2] K. L. Lear, K. D. Choquette, R. P. Schneider, Jr., S. P. Kilcoyne, and K. M. Geib, "Selectively oxidised vertical cavity surface emitting lasers with 50 % power conversion efficiency", *Electron. Lett.*, **vol. 31**, no. 3, pp. 208-209, 1995.

[3] M. H. MacDougal, P. D. Dapkus, V. Pudikov, H. Zhao, and G. M. Yang, "Ultralow threshold current vertical-cavity surface-emitting lasers with AlAs oxide-GaAs distributed Bragg reflectors", *IEEE Photon. Technol. Lett.*, vol. 7, no. 3, pp. 229-231, 1995.

[4] G. M. Yang, M. H. MacDougal, and P. D. Dapkus, '"Ultralow threshold VCSELs fabricated by selective oxidation from all epitaxial structure" *Conference on Lasers and Electro-Optics (CLEO)*, postdeadline paper CPD4, Bultimore, MD, May 22-26, (1995).

[5] J. W. Scott, R. S. Geels, S. W. Corzine, and L. A. Coldren, "Modeling temperature effects and spatial hole burning to optimize vertical-cavity surface-emitting laser performance", *IEEE J. Quantum Electron.*, **vol. 29**, no. 5, pp. 1295-1308, 1993.

[6] D. V. Kuksenkov, H. Temkin, and S. Swirhun, "Measurement of internal quantum efficiency and losses in vertical cavity surface emitting lasers", *Appl. Phys. Lett.*, **vol. 66**, no. 14, pp. 1720-1722, 1995.

[7] see, for example, M. Born and E. Wolf, *Principles of Optics*, Pergamon, Oxford (1994).

[8] N. C. Frateschi, S. G. Hummel, and P. D. Dapkus, "In situ laser reflectometry applied to the growth of $Al_xGa_{1-x}As$ Bragg reflectors by metalorganic chemical vapor deposition", *Electron. Lett.*, **vol. 27**, no. 2, pp. 155-157, 1991.

[9] S. W. Corzine, R. S. Geels, J. W. Scott, R. H. Yan, and L. A. Coldren, "Design of Fabry-Perot surface-emitting lasers with a periodic gain structure", *IEEE J. Quantum Electron.*, **vol. 25**, no. 6, pp. 1513-1524, 1989.

[10] D. I. Babic and S. W. Corzine, "Analytic expressions for the reflection delay, penetration depth, and absorptance of quarter-wave dielectric mirrors", *IEEE J. Quantum Electron.*, **vol. 28**, no. 2, pp. 514-524, 1992.

[11] T. A. DeTemple and C. M. Herzinger, "On the semiconductor laser logarithimic gain-current density relation", *IEEE J. Quantum Electron.*, **vol. 29**, no. 5, pp. 1246-1252, 1993.

[12] H. Zhao, *The development of low threshold laser arrays and their applications in parallel optical datalinks*, Ph. D. Dissertation, University of Southern California (1994).

## Figure Captions

Fig. 1 Schematic cross section of VCSEL with a native-oxide constriction layer and binary material DBRs.

Fig. 2 Continuous-wave room-temperature light output against current characteristics for different numbers of pairs in the top mirror.

Fig. 3, Inverse external efficiency as a function of $1/\ln(1/R)$, where R is the mean power reflectivity. To obtain the external efficiency for total emission, the top emission external efficiency is corrected by the power emitted through the bottom Bragg mirror taking into error in layer thicknesses.

Fig. 4 Threshold current density of the VCSEL's with various reflectivities. Here, a plot of $\log(J_{th})$ versus $\ln(1/R)$ is being presented.

Fig. 1

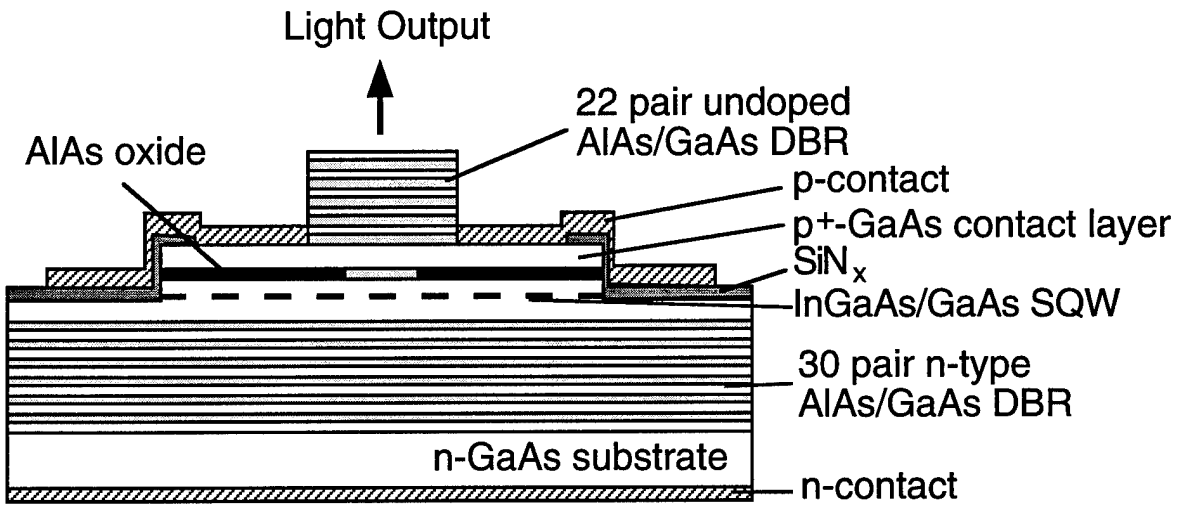
Light Output
22 pair undoped
AlAs/GaAs DBR
AlAs oxide
p-contact
p+-GaAs contact layer
SiNx
InGaAs/GaAs SQW
30 pair n-type
AlAs/GaAs DBR
n-GaAs substrate
n-contact

Fig. 2

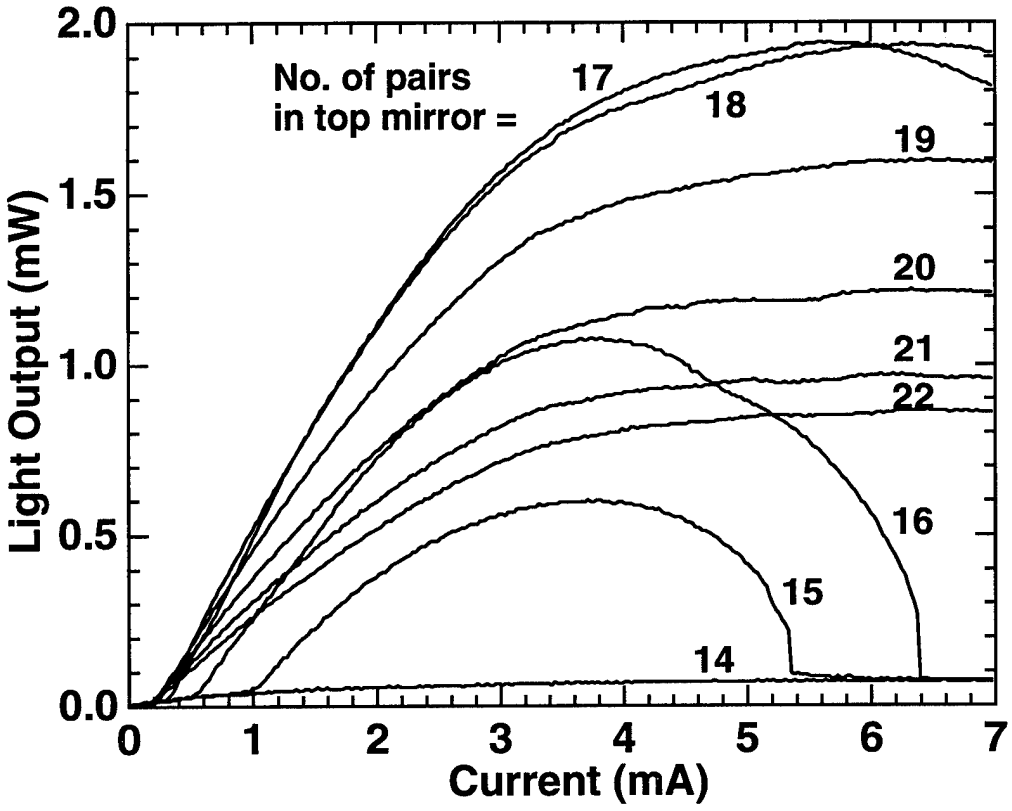
No. of pairs
in top mirror =
17
18
19
20
21
22
16
15
14
Light Output (mW)
Current (mA)
0.0
0.5
1.0
1.5
2.0
0
1
2
3
4
5
6
7

Fig. 3

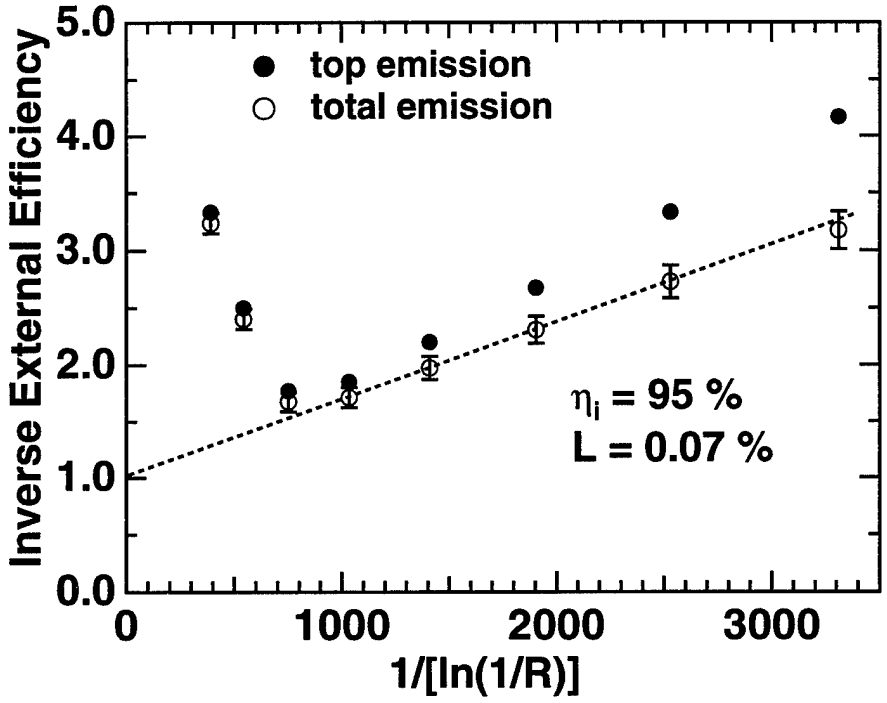
Inverse External Efficiency
5.0
4.0
3.0
2.0
1.0
0.0
0
1000
2000
3000
1/[ln(1/R)]
top emission
total emission
$\eta_i$ = 95 %
L = 0.07 %

Fig. 4

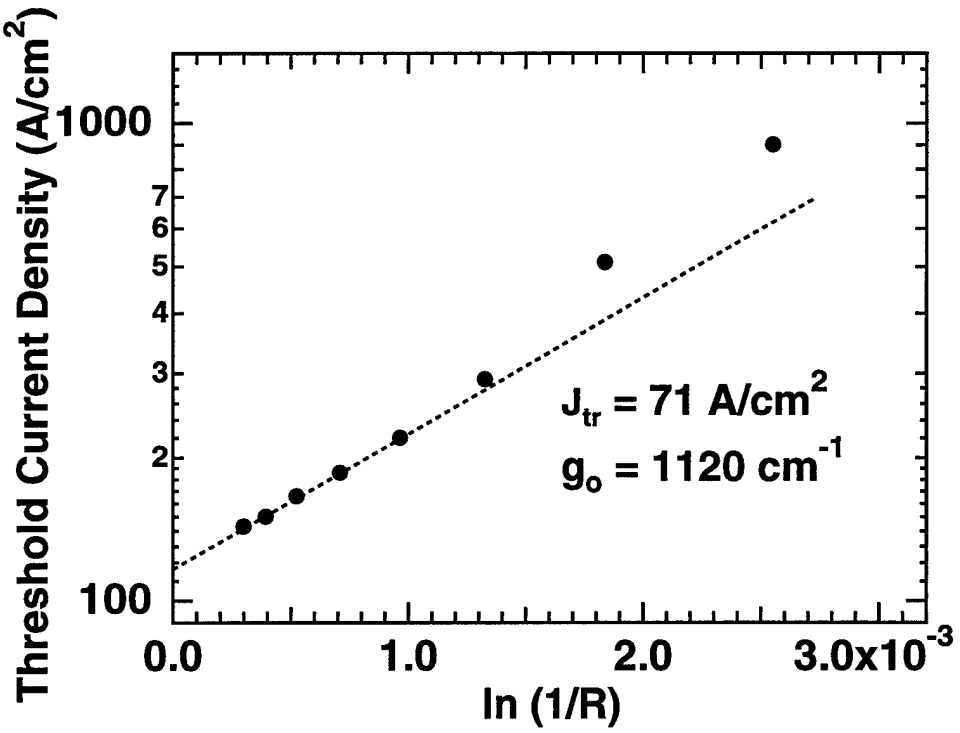
Threshold Current Density (A/cm$^2$)
1000
7
6
5
4
3
2
100
0.0
1.0
2.0
3.0x10$^{-3}$
ln (1/R)
$J_{tr}$ = 71 A/cm$^2$
$g_o$ = 1120 cm$^{-1}$

## 2.3 VCSEL's EMPLOYING OXIDE SEMICONDUCTOR BRAGG MIRRORS

# Wide-bandwidth distributed Bragg reflectors using oxide/GaAs multilayers

M. H. MacDougal, H. Zhao, P. D. Dapkus, M. Ziari and W. H. Steier

*Indexing terms: Distributed Bragg reflector lasers, Vertical cavity surface emitting lasers*

The authors have designed and fabricated a wide bandwidth high reflectivity distributed Bragg reflector (DBR) using the native oxide of AlAs as the low refractive index layer and GaAs as the high refractive index layer. Results show that the refractive index of the native oxide is 1.55±0.01, the peak reflectivity of the DBR is over 99%, and the reflectivity bandwidth is ~460nm.

Distributed Bragg reflectors (DBRs) are used in a wide variety of optoelectronic devices, including vertical cavity surface emitting lasers (VCSELs) [1] and resonant cavity devices [2]. Because of the low refractive index ratio of 3.5/3.0 for typical epitaxial materials, many pairs of the constituent materials must be grown to achieve a reflectivity of greater than 99%, and the band for which the reflectivity is greater than 90% is only around 110nm. Furthermore, the reflectivity and spectral bandwidth are very sensitive to the thickness and thickness uniformity of the layers. To relax this constraint as well as increase the spectral bandwidth, the use of two materials that have a much larger refractive index difference is necessary. In this Letter, we describe the fabrication of epitaxially grown wide bandwidth high reflectivity DBRs using the native oxide of AlAs [3–5] as the low refractive index layer and GaAs as the high refractive index layer so that the refractive index ratio is increased from 1.2in GaAs/AlAs to 2.3in GaAs/AlAs oxide. We and others have previously demonstrated the highest index ratio mirrors possible by fabricating GaAs/air Bragg reflectors [6, 7]. In these structures, the AlAs is etched away and replaced either with air or acrylic resin. This approach requires great care to keep the DBR from collapsing and requires supports on the side to hold up the GaAs layers. In contrast, the AlAs oxide/GaAs DBR structure we report here is a robust, self-supporting structure. In addition to its physical robustness, the oxide/GaAs structure will exhibit a wide bandwidth and wide angular acceptance. These attributes are expected to show benefits in broadband devices such as light emitting diodes (LEDs) and solar cells by increasing the angular spectrum of light that is reflected.

To design and simulate the DBR, the refractive index and thickness of each layer must be known. The thickness of the AlAs and GaAs epitaxial layers used in this structure is controlled by laser reflectometry [8, 9] and the refractive indices for these materials are well known [10, 11]. Our structure uses the native oxide of AlAs [4] as one of the reflector layers, but little data are available about its optical properties. Sugg and co-workers have measured the refractive index of the native oxide of $Al_{0.8}Ga_{0.2}As$ to be 1.63 [12]. Using ellipsometry, we have measured the refractive index of the native oxide of AlAs to be between 1.5 and 1.56, depending on oxidation conditions. The thickness of the oxide layer is also a variable because AlGaAs has been observed to contract in thickness by 60–70% when oxidised [4]. Owing to the limited data available on the native oxide, we designed the layer thicknesses for the Bragg reflector under the assumption that the oxide index of refraction is 1.54 and that there is no contraction in the thickness. The centre wavelength of the DBR is designed to be at 1 μm.

The designed structure, shown in Fig. 1, is grown by MOCVD. After growth, the wafer is coated with $SiN_x$, photolithographically patterned, and etched through the top three DBR pairs to expose edges of the AlAs for oxidation. The native oxide of AlAs is formed by flowing $N_2$, bubbled through $H_2O$ at 90°C, over the sample at 425°C [3, 5]. The oxidation of the AlAs starts at the sides of the mesa, as shown in Fig. 2, and moves toward the middle, until the whole AlAs layer is oxidised. The growth rate calibration layers are not exposed and thus left unoxidised. For our mesa width of 57μm, the oxidation time required for all three AlAs layers to oxidise completely is 45 min.

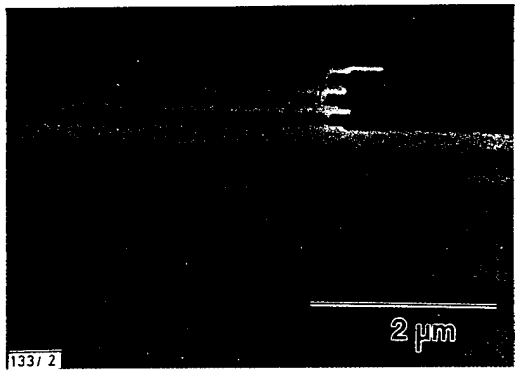


**Fig. 2** *SEM of one side of DBR mesa after oxidation*

The reflectivity of the DBR, shown in Fig. 3, is measured by a Cary spectrophotometer in reflection mode. Because the refractive index and the thickness of the oxide are unknowns, these variables have been varied in the simulation to match the measured spectrum. To achieve optimal matching in the simulation, the oxide index of refraction is 1.55, and the oxide thickness is 1427Å or 87.9% of the original intended AlAs thickness. When the layers at the bottom of the vias were added into the simulation in proportion to their aerial coverage, they drastically changed the shape of the simulated spectrum, and the simulation could not be made to fit the measured spectrum. Presumably, these layers do not contribute to the measured spectrum because the etched surface does not reflect the light specularly. The reflectance is measured at one wavelength (λ = 1.064μm) on the DBR and an Au film of known reflectivity using a microscope objective to focus the light on each to obtain the absolute reflectance of the DBR at this wavelength. The ratio between this absolute reflectance and the reflectance measured by the spectrophotometer at the same wavelength is

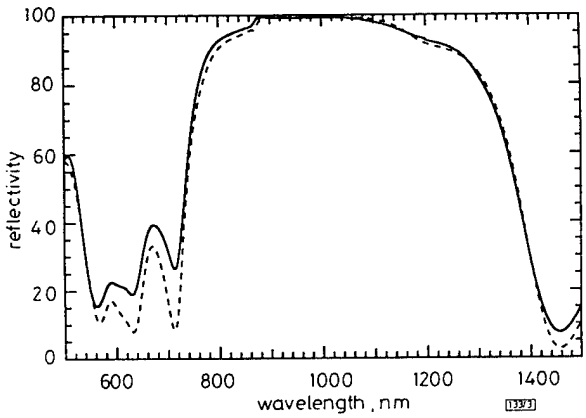


**Fig. 3** *Measured and simulated reflectivity of AlAs oxide/GaAs DBR*

Structure in Fig. 1 is used for reflectivity simulation

——— measured
– – – – simulated

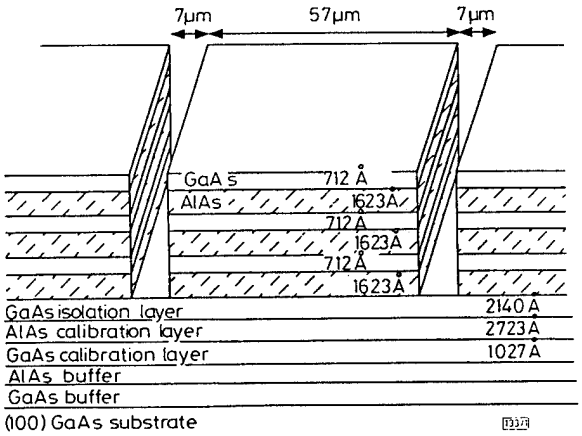


**Fig. 1** *Schematic diagram of DBR after patterning*

multiplied with the rest of the measured spectrum to obtain the absolute reflectivity for the other wavelengths. The peak reflectivity is ~960nm and is greater than 99%. The bandwidth, the range of wavelengths for which the reflectivity is greater than 90%, is 460nm. By comparison, a DBR with 16 pairs of AlAs/GaAs gives a reflectivity of 99.5% and a bandwidth of only 110nm. The fact that a high reflectivity is achieved, even when the oxide layer thickness is more than 10% off its designed thickness, demonstrates the thickness insensitivity of this type of DBR. In addition to the advantages of our DBR mentioned above, it achieves high reflectivity with only three pairs and a total epitaxial thickness of ~7000Å. When simulating four pairs, the reflectivity increases to 99.7%, which is suitable for use in VCSELs. The large bandwidth of this structure makes it an ideal candidate as a broadband reflector. Because it can be grown under the active region unlike dielectric reflectors such as ZnS and $SiO_2$, it could be placed beneath an LED and increase its power efficiency. Of course, its use will also complicate the contacting geometry because the oxide layers are insulating.

In this Letter, we have presented the design and fabrication of a wide bandwidth, high reflectivity distributed Bragg reflector. The DBR makes use of the large refractive index ratio between GaAs and the native oxide of AlAs to achieve these advantages.


*12 May 1994*
*Electronics Letters Online No: 19940754*

M. H. MacDougal, H. Zhao, P. D. Dapkus, M. Ziari and W. H. Steier (*Department of Electrical Engineering/Electrophysics University of Southern California, Los Angeles, CA 90089-0483, USA*)

## References

1 SAKAGUCHI, T., KOYAMA, F., and IGA, K.: 'Vertical cavity surface-emitting laser with an AlGaAs/AlAs Bragg reflector', *Electron. Lett.*, 1988, 24, (15), pp. 928–929

2 DODABALAPUR, A., and CHANG, T. Y.: 'Resonant-cavity InGaAlAs/InGaAs/InAlAs phototransistors with high gain for 1.3–1.6μm', *Appl. Phys. Lett.*, 1992, 60, (8), pp. 929–931

3 DALLESASSE, J. M., HOLONYAK, N., SUGG, A. R., RICHARD, T. A., and EL-ZEIN, N.: 'Hydrolyzation oxidation of $Al_xGa_{1-x}As$-AlAs-GaAs quantum well heterostructures and superlattices', *Appl. Phys. Lett.*, 1990, 57, (26), pp. 2844–2846

4 SUGG, A. R., HOLONYAK, N., BAKER, J. E., KISH, F. A., and DALLESASSE, J. M.: 'Native oxide stabilization of AlAs-GaAs heterostructures', *Appl. Phys. Lett.*, 1991, 58, (11), pp. 1199–1201

5 SUGG, A. R., CHEN, E .I., RICHARD, T. A., HOLONYAK, N., and HSIEH, K. C.: 'Native oxide-embedded $Al_yGa_{1-y}As$-GaAs-$In_xGa_{1-x}As$ quantum well heterostructure lasers', *Appl. Phys. Lett.*, 1993, 62, (11), pp. 1259–1261

6 HO, S.-T., MCCALL, S. L., SLUSHER, R. E., PFEIFFER, L. N., WEST, K. W., LEVI, A. F. J., BLONDER, G. E., and JEWELL, J. L.: 'High index contrast mirrors for optical microcavities', *Appl. Phys. Lett.*, 1990, 57, (14), pp. 1387–1389

7 BEYLER, C. A., HUMMEL, S. G., FRATESCHI, N., and DAPKUS, P. D.: 'Small dimension Bragg reflectors formed by air-isolated GaAs layers', *Electron. Lett.*, 1991, 27, (7), pp. 588–589

8 FRATESCHI, N., HUMMEL, S. G., and DAPKUS, P. D.: 'In situ laser reflectometry applied to the growth of $Al_xGa_{1-x}As$ Bragg reflectors by metalorganic chemical vapour deposition', *Electron. Lett.*, 1991, 27, (2), pp. 155–156

9 HUMMEL, S.G.: 'The growth and characterisation of multilayer structure by metal-organic chemical vapor deposition'. PhD Dissertation, University of Southern California, 1993

10 ASPNES, D. E., and STUDNA, A. A.: 'Dielectric functions and optical parameters of Si, Ga, GaP, GaAs, GaSb, InP, InAs, and InSb from 1.5 to 6.0eV', *Phys. Rev. B*, 1983, 27, (2), pp. 985–1009

11 FERN, R. E., and ORTON, A.: 'Refractive index of AlAs', *J. Appl. Phys.*, 1971, 42, (9), pp. 3499–3500

12 SUGG, A. R., CHEN, E. I., HOLONYAK, N., HSIEH, K. C., BAKER, J. E., and FINNEGAN, N.: 'Effects of low-temperature annealing on the native oxide of $Al_xGa_{1-x}As$', *J. Appl. Phys.*, 1993, 74, (6), pp. 3880–3885

*Accepted for Publication in Photonic Technology Letters*

# Epitaxial (Al,Ga)InP/oxide distributed Bragg reflectors for use in visible wavelength optical devices

Michael H. MacDougal, Steven G. Hummel*, P. Daniel Dapkus, Hanmin Zhao, and Yong Cheng

*University of Southern California*
*Department of Electrical Engineering/Electrophysics*
*Los Angeles, CA 90089-0483*

**Hewlett-Packard Laboratories*
*3500 Deer Creek Rd. PO Box 10350*
*Palo Alto, CA 94303-0867*

**Abstract**

Epitaxially-grown distributed Bragg reflectors(DBRs) employing thermally oxidized AlAs as the low refractive index constituent and (Al,Ga)InP as the high index constituent are fabricated. The 4.5 pair $Ga_{0.5}In_{0.5}P$/oxide and $Al_{0.5}In_{0.5}P$/oxide DBRs exhibit high reflectivity (>90%) over a range of 635-967 nm and 470-676 nm, respectively. The (Al,Ga)InP/oxide DBRs are shown to require less material to obtain high reflectivity and have much wider bandwidth than available all-semiconductor DBRs used in the visible spectrum.

## I. Introduction

Distributed Bragg reflectors (DBRs) are used in a wide variety of optoelectronic devices, including vertical cavity surface emitting lasers (VCSELs) and asymmetric Fabry-Perot light modulators. These multilayer structures are also used to enhance the performance of light emitting diodes (LEDs) by reflecting light away from an absorbing substrate.[1,2] DBRs employed

in cavity-based, near-IR and IR wavelength devices pose many challenges by requiring high reflectivity at specific wavelengths, which is problematic due to the small index difference available between the constituent materials.[3] In this letter, we present epitaxially-grown DBRs employing thermally oxidized AlAs as the low refractive index constituent and $(Al,Ga)_{0.5}In_{0.5}P$ as the high index constituent. The large refractive index ratio (~2) between these materials leads to DBRs possessing reflectivity greater than 90% and wide spectral bandwidth of greater than 200 nm. Furthermore, since these DBRs are epitaxially grown, they can be freely located within a device structure, and not limited to the surface as is the case for deposited dielectric mirrors.

AlAs is converted from a high index (n~3.0) material to a low index (n~1.55) material by wet thermal oxidation. Dallesasse and coworkers demonstrated that applying this technique results in a robust oxide unlike the poor quality oxide generated by the oxidation of AlAs at room temperature.[4] Sugg and coworkers reported that AlAs could be laterally oxidized while adjacent GaAs layers remain unoxidized.[5] This property has been utilized to create high reflectivity, wide-bandwidth DBRs centered at 960 nm by using AlAs oxide/GaAs pairs.[6]

## II. Fabrication

The use of GaAs as one of the constituent materials in a DBR operating in the visible wavelength region will limit available reflectivity due to absorbing characterics below 860 nm. In this work, AlAs oxide is paired with $Ga_{0.5}In_{0.5}P$ and $Al_{0.5}In_{0.5}P$, whose absorption cutoffs of 650 nm and 500 nm, respectively, permit high reflectivity in much of the visible region. The 4.5 period DBR structures have five layers of AlAs and 4 layers of $(Al,Ga)_{0.5}In_{0.5}P$ and are grown by low-pressure metalorganic chemical vapor deposition

(MOCVD) on (100) $n^+$ doped GaAs substrates. In the $Ga_{0.5}In_{0.5}P$ based structure, each period consists of 540 Å of $Ga_{0.5}In_{0.5}P$ and 1330Å of AlAs to achieve a center reflectance wavelength of 740 nm after thermal oxidation. In the $Al_{0.5}In_{0.5}P$ based structure, each period consists of 390Å of $Al_{0.5}In_{0.5}P$ and 970Å of AlAs to achieve a center wavelength of 540 nm.

The samples are processed and oxidized identically. The thermal oxidation process requires that the edges of the layers first be exposed. $SiN_x$ is deposited on the sample to protect the surface from any oxidation affects. Trenches are defined through photolithographically defined stripes which are 3 μm wide and 55 μm apart. Ion beam etching (IBE) is then used to isotropically etch the trenches and expose the AlAs layers. The photoresist is removed by chemical stripping.

At this point the samples are ready for oxidation. The native oxide of AlAs is formed by flowing $N_2$, which is first bubbled through $H_2O$ at 90°C, over the sample at 425°C. The samples are oxidized for 45 minutes to ensure that all AlAs layers are fully transformed. Since the $Ga_{0.5}In_{0.5}P$ layers do not contain any Al, they are left unaffected by the oxidation. Although the $Al_{0.5}In_{0.5}P$ contains Al, its oxidation rate at this temperature is much lower than that of the AlAs.[7] $Al_{0.5}In_{0.5}P$ begins to oxidize appreciably at 500°C, and even then at only a small rate, whereas AlAs oxidizes rapidly at 400°C. No evidence of $Al_{0.5}In_{0.5}P$ oxidation is observed in these samples under the optical microscope.

## III. Optical Characterization

The resulting reflectance vs. wavelength behavior for the 4.5 pair $Ga_{0.5}In_{0.5}P$/oxide and $Al_{0.5}In_{0.5}P$/oxide DBRs are shown in Figures 1 and 2, respectively. These measurements are performed with a spectrophotometer

in the reflectance mode. To determine the absolute reflectance of the mirrors, monochromatic light is focussed down to a 15 μm spot on a mesa and the reflected light intensity is measured and compared to the reflected intensity off a calibrated reflector. A Ti-sapphire laser at 791 nm is used for the InGaP/oxide DBR, and a He-Ne laser at 594 nm is used to for the $Al_{0.5}In_{0.5}P$ /oxide DBR. Because the trenches are quite small compared with the mirror area and do not specularly reflect due to rough etching, they do not contribute to the shape of the reflectivity spectrum. The $Ga_{0.5}In_{0.5}P$/oxide DBR has a reflectance bandwidth ($\Delta\lambda_{90}$), defined here as the wavelength range for which reflectance is greater than 90%, of 332 nm, with the stop band extending slightly beyond the absorption cutoff to 640 nm. The $Al_{0.5}In_{0.5}P$/oxide reflector demonstrates a bandwidth of 206 nm with reflectance greater than 90% extending to 470 nm. These bandwidths are limited by the absorption cutoff on the short wavelength side, since one of the objectives of this study is to determine the shortest wavelength at which high reflectivity is attained. They would be wider if the center wavlength were moved farther away from the absorption cutoff. The peak reflectivity of both DBRs are greater than 98.5%.

## IV. Discussion

In an earlier study of GaAs/oxide DBRs[6], the index of refraction of AlAs oxide was found to be 1.55 and the oxide layer's thickness was found to be ~88% of the original AlAs layer's thickness. Using these numbers along with predicted indices[8] for the $(Al,Ga)_{0.5}In_{0.5}P$ layers to simulate the reflectivity spectrum of the grown structure, a close match is found with the measured data as shown in Figs. 1 and 2. This match indicates that the oxide stops at the the interface of the $(Al,Ga)_{0.5}In_{0.5}P$/AlAs layers and does not

encroach into the $(Al,Ga)_{0.5}In_{0.5}P$ significantly and verifies that the oxide data is also correct when used with this material system.

Having verified that the refractive index and thickness change for the oxide is accurate when used with this material system, we can calculate the reflectivity of the oxide-based DBRs at other center wavelengths and compare it to the reflectivity of all-semiconductor DBRs. Since the beneficial impact of (Al,Ga)InP/oxide DBRs becomes more apparent at shorter wavelengths, a comparison is made using DBRs centered at 650 nm since that is near the shortest wavelength at which current state-of-the-art VCSELs are fabricated[9]. The DBR pair that is normally used in visible VCSELS is composed of $Al_{0.5}Ga_{0.5}As$ and AlAs whose refractive indices are well known[10]. Figure 3a shows the difference between a 5 pair $Al_{0.5}In_{0.5}P$/oxide DBR and a 35 pair $Al_{0.5}Ga_{0.5}As$/AlAs DBR. The peak reflectivities are 99.93 for both types. However, the oxide semiconductor DBR requires less than one quarter of the material thickness and many fewer pairs than an all-semiconductor DBR of the same reflectivity. The advantages of thinner DBRs iclude reduced epitaxial growth time and a reduction in absorption, scattering, and diffraction losses. Furthermore, the bandwidth of the oxide-based DBR is 302 nm, over seven times larger than the 41 nm bandwidth of all-semiconductor DBR. A major benefit that follows from the wide bandwidth of the oxide-based DBR is the flatter phase response on reflection, which relaxes the precise growth targets normally required to obtain high reflectivity in resonant cavity devices such as VCSELs. . The calculated phase responses for the two different types of DBRs are shown in Figure 3b. For a cavity surrounded by $Al_{0.5}In_{0.5}P$/oxide DBRs, the flatter phase response makes the resonant wavelength of the cavity less sensitive to thickness deviation within

the DBRs, and, consequently, makes it easier to align the cavity resonance with the gain peak than for a cavity surrounded by $Al_{0.5}Ga_{0.5}As/AlAs$ DBRs.

## V. Conclusions

In conclusion, we have demonstrated DBRs possessing extremely wide bandwidth and high reflectivity across the visible wavelength region. These performance features, combined with the ability to be epitaxially integrated below or above an active region, suggests the use of such DBR structures in VCSEL and LED devices emitting at visible wavelengths. The performance of the oxide-based DBRs has been compared with all-semiconductor DBRs and shown to be superior in reflectivity bandwidth and to reduce the amount of material required for high reflectivity. The wide bandwidth properties can be advantageously applied through relaxation of the extreme growth precision required for VCSELs, as well as through an increase in angular capture of available photons in visible LEDs. The $Ga_{0.5}In_{0.5}P$/oxide combination would be preferable in the red region due to the higher conductivity of $Ga_{0.5}In_{0.5}P$ and absence of Al in the semiconductor region. The $Al_{0.5}In_{0.5}P/oxide$ combination would provide higher reflectance in the yellow, orange and green regions due to decreased absorption.

## VI. Acknowledgements

The authors acknowledge the support of the Office of Naval Research, the Army Research Office, the Advanced Research Projects Agency, and the Ballistic Missile Defense Organization for support of portions of this work.

Figure 1. Reflectance spectra for the 4.5 pair $Ga_{0.5}In_{0.5}P$/oxide DBR.

Figure 2. Reflectance spectra for the 4.5 pair $Al_{0.5}In_{0.5}P$/oxide DBR.

Figure 3. Comparison of reflection characteristics between a 5 pair $Al_{0.5}In_{0.5}P$/oxide DBR and a 35 pair $Al_{0.5}Ga_{0.5}As$/AlAs DBR. (a) Calculated reflectance spectra where the peak reflectivities for both spectra are 99.93%. (b) Calculated phase response on reflection.

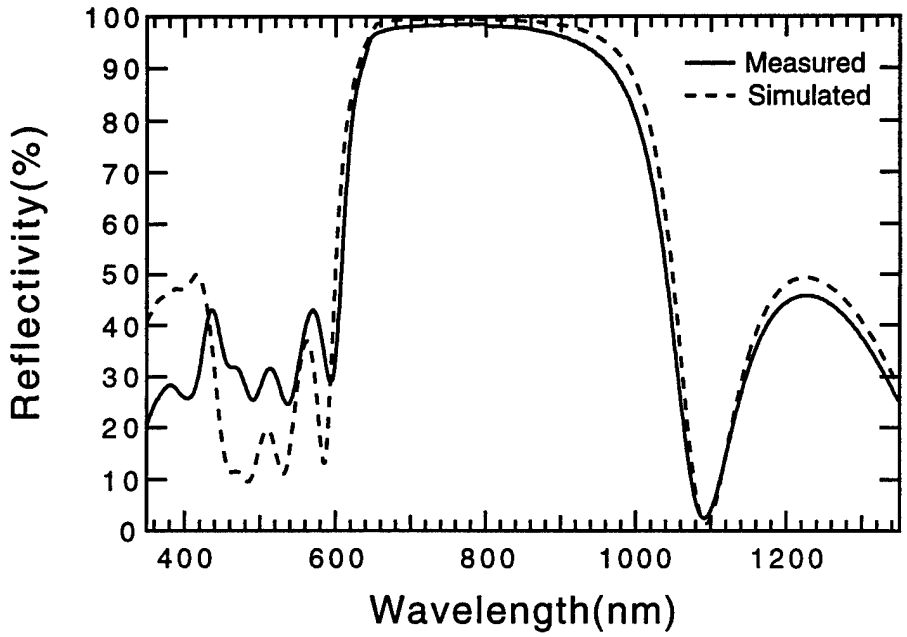
Reflectivity(%)
100
90
80
70
60
50
40
30
20
10
0
400
600
800
1000
1200
Wavelength(nm)
Measured
Simulated

**Figure 1**

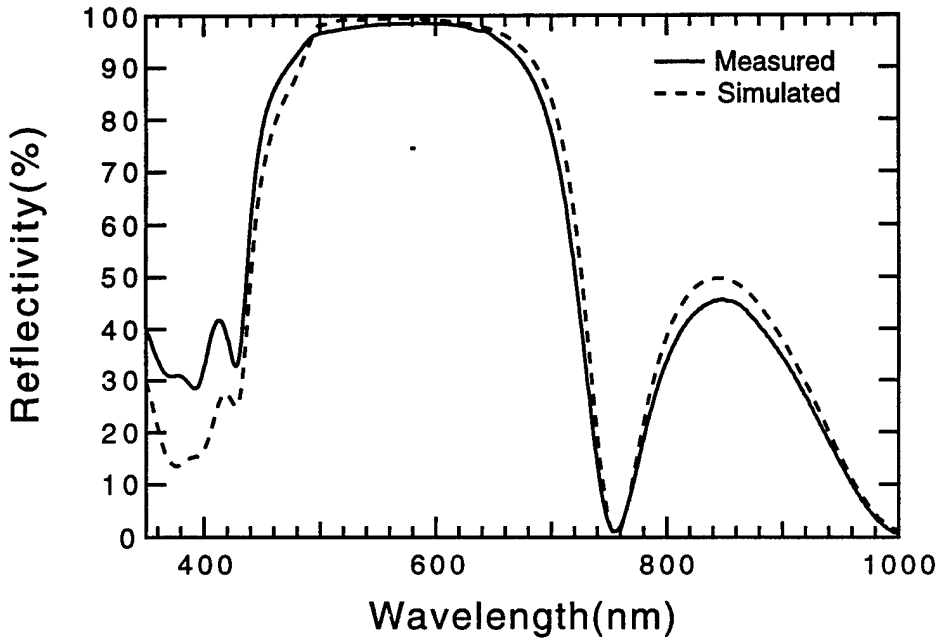
Reflectivity(%)
100
90
80
70
60
50
40
30
20
10
0
400
600
800
1000
Wavelength(nm)
Measured
Simulated

**Figure 2**

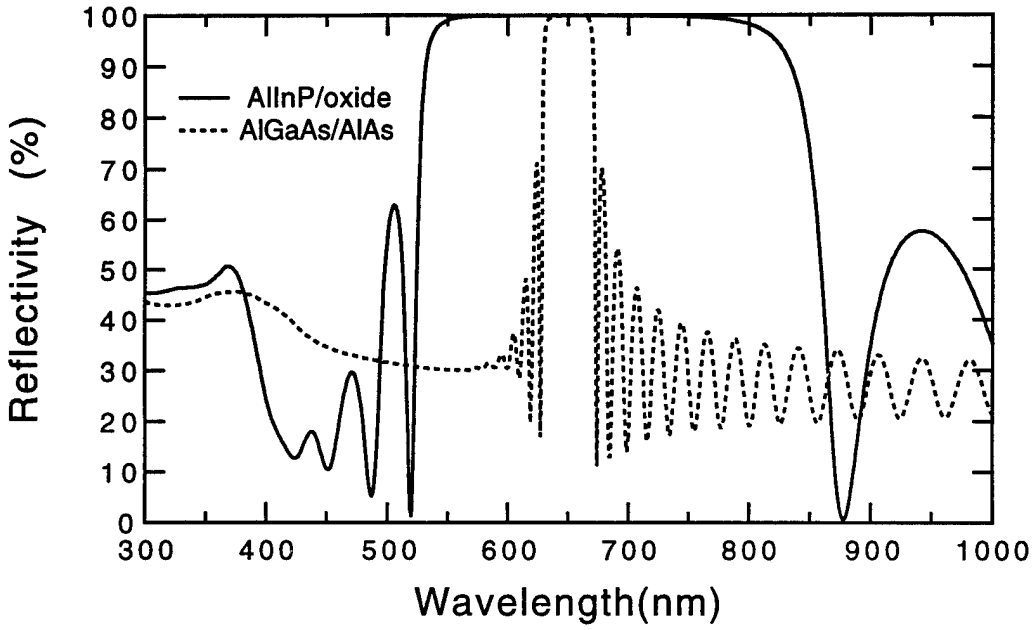
AlInP/oxide
AlGaAs/AlAs
Reflectivity (%)
Wavelength(nm)
0
10
20
30
40
50
60
70
80
90
100
300
400
500
600
700
800
900
1000

**Figure 3a**

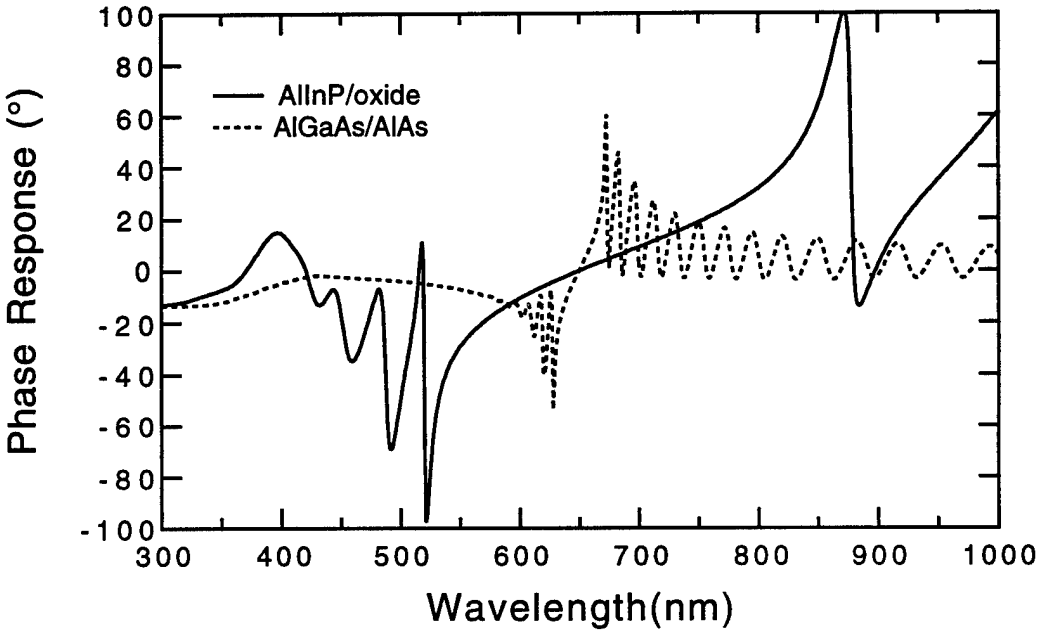
Phase Response (°)
100
80
60
40
20
0
-20
-40
-60
-80
-100
AlInP/oxide
AlGaAs/AlAs
300
400
500
600
700
800
900
1000
Wavelength(nm)

**Figure 3b**

## References

1. M.G. Craford and F.M. Steranka, *Light Emitting Diodes*, in *Encyclopedia of Applied Physics*, G. Trigg, ed., VCH, New York, (1994).

2. H. Sugawara, A. Itaya, H. Nozaki, and G. Hatakoshi, "High-brightness InGaAlP green light-emitting diodes", *Applied Physics Letters*, 1992, **Vol. 61,** No. 15, p. 1775-1777.

3. R.P. Schneider Jr., R.P. Bryan, J.A. Lott, E.D. Jones, and G.R. Olbright, "MOVPE growth of InAlGaP-based visible vertical-cavity surface-emitting lasers", *Journal of Crystal Growth*, 1992, **Vol. 124,** No. p. 763-771.

4. J.M. Dallesasse, N. Holonyak Jr., A.R. Sugg, T.A. Richard, and N. El-Zein, "Hydrolyzation oxidation of $Al_xGa_{1-x}As$-AlAs-GaAs quantum well heterostructures and superlattices", *Applied Physics Letters*, 1990, **Vol. 57,** No. 26, p. 2844-2846.

5. A.R. Sugg, E.I. Chen, T.A. Richard, N. Holonyak Jr., and K.C. Hsieh, "Native oxide-embedded $Al_yGa_{1-y}As$-GaAs-$In_xGa_{1-x}As$ quantum well heterostructure lasers", *Applied Physics Letters*, 1993, **Vol. 62,** No. 11, p. 1259-1261.

6. M.H. MacDougal, H. Zhao, P.D. Dapkus, M. Ziari, and W.H. Steier, "Wide-bandwidth distributed Bragg reflectors using oxide/GaAs multilayers", *Electronics Letters*, 1994, **Vol. 30,** No. p. 1147-1149.

7. F.A. Kish, S.J. Caracci, N. Holonyak Jr., K.C. Hseih, J.E. Baker, S.A. Maranowski, A.R. Sugg, and J.M. Dallesasse, "Properties and use of $In_{0.5}(Al_xGa_{1-x})_{0.5}P$ and $Al_xGa_{1-x}As$ native oxides in heterostructure lasers", *Journal of Electronic Materials*, 1992, **Vol. 21,** No. 12, p. 1133-1139.

8. H. Tanaka, Y. Kawamura, and H. Asahi, *Journal of Applied Physics*, 1986, **Vol. 59,** No. p. 985.

9. R.P. Schneider Jr. and J.A. Lott, "Cavity design for improved electrical injection in InAlGaP/AlGaAs visible (639-661 nm) vertical-cavity surface-emitting laser diodes", *Applied Physics Letters*, 1993, **Vol. 63,** No. 7, p. 917-919.

10. S. Adachi, "GaAs, AlAs, and $Al_xGa_{1-x}As$: Material parameters for use in research and device applications", *Journal of Applied Physics*, 1985, **Vol. 58,** No. 3, p. R1-R29.

# Ultralow threshold current vertical-cavity surface-emitting lasers with AlAs oxide/GaAs distributed Bragg reflectors

Michael H. MacDougal, P. Daniel Dapkus, Vasily Pudikov, Hanmin Zhao, and Gye Mo Yang
*Department of Electrical Engineering/Electrophysics*
*University of Southern California, Los Angeles, CA 90089-0483*

**Abstract**

An electrically-pumped vertical-cavity surface-emitting laser(VCSEL) using an AlAs oxide/GaAs DBR above the AlGaAs/GaAs/InGaAs gain region and a conventional AlAs/GaAs DBR below is described. By selective oxidation, devices with current flow apertures of different areas are fabricated, and in 8 μm square devices, threshold currents as low as 0.22 mA are achieved. Being the first electrically-pumped VCSEL to utilize the oxide-based DBR, it demonstrates that the oxide-based DBR is of sufficient quality to realize submilliampere threshold currents.

## I. Introduction

Vertical-cavity surface-emitting lasers (VCSELs) are promising candidates as light sources in optical systems. They are inherently integrable into arrays, can be coupled efficiently into fibers, and are amenable to on-wafer testing. These advantages must be weighed against the stringent epitaxial layer thickness control required in their fabrication. In VCSELs, very high reflectivity mirrors are required on each side of the resonant cavity since the gain region is small, especially compared with that of edge-emitting lasers. Epitaxial semiconductor distributed Bragg reflectors (DBRs) can be placed above and below the active region allowing the VCSEL to be grown in one step; however, the requirements

on thickness precision are high and the DBR pairs must be repeated many times (>20) to achieve high reflectivity (>99%). The difference in index of refraction between the DBR pairs is small (3.5/3.0 for GaAs/AlAs), resulting in a narrow stop band and a strong variation of the reflection phase change within the stopband. These factors place stringent requirements on the layer thickness precision (±1%) to ensure that the cavity resonance is aligned with the gain peak. Single-wafer, in-situ thickness measurement techniques are used to achieve the high degree of control needed to reproducibly grow these structures[1,2].

In contrast to semiconductor DBRs, dielectric mirrors which have been used in VCSELs have a high index difference (2.98/1.37 for $Sb_2S_3/MgF_2$), a wide stopband, and high reflectivity using relatively few layers. As a result, the alignment of the cavity resonance with the gain peak is not as difficult as in semiconductor DBRs. In addition, Huffaker et al. have suggested that the use of high refractive index contrast mirrors on both sides of the active region reduces the fundamental lateral spread of the cavity mode and allow extremely low threshold currents to be achieved[3]. It is difficult, however, to fabricate VCSELs with deposited dielectric mirrors on both sides of the active region.

To take advantage of the favorable properties of each type of DBR, we recently fabricated an epitaxially-grown 3-pair DBR with high reflectivity and a wide stopband using the combination of AlAs oxide/GaAs[4]. The refractive index difference of this pair is high (1.55/3.5), and the AlAs/GaAs pair can be epitaxially grown and later oxidized. Holonyak and coworkers have pioneered the technique of wet oxidation of AlGaAs[5,6] and have shown that AlAs can be oxidized without significantly affecting the GaAs[7]. In fact, they have recently used the AlAs oxide/GaAs DBR to make a photopumped laser which emits through the sides as well as vertically[8]. In this paper, we present an electrically-

pumped VCSEL using an AlAs oxide/GaAs DBR above the gain region and a conventional AlAs/GaAs DBR below and show that the oxide DBR is of sufficient quality to realize submilliampere threshold currents.

## II. Design, Growth, and Fabrication

The basic structure, shown in Fig. 1, consists of a 30-pair n-doped quarter-wave AlAs/GaAs DBR stack, an AlGaAs/GaAs/InGaAs resonant cavity, p-doped contact layers and a 4-pair undoped quarter-wave AlAs oxide/GaAs DBR. The AlAs/GaAs DBR is doped n-type with a doping level of ~2 x $10^{18}$ $cm^{-3}$ and has a calculated reflectivity of 99.992%. The undoped active region contains three 60Å $In_{0.15}Ga_{0.85}As$ quantum wells (QWs) separated by 100Å GaAs barriers. On either side are 100Å GaAs layers to separate the QWs from the $Al_{0.5}Ga_{0.5}As$ confinement layers. The doped $Al_{0.5}Ga_{0.5}As$ layers are used to center the active region on the electric field standing wave peak in a one-wavelength cavity and to provide carrier confinement. The top DBR does not conduct current when oxidized so one additional doped Bragg pair, whose constituent layers are multiples of quarter wavelengths are placed between the top DBR and the cavity. These p-doped layers provide an electrical path for the current to reach the active region. A 0.25λ p-type AlAs layer borders the cavity followed by a 1.75λ $p^+$ GaAs layer. The AlAs is non-intentionally doped and has a doping level of ~$10^{17}$ $cm^{-3}$, and the GaAs has a doping level of ~4 x $10^{18}$ $cm^{-3}$. The AlAs serves a dual function as a current constriction as well as a quarter-wave Bragg layer. An insulating current constriction, created by laterally oxidizing the AlAs until the oxide front is underneath the top DBR[9], forces the current path and gain region into the optical mode. This current constriction layer allows the top DBR to be wider than the current injection layer thereby decreasing leakage of the optical mode from the waveguide[10]. The refractive index is 1.55 in the oxidized region

of the current constriction layer and 2.96 in the unoxidized region of the current constriction layer, and this index step provides a measure of index guiding in the cavity. Together, these qualities contribute to low threshold currents when matched with high reflectivity mirrors. The top DBR is made up of four AlAs/GaAs pairs before processing. From previous studies[4], we have determined the refractive index of AlAs oxide to be 1.55 and the thickness of the oxide to be 90% of the original AlAs thickness. After processing, it becomes a quarter wave AlAs oxide/GaAs DBR. The reflectivity spectrum of a typical 4-pair oxide DBR is shown in Fig. 2. It has a peak reflectivity of 99.8% (calculated) and a stopband of 540 nm. Output power is limited by the very high reflectivity of these mirrors, but the original intent of this study was to demonstrate that the reflectivity of the native oxide DBR was sufficient to obtain lasing in a vertical cavity. Across the wafer, the gain peak varies from 940 - 950 nm as determined by photoluminescence measurements and the cavity peak varies from 920 - 950 nm as determined by laser spectra. This variation is caused by inadvertent nonuniformity of deposition rates in our growth chamber.

The VCSELs are grown by atmospheric-pressure metal-organic chemical vapor deposition (MOCVD). In-situ laser reflectometry is used to monitor the thickness at the center of the wafer[1,11]. The sources are trimethylgallium, trimethylaluminium, trimethylindium, and arsine. The dopants are disilane and diethylzinc. After growth, 15 μm square mesas are wet etched through the top DBR down to the GaAs contact layer. The exposed AlAs is oxidized at 425°C for 10 minutes. The selectivity of this process transforms the AlAs to AlAs oxide while leaving the GaAs unaffected. Then, 50 μm square mesas, whose centers coincide with the centers of the 15 μm mesas, are defined, and the p-type GaAs contact layer and AlAs current constriction layer are selectively etched to expose

the AlAs so that it may be oxidized. Current flow apertures of 15 μm and 8 μm are created by oxidizing the AlAs at 425°C for 8 minutes and 10 minutes, respectively. $SiN_x$ is deposited outside and on the edges of the 50 μm square to isolate the p-type metal from the active region The p contact is made with Ti/Pt/Au and the n contact is made with AuSn.

## III. Results

Devices were tested with no temperature control under cw excitation. No heat sinking was present other than the contact with the metal test stage to the bottom of the chip. Laser characteristics for the 15 μm square and 8 μm square devices are shown in Figs. 2 and 3. The 15 μm and 8 μm devices have minimum threshold currents of 1.55 mA and 0.22 mA, respectively. These low numbers demonstrate that the oxide DBR is a viable mirror option in electrically-pumped VCSELs and can be used to achieve very low threshold currents. The threshold current density for the 15 μm device (667 $A/cm^2$) is higher than that for the smaller 8 μm device (344 $A/cm^2$) because the current aperture is equal to or greater than the top mirror mesa. This causes reduced reflectivity and increases scattering. These effects are reflected in both the higher threshold current density and lower efficiency of the 15 μm aperture laser. In addition, the higher current density causes the 15 μm device to have a higher threshold voltage drop of 3.56V as compared to a 2.55V drop for the 8 μm device. The emission wavelengths of the 15 μm and 8 μm device are 949 nm and 936 nm, respectively. The difference in wavelength is due to the different growth rates across the wafer causing the bottom reflector stopband to vary. As expected, the best devices occurred when the QW emission wavelength and the cavity resonance wavelength were close to one another. The 8 μm device emits in a single mode

and has a next order transverse mode suppression of 35 dBm. The 15 μm device has a smaller mode suppression due to the appearance of transverse modes in the wide aperture oxide-defined device as noted by Huffaker et al.[12] These first generation devices exhibit low threshold currents and good modal quality using an 8 μm square current aperture and, with further optimization, should have higher power output.

## IV. Summary

In conclusion, we have demonstrated the use of AlAs oxide/GaAs DBRs in electrically-pumped VCSELs. The top mirror is a 4-pair quarter-wave stack with peak reflectance of 99.8% (calculated) and a stopband of 540 nm. Employing an oxide DBR above the active region and a semiconductor below, VCSELs achieve submilliampere thresholds, which suggests that little scattering or absorption occurs in the oxide DBRs. These high-contrast DBRs have a short effective penetration depth which may lead to extremely low threshold currents (<10 μA) when placed on both sides of the active region. The device presented here indicates that such an extremely low threshold device is feasible.

## V. Acknowledgments

The authors would like to thank S. Hummel(Hewlett-Packard Labs) and R. Schneider(Sandia National Labs) for useful discussions and comments, and S. Dubovitsky for assistance with laser measurements. This work was supported by the Office of Naval Research, the Army Research Office, the Ballistic Missile Defense Organization, and ARPA.

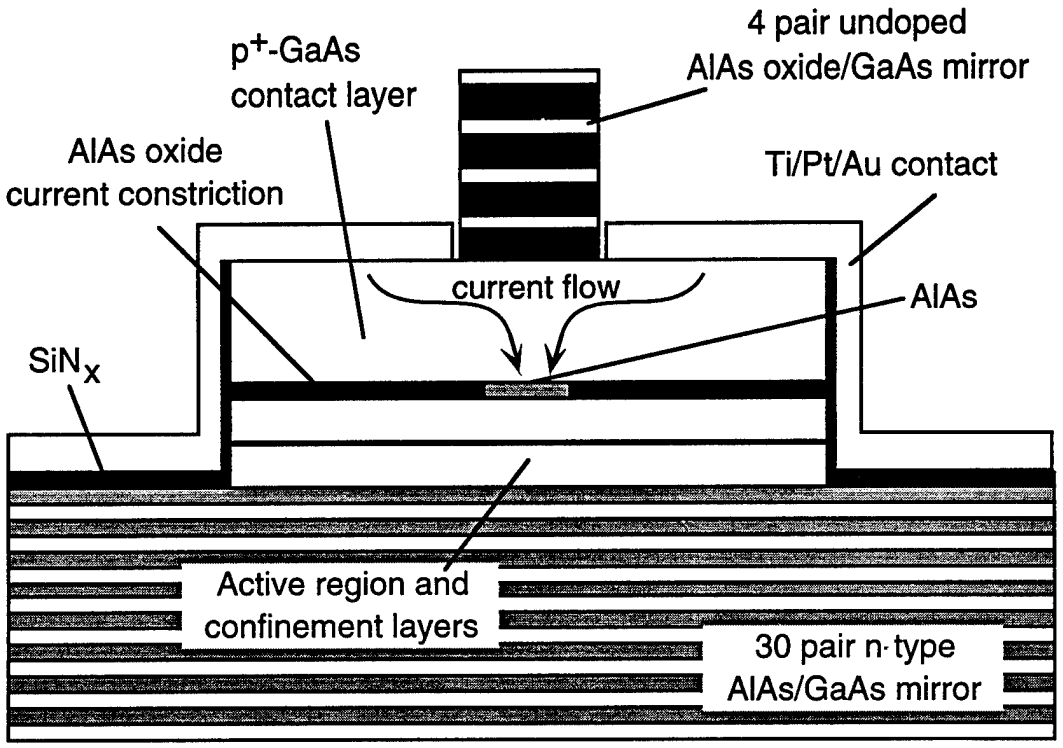
4 pair undoped
AlAs oxide/GaAs mirror
p+-GaAs
contact layer
AlAs oxide
current constriction
Ti/Pt/Au contact
current flow
AlAs
SiNx
Active region and
confinement layers
30 pair n-type
AlAs/GaAs mirror

Figure 1

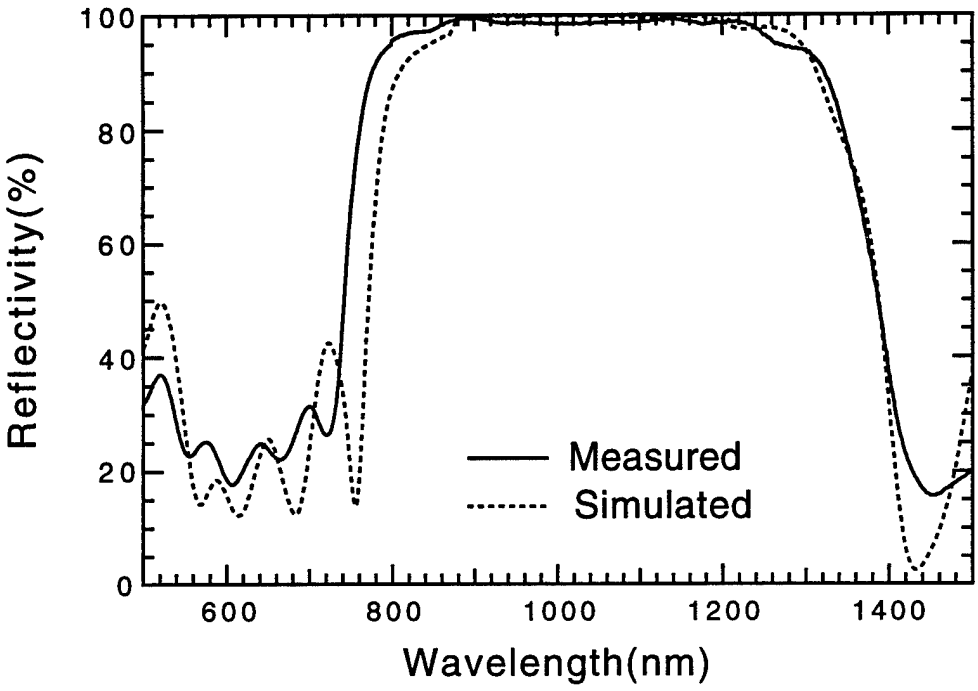
100
80
60
40
20
0
Reflectivity(%)
600
800
1000
1200
1400
Wavelength(nm)
Measured
Simulated

Figure 2

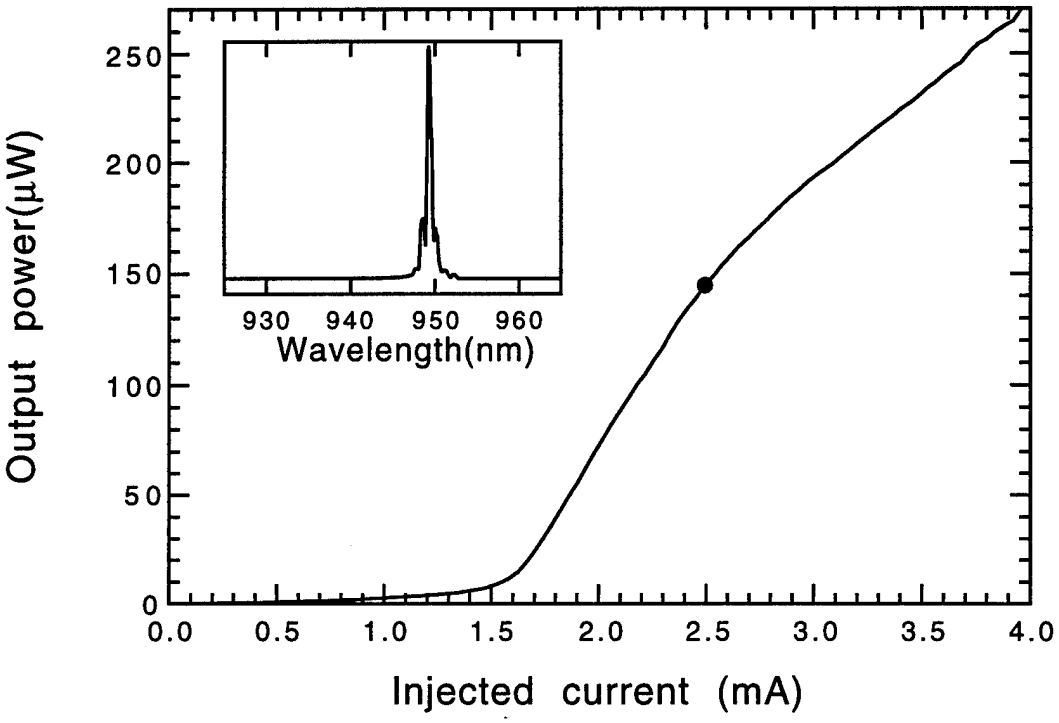
Output power(μW)
250
200
150
100
50
0
0.0
0.5
1.0
1.5
2.0
2.5
3.0
3.5
4.0
Injected current (mA)
930
940
950
960
Wavelength(nm)

Figure 3

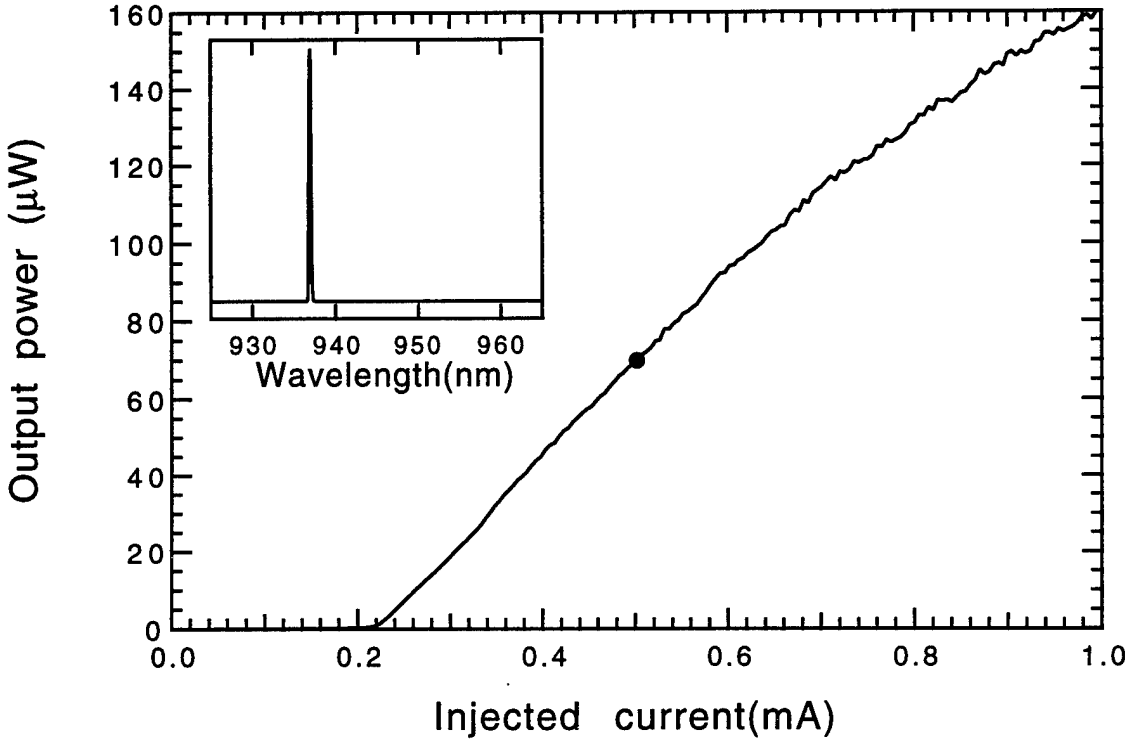
Output power (μW)
160
140
120
100
80
60
40
20
0
0.0
0.2
0.4
0.6
0.8
1.0
Injected current(mA)
930
940
950
960
Wavelength(nm)

Figure 4

## Figure Captions

Figure 1.Schematic of VCSEL utilizing native oxide constriction layer and an AlAs oxide/GaAs DBR.

Figure 2. Reflectivity of 4 pair quarter wavelength AlAs oxide/GaAs DBR stack.

Figure 3. Light versus current curve for VCSEL with 15 μm square current aperture measured under cw excitation at room temperature. The inset shows laser spectra when operated at 2.5 mA, cw.

Figure 4. Light versus current curve for VCSEL with 8 μm square current aperture measured under cw excitation at room temperature. The inset shows laser spectra when operated at 0.5 mA, cw.

## References

1. N.C. Frateschi, S.G. Hummel, and P.D. Dapkus, "In situ laser reflectometry applied to the growth of $Al_xGa_{1-x}As$ Bragg reflectors by metalorganic chemical vapour deposition", *Electronics Letters*, 1991, **Vol. 27,** No. 2, p. 155-156.

2. S.A. Chalmers and K.P. Killeen, "Method for accurate growth of vertical-cavity surface-emitting lasers", *Applied Physics Letters*, 1993, **Vol. 62,** No. 11, p. 1182-4.

3. D.L. Huffaker, C.C. Lin, D.G. Deppe, B.G. Streetman, and T.J. Rogers, "Mode dependence on mirror contrast in Fabry-Perot microcavity lasers", *IEEE Photonics Technology Letters*, 1994, **Vol. 6,** No. 2, p. 135-8.

4. M.H. MacDougal, H. Zhao, P.D. Dapkus, M. Ziari, and W.H. Steier, "Wide-bandwidth distributed Bragg reflectors using oxide/GaAs multilayers", *Electronics Letters*, 1994, **Vol. 30,** No. p. 1147-1149.

5. J.M. Dallesasse, N. Holonyak Jr., A.R. Sugg, T.A. Richard, and N. El-Zein, "Hydrolyzation oxidation of $Al_xGa_{1-x}As$-AlAs-GaAs quantum well heterostructures and superlattices", *Applied Physics Letters*, 1990, **Vol. 57,** No. 26, p. 2844-2846.

6. A.R. Sugg, N. Holonyak Jr., J.E. Baker, F.A. Kish, and J.M. Dallesasse, "Native oxide stabilization of AlAs-GaAs heterostructures", *Applied Physics Letters*, 1991, **Vol. 58,** No. 11, p. 1199-1201.

7. A.R. Sugg, E.I. Chen, T.A. Richard, N. Holonyak Jr., and K.C. Hsieh, "Native oxide-embedded $Al_yGa_{1-y}As$-GaAs-$In_xGa_{1-x}As$ quantum well heterostructure lasers", *Applied Physics Letters*, 1993, **Vol. 62,** No. 11, p. 1259-1261.

8. M.J. Ries, T.A. Richard, S.A. Maranowski, N. Holonyak Jr., and E.I. Chen, "Photopumped room-temperature edge- and vertical-cavity operation of AlGaAs-GaAs-InGaAs quantum-well heterostructure lasers utilizing native oxide mirrors", *Applied Physics Letters*, 1994, **Vol. 65,** No. 6, p. 740-2.

9. D.L. Huffaker, D.G. Deppe, K. Kumar, and T.J. Rogers, "Native-oxide defined ring contact for low threshold vertical-cavity lasers", *Applied Physics Letters*, 1994, **Vol. 65,** No. 1, p. 97-9.

10. J.W. Scott, R.S. Geels, S.W. Corzine, and L.A. Coldren, "Modeling temperature effects and spatial hole burning to optimize vertical-cavity surface-emitting laser performance", *IEEE Journal of Quantum Electronics*, 1993, **Vol. 29,** No. 5, p. 1295-1308.

11. S.G. Hummel and P.D. Dapkus, 1993 (unpublished).

12. D.L. Huffaker, D.G. Deppe, and T.J. Rogers, "Transverse mode behavior in native-oxide-defined low threshold vertical-cavity lasers", *Applied Physics Letters*, 1994, **Vol. 65,** No. 13, p. 1611-3.

## 3.0 SUMMARY OF ACCOMPLISHMENTS

## 4.0. FUTURE RESEARCH

## 3.0 SUMMARY OF ACCOMPLISHMENTS

There have been numerous accomplishments during the short span of this program. The most important are listed below:

1. New design paradigm for vertical cavity surface emitting lasers emphasizing minimization of optical loss to achieve low threshold.
2. Achievement of the lowest threshold current laser ever fabricated, 8.7 μA.
3. The lowest threshold current density VCSEL ever fabricated, 140 A/cm$^2$.
4. The first oxide / semiconductor Bragg mirrors.
5. The first oxide / semiconductor Bragg mirror to operate in the visible.
6. The first VCSEL's employing oxide / semiconductor Bragg mirrors.
7. The lowest threshold buried oxide edge emitting lasers.
8. The lowest threshold folded cavity surface emitting lasers.

## 4.0 FUTURE RESEARCH

The integration of optical and electrical devices is now closer to reality as a result of this program. Several issues remain to be resolved before a viable technology is available. First, low resistance VCSEL's with two oxide /semiconductor DBR's must be demonstrated. Second, low resistance contact schemes for these devices must be devised. Third, oxide isolated electronic devices must be demonstrated that can be integrated with the VCSEL's to form OEIC's. Finally, a compatible process sequence for integration must be developed. these issues will form the basis of future work in the program that is to follow.

# APPENDIX

# PUBLISHED PAPERS

# Folded-Cavity Surface-Emitting InGaAs–GaAs Lasers with Low-Threshold Current Density and High Efficiency

Yong Cheng, Gye Mo Yang, and P. Daniel Dapkus, *Fellow, IEEE*

***Abstract*—Folded-cavity surface-emitting InGaAs–GaAs lasers (FCSEL's) that employ high-quality internal 45° deflectors are demonstrated with low-threshold current density and high efficiency. A simplified process involving a stop etch to position the surface emitting output mirror close to the waveguide and ion-beam-etching (IBE) to form the 45° deflecting mirror is presented. FCSEL's (cavity length 800 $\mu$m) with two 45° deflectors, are obtained with threshold current density as low as 112.5 A/cm$^2$ and surface-emission external quantum efficiency as high as 65% (0.82 W/A). The additional loss contributed by the folded-cavity design is estimated as 4.2 cm$^{-1}$.**

## I. Introduction

HIGH-PERFORMANCE surface-emitting lasers needed for sources in optoelectronic integrated circuits. Lasers with internal 45° total reflection mirrors [referred to as folded-cavity surface emitting lasers (FCSEL's)] may be utilized to couple the light in a horizontal cavity toward the surface. To date, threshold currents as low as 8 mA for InGaAs–GaAs FCSEL's incorporating high reflectivity epitaxial Bragg reflectors have been reported [1], [2]. High-power GaAs–AlGaAs narrow ridge waveguide [3] and broad area [4] FCSEL's, as well as high-power two-dimensional (2-D) arrays of FCSEL's [5]–[7] have been demonstrated. In a FCSEL, additional losses, such as diffraction loss in the folded unguided region, coupling loss owing to angular inaccuracy of the 45° mirror, and scattering loss due to roughness of dry-etched facets, are introduced that may limit the performance. In this letter, we present a design that minimizes these losses and permits high efficiency operation.

A schematic diagram of the laser we present is shown in Fig. 1. The laser positions the output mirror close to the waveguide to minimize the distance over which the deflected beam travels unguided [8], [9]. Analysis predicts that this distance is the critical factor in determining the effective loss in the folded cavity [8]. A high-quality 45° deflector is required in which the facet angle is controlled to within $\pm 1°$ and the roughness must be $< 0.1$ mm RMS. The lasers we describe here employ 45° deflectors fabricated by ion-beam-etching (IBE). The lasers use a GaAs etch stop layer to permit the cladding layer to be etched to within 0.4 $\mu$m from the cavity at the output mirror [9]. FCSEL's (cavity length 800 mm), with two 45° deflectors, are obtained with threshold current density as low as 112.5 A/cm$^2$ and surface-emission external quantum efficiency as high as 65% (0.82 W/A). The performance of these monolithic FCSEL's is very close to that of cleaved edge-emitting lasers. The additional loss due to the folded-cavity design is estimated to be 4.2 cm$^{-1}$.

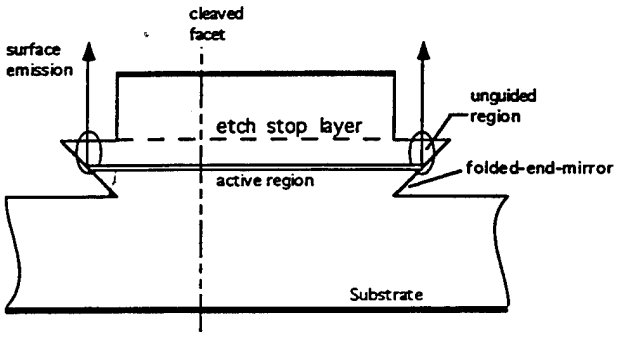


Fig. 1. The schematic diagram of a FCSEL structure.

The laser structure designed for FCSEL's is a symmetric single quantum-well graded-index separate-confinement heterojunction grown by metalorganic chemical vapor deposition with 1.5-$\mu$m-thick $Al_{0.6}Ga_{0.4}As$ cladding layers and a 330-nm-thick graded waveguide region. The $Al_xGa_{1-x}As$ graded regions vary in composition from $x = 0.6$ to $x = 0.2$ over 150 nm. The quantum-well region consists of an 8-nm $In_{0.24}Ga_{0.76}As$ quantum well with 12-nm GaAs layers on either side. A 50-nm-thick GaAs stop etch layer in the p-cladding region and its image are positioned 400 nm from the waveguide region. The material is fabricated into devices with a process sequence that begins with mesa etching to define broad area stripes. Mesas 100-$\mu$m wide and 0.6-$\mu$m high are etched in a solution of $H_2SO_4 : H_2O_2 : H_2O$ (1 : 8 : 160). A 1000 Å $Si_3N_4$ layer is then deposited on the sample, using plasma enhanced chemical vapor deposition. In order to make contact to the p-layer, photoresist is applied to open windows (800 $\mu$m × 100 $\mu$m, separated by 50 $\mu$m) on the mesa top for $CF_4$ etching of the $Si_3N_4$. Ti–Pt–Au is e-beam deposited as p-contact. Lithographic patterning to define the output mirror opening is followed by selective etching to remove the GaAs cap layer (Citric Acid:$H_2O_2$/4:1) and the AlGaAs cladding layer (HF).

Manuscript received March 27, 1995; revised May 30, 1995. This work was supported by ARPA through the Ultra program and by the Office of Naval Research.

The authors are with the National Center for Integrated Photonic Technology, Department of Electrical Engineering/Electrophysics, University of Southern California, Los Angeles, CA 90089-0483 USA.

IEEE Log Number 9414246.

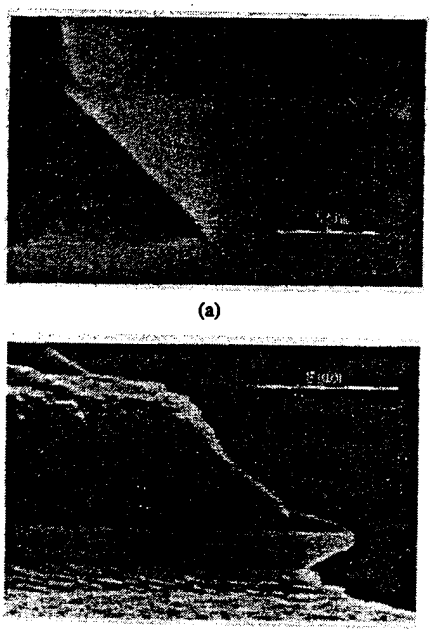

Fig. 2. (a) A SEM picture showing the cross section of an ion-beam-etched 45° deflector. (b) A SEM picture showing the smoothness of an ion-beam-etched 45° deflector.

The quality of the single-layer IBE photoresist mask, in terms of profile and smoothness, is crucial to good results in IBE of the 45° deflecting mirrors. Nearly vertical side walls and smooth edges must be achieved to etch facets with high quality. IBE is performed at $9 \times 10^{-5}$ torr with an $Ar^+$ ion beam at 800 eV on Technics 300 Series TLA 5.5 ion beam milling system. For a 1-$\mu$m-deep 45° undercut, the sample is tilted by 70° and etched for 180 min. The SEM pictures, shown in Fig. 2(a) and (b), indicate that smooth etched 45° deflectors have been obtained. An optimum separation between the IBE window and the end of the p-contact is required to allow efficient mode coupling, while at the same time allowing efficient pumping of the end of the active region. This separation is chosen to be 2–5 $\mu$m. After the sample is lapped down to about 100 $\mu$m, AuGe–Ni–Au is e-beam deposited on the bottom of the sample and alloyed at 400° for 40 s as the n-contact.

The FCSEL design employed here positions the output mirror as close to the waveguide as possible to reduce the light path through unguided region to minimize the diffraction loss. The calculations reported by N. C. Frateschi *et al.* [8] indicate an increase of the beam divergence and a strong reduction of the feedback as the unguided region path is increased. In our FCSEL structure, the unguided region can be easily reduced by controlling output mirror position relative to the waveguide with the stop etch layer. In this work we choose 0.4 mm.

The lasers are tested under pulsed operation (500 ns pulse width, 10 kHz repetition rate). The emission spectra exhibit multiple modes centered around ~990 nm. Fig. 3 shows a typical *L–I* curve for a FCSEL ($L$ = 640 mm) consisting of one vertical output mirror and one cleaved facet. The threshold current density is 133 A/cm$^2$ and the external quantum efficiencies are 41% (0.52 W/A) and 38% (0.48 W/A)

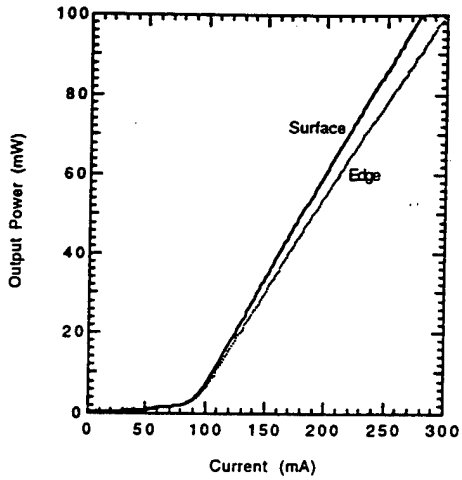


Fig. 3. Typical *L–I* curves of emission from surface and edge for a FCSEL ($L$ = 640 mm), consisting of a vertical output mirror, $\alpha_n$ = internal 45° deflector and a cleaved mirror, under pulsed operation at room temperature.

for the light output from the top surface and the cleaved facet, respectively, which gives a total external quantum efficiency of 79%. The slight improvement of the surface output over the cleaved edge suggests that the effective reflectivity here may be slightly smaller. For comparison, broad-area cleaved lasers ($L$ = 650 mm) made from this material have the threshold current density of 108 A/cm$^2$ and the external quantum efficiency of 78%.

Fig. 4 shows a typical *L–I* curve for a broad area FCSEL ($L$ = 800 mm), consisting of two vertical output mirrors and two internal 45° deflectors. The threshold current density is 112.5 A/cm$^2$ and the external quantum efficiency is 65% (0.82 W/A) for surface emission. The performance of these monolithic FCSEL's can be compared to cleaved edge-emitting lasers fabricated from the same material. Additional losses such as diffraction loss ($\alpha_{\text{diff}}$), coupling loss ($\alpha_{\text{coupl}}$), and scattering loss ($\alpha_{\text{scatt}}$) are introduced in FCSEL's that will compromise the performance. These additional losses resulting from a folded-cavity can be written as

$$\alpha_{\text{FC}} = \alpha_{\text{diff}} + \alpha_{\text{coupl}} + \alpha_{\text{scatt}}. \tag{1}$$

The external quantum efficiency $\eta_d$ of a FCSEL is defined as

$$\eta_d = \eta_i \frac{\alpha_m}{\alpha_m + \alpha_{\text{int}} + \alpha_{\text{FC}}} \tag{2}$$

where $\eta_i$ is the internal quantum efficiency, $\alpha_m$, $\alpha_{\text{int}}$ are the mirror loss and the internal loss, respectively. The internal quantum efficiency and the internal loss for the edge-emitting lasers made from this material are 92% and 1.7 cm$^{-1}$, respectively. Using the 65% for the total external quantum efficiency of the FCSEL, therefore, the additional loss due to the folded-cavity, $\alpha_{\text{FC}}$, is estimated as 4.2 cm$^{-1}$ for the above devices.

The broad-area GaAs–AlGaAs FCSEL's ($L$ = 500 $\mu$m), reported by S. S. Ou *et al.* [4], have threshold current density of 360 A/cm$^2$ and surface-emission quantum efficiency of 22%. W. D Goodhue *et al.* [7] demonstrated 2-D arrays of InGaAs–AlGaAs FCSEL's ($L$ = 1000 mm) with threshold current density of 185 A/cm$^2$ and surface-emission quantum

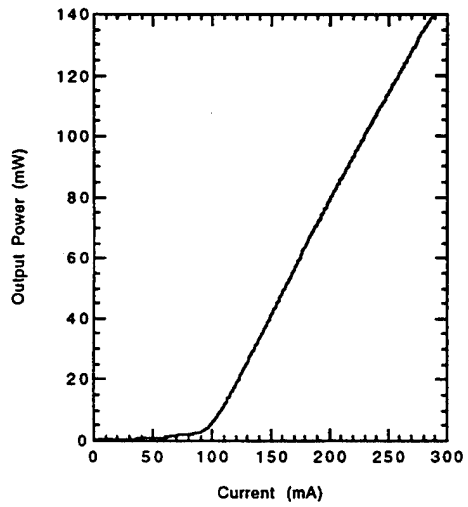


Fig. 4. A typical $L$–$I$ curve of surface emission for the FCSEL's ($L$ = 800 mm), consisting of two output mirror and two internal 45° deflectors, underpulsed operation at room temperature.

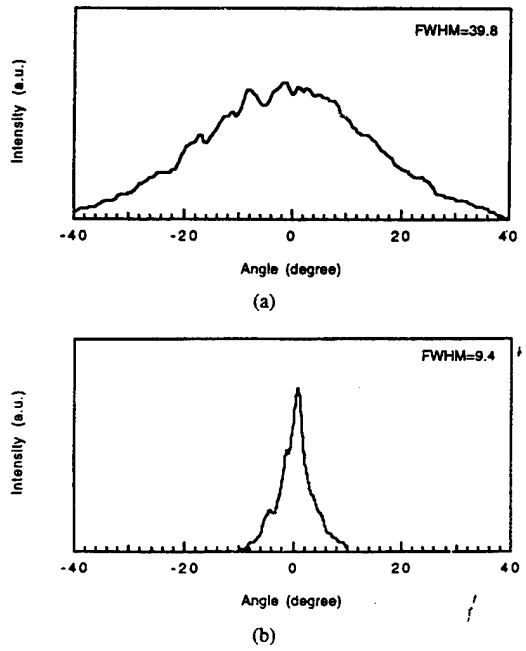


Fig. 5. The far-field profiles for the surface emission (a) perpendicular to the junction and (b) parallel to the junction.

efficiency of 28% per facet. To the best of our knowledge, the FCSEL's ($L$ = 800 mm) reported here, have the lowest threshold current density (112.5 A/cm$^2$) and the highest total quantum efficiency (65%).

The surface emission far-field patterns were measured at 40 mW output power level under CW operation. Fig. 5 shows the far-field profiles for surface emission perpendicular and parallel to the junction. The full widths at half maximum (FWHM) of the far-field perpendicular ($\theta_\perp$) and parallel ($\theta_{//}$) to the junction are 39.8° and 9.4°, respectively. These FWHM values are comparable to those of edge-emitting broad-area lasers.

## II. Conclusion

In conclusion, we report the fabrication of high-quality 45° deflectors using ion-beam-etching (IBE) technique, and the characteristics of simply designed InGaAs–GaAs FCSEL's with high performance. The FCSEL's (cavity length 800 mm), consisting of two internal 45° deflectors, are obtained with a threshold current density of 112.5 A/cm$^2$ and an external quantum efficiency of 65% (0.82 W/A) for surface emission. The additional loss due to the folded-cavity is estimated as 4.2 cm$^{-1}$. It may be possible to improve the performance of the FCSEL's presented here. For example, the 0.4 mm separation between the horizontal output mirror and the top waveguide layer of the FCSEL may not be optimum. It may be further reduced to decrease the diffraction loss. Second, antireflection (AR) and high-reflection (HR) coatings may be applied to the output mirrors so that more surface-emitting power can be achieved at one mirror. The high-quality 45° deflectors and the resulting high performance InGaAs–GaAs FCSEL's, presented here, suggest the potential fabrication of high-performance monolithic 2-D arrays of FCSEL's.

## Acknowledgment

The authors wish to thank S. S. Ou for help on the IBE technique, F. Fang, M. Jansen, K. Walker, and J. J. Yang for testing assistance, H. Zhao, M. H. MacDougal, and K. Uppal for useful discussions.

## References

[1] C. P. Chao, K. K. Law, and J. L. Merz, "Design and fabrication of ridge waveguide folded-cavity in-plane surface-emitting lasers," *IEEE Photon. Technol. Lett.*, vol. 4, pp. 223–227, 1992.

[2] N. C. Frateschi, P. D. Dapkus, S. S. Ou, J. J. Yang, and M. Jansen, "Low threshold InGaAs/GaAs 45° folded-cavity surface-emitting lasers grown on structured substrates," *IEEE Photon. Technol. Lett.*, vol. 5, pp. 741–743, 1993.

[3] F. R. Gfeller, P. Buchmann, K. Dätwyler, J. P. Reithmaier, P. Vettiger, and D. J. Webb, "50 mW CW operated single-mode surface-emitting AlGaAs lasers with 45° total reflection mirrors," *IEEE Photon. Technol. Lett.*, vol. 4, pp. 698–700, 1992.

[4] S. S. Ou, M. Jansen, J. J. Yang, and M. Sergant, "High-power CW operation of GaAs/AlGaAs surface-emitting lasers mounted in the junction-up configuration," *Appl. Phys. Lett.*, vol. 59, pp. 1037–1039 1991.

[5] D. W. Nam, R. G. Waarts, D. F. Welch, and D. R. Scifres, "Operating characteristics of high continuous power (50 W) two-dimensional surface-emitting laser arrays," *IEEE Photon. Technol. Lett.*, vol. 5, pp. 281–284, 1993.

[6] J. P. Donnelly, W. D. Goodhue, C. A. Wang, R. J. Bailey, G. A. Lincoln, G. D. Johnson, L. J. Missaggia, and J. N. Walpole, "CW operation of monolithic arrays of surface-emitting folded-cavity InGaAs/AlGaAs diode lasers," *IEEE Photon. Technol. Lett.*, vol. 5, pp. 747–750, 1993.

[7] W. D. Goodhue, J. P. Donnelly, C. A. Wang, G. A. Lincoln, K. Rauschenbach, R. J. Bailey and G. D. Johnson, "Monolithic two-dimensional surface-emitting strained-layer InGaAs/AlGaAs and AlInGaAs/AlGaAs diode laser arrays with over 50% differential quantum efficiencies," *Appl. Phys. Lett.*, vol. 59, pp. 632–634, 1991.

[8] N. C. Frateschi, P. D. Dapkus, S. S. Ou, J. J. Yang, and M. Jansen, "Analysis of nonplanar wave propagation through multilayer bragg reflectors for folded cavity and vertical cavity surface emitting laser structures," *IEEE J. Quantum Electron.*, vol. 31, no. 4, pp. 627–635, 1995.

[9] C. P. Chao, G. J. Shiau, and S. R. Forrest, "1.3 mm wavelength, InGaAsP-InP folded-cavity surface-emitting lasers grown by gas-source molecular-beam epitaxy," *IEEE Photon. Technol. Lett.*, vol. 6, pp. 1406–1408, 1994.

# Lasing Characteristics of High-Performance Narrow-Stripe InGaAs–GaAs Quantum-Well Lasers Confined by AlAs Native Oxide

Yong Cheng, P. Daniel Dapkus, *Fellow, IEEE*, Michael H. MacDougal, *Student Member, IEEE*, and Gye Mo Yang

*Abstract*— **High-performance narrow-stripe InGaAs–GaAs quantum-well lasers with integral buried AlAs native-oxide layers have been fabricated. AlAs native-oxide layers above and below waveguide region were employed for current and optical confinement to form narrow-stripe lasers. A low temperature (400 °C) anisotropic wet oxidation technique was used to selectively oxidize AlAs layers in the epitaxial structure. The devices demonstrated continuous wave threshold currents of 3.5 mA, external quantum efficiencies of 82%, and a characteristic temperature of 133 K for 1.8 $\mu$m-wide aperture, 400 $\mu$m-long devices. Threshold currents of 1.7 mA were obtained by applying HR/HR coatings.**

## I. Introduction

SEMICONDUCTOR laser diodes with near-mA threshold currents and high quantum efficiencies are needed for application to optoelectronic integrated circuits (OEIC's) and in optical interconnects. High-performance index-guided lasers have been reported by several groups [1], [2]. These devices usually require more complex processing than, for example, ridge waveguide or oxide stripe lasers. Oxide stripe gain-guided lasers are simple to fabricate but current spreading and lateral carrier diffusion in the active layer adversely influence the emission properties and limit the practical applications of these devices [3].

There has been interest in recent years to apply buried layers of a native oxide to optoelectronic devices because it is an insulator and has a low refractive index ($n \sim 1.55$). The native-oxide of AlGaAs provides both electronic and optical confinement making it possible to fabricate low threshold, high efficiency lasers. In addition, its use simplifies processing of lasers. For edge-emitting lasers, the native-oxide of AlGaAs has been utilized to fabricate stripe-geometry lasers [4] and index-guided lasers [5]. For vertical-cavity surface-emitting lasers, the native-oxide of AlAs has been employed in DBR structures, [6] and for current constriction [7], [8] to achieve low threshold devices. Maranowski *et al.* [4] demonstrated a stripe-geometry structure in which the laser stripe is defined by both top and bottom native-oxide layers. AlGaAs native-oxide confined InGaAs–GaAs narrow-stripe lasers (~2.5 $\mu$m-wide aperture, 305 $\mu$m-long cavity) were reported with threshold currents of 8 mA and quantum efficiency of 61%. This paper explores further the design and properties of these lasers with the goal of optimizing their performance, quantifying the degree of optical and carrier confinement and comparing their properties to state of the art buried heterostructure lasers.

Manuscript received September 1, 1995; revised October 25, 1995. This work is supported in part by ARPA through the Ultra program and by the Office of Naval Research.

The authors are with the Department of Electrical Engineering/Electrophysics, National Center for Integrated Photonic Technology, University of Southern California, Los Angeles, CA 90089-0483 USA.

Publisher Item Identifier S 1041-1135(96)00924-X.

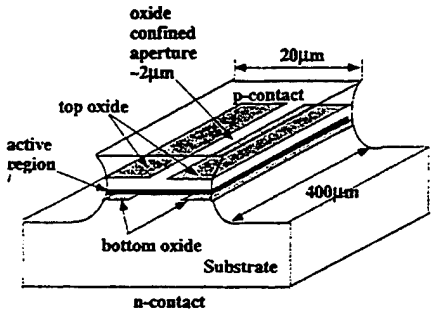


Fig. 1. Schematic diagram of narrow-stripe InGaAs–GaAs quantum-well laser confined by native oxide layers above and below the waveguide region.

## II. Device Design and Fabrication

The device design is schematically shown in Fig. 1. The AlAs layers above and below the waveguide region are oxidized from the edge of an etched mesa to form a narrow-stripe structure. Since the native-oxide of AlAs is an insulator with a small refractive index, both electronic and optical confinement is expected in this structure. Because the oxidation rate of AlGaAs depends strongly on Al composition, [9] AlAs is used in our devices to minimize effect of composition nonuniformity and to increase reproducibility. Use of the binary AlAs instead of the ternary AlGaAs relaxes the composition requirements to obtain the desired oxide profile and also decreases the oxidation time. Ultimately, an alloy would be used in the oxide layer to guarantee reliability. Since the top native-oxide layer forms a current constriction aperture, it must be placed close to the waveguide to minimize current spreading effects.

The laser structure in this work is a single quantum-well graded-index separate-confinement heterojunction grown by metalorganic chemical vapor deposition. 1000 Å n- and p-type AlAs layers are placed below and above the InGaAs–GaAs active region, respectively. The top AlAs layer is about 2500 Å above the active region. The mesas to expose the edge of the AlAs layers for oxidation are formed by wet chemical

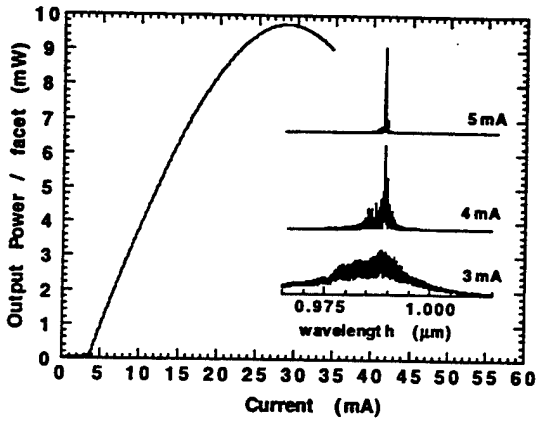


Fig. 2. A typical L–I curve for device with 1.8 $\mu$m-wide aperture, 400 $\mu$m-long cavity under CW operation at room temperature. The inset shows the spectra for the device at different pumping levels.

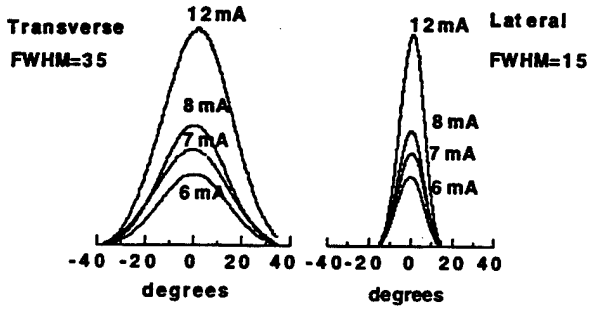


Fig. 3. The far-field patterns of the device at different pumping levels from 6–12 mA.

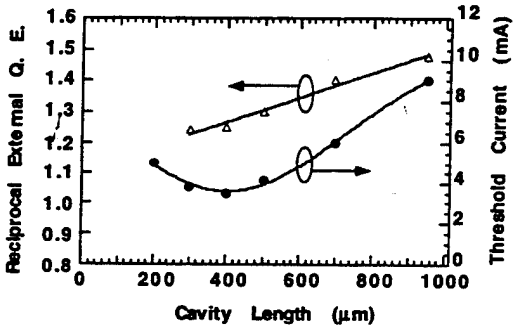


Fig. 4. The cavity length dependence of the threshold current and the reciprocal external quantum efficiency ($\eta_d^{-1}$).

etching using an $H_2O$–$H_2O_2$–$H_2SO_4$ (160:8:1) solution. The oxidation is performed at 400 °C in $H_2O$-vapor-saturated $N_2$. The aperture defined by top AlAs oxide layer is about 1.8 $\mu$m after 8.5 min oxidation. The lower oxide aperture is wider owing to the doping dependence of the oxidation process [10]. After oxidation, the sample is fully covered by $Si_3N_4$ using PECVD and 10 $\mu$m-wide stripes are opened on the mesa top using a $CF_4$ plasma etching. Ti–Pt–Au is e-beam deposited on the mesa top as the p-contact. After the sample is lapped down to about 100 $\mu$m, AuGe–Ni–Au is e-beam deposited on the bottom of the sample as the n-contact. Finally, the sample is alloyed at 400 °C for 40 s. The wafer is then cleaved into laser bars for testing.

## III. Device Characteristics

The devices are probe-tested under continuous wave operation at room temperature without an intentional heat sink. A typical light output versus current curve for device with 1.8 $\mu$m-wide aperture, 400 $\mu$m-long cavity is shown in Fig. 2. A threshold current of 3.5 mA ($J_{th} \sim 490$ A/cm$^2$) is obtained with external quantum efficiency of 82%. The pulsed threshold current density of broad area lasers (100 $\mu$m-wide) made from the same material is 70 A/cm$^2$ for a 1500 $\mu$m cavity length. Thermal effects influence the output power when the pumping current is 25 mA or more in these unbonded devices. The devices have operated stably in the laboratory under all test conditions. No evidence for short term degradation has been observed in our limited testing nor in VCSEL strucutres tested at Sandia [11]. By applying high-reflection (HR) dielectric ($SiO_2$–Si) coating on one facet, a threshold current of 2.6 mA is obtained. The threshold current is 1.7 mA with both facets HR coated. The inset in Fig. 2 shows the spectra for the uncoated device at different pumping levels. From 3–4 mA, the spectrum narrows down considerably. In the above-threshold regime, particularly when $I > 5$ mA, single longitudinal mode operation becomes dominant as the power in side modes saturates. This suggests that good current and optical confinement exist in these narrow-stripe structures.

The far-field patterns are measured under CW operation at room temperature at different pumping levels from 6–12 mA, as shown in Fig. 3. The full width at half maximum (FWHM) of the far-field perpendicular and parallel to the junction plane are 35° and 15°, respectively. The CW threshold currents vary from 3–4.7 mA in the temperature range of 0–50 °C with a characteristic temperature of 133 K.

Fig. 4 shows the cavity length dependence of the threshold current and the reciprocal external quantum efficiency ($\eta_d^{-1}$). Low threshold currents can be expected for laser cavity lengths in the range of 300–500 $\mu$m. The threshold current increases anomalously as the cavity length exceeds 500 $\mu$m. The cause of this increase is under investigation, but we speculate that some nonuniformity of oxide aperture along the laser may be the cause. From the cavity length dependence of $\eta_d^{-1}$, the internal quantum efficiency and the internal losses for such narrow-stripe lasers are estimated as 90.2% and 4.1 cm$^{-1}$, respectively.

In Fig. 5, the threshold currents for devices with different current aperture widths are plotted. Compared with the device reported by Maranowski *et al.* [4], the lasers in this work have lower threshold and higher efficiency. The data reported by H. Zhao *et al.* [1] for buried-heterostructure lasers grown on the nonplanar substrates are also shown in Fig. 5 for comparison. Those devices exhibit lower threshold current at comparable width, presumably due to better lateral confinement of the carriers and the optical fields.

In Fig. 6, the threshold currents and quantum efficiencies for 25 devices (400 $\mu$m-long cavity) on a laser bar are plotted. It can be seen that the threshold currents and the quantum efficiencies are 3.8 ± 0.3 mA and 79 ± 3%, respectively, for the devices along the bar. Such good uniformity of high perfor-

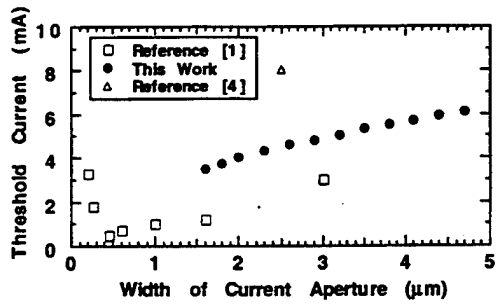


Fig. 5. Threshold currents for the devices with different width of current aperture. Data from [1] and [4] are also shown for comparison.

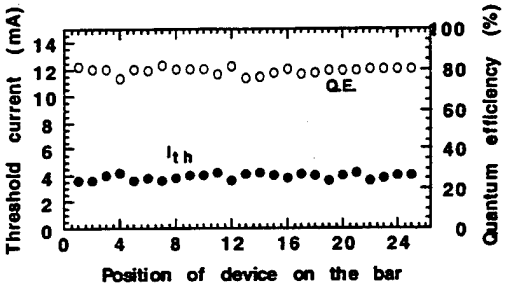


Fig. 6. The distribution of threshold current and quantum efficiency for 25 devices (400 $\mu$m-long cavity) on a laser bar.

mance lasers suggests potential application of this technology to laser arrays.

## IV. Summary

In conclusion, we report the fabrication and characteristics of the low threshold current and high efficiency narrow-stripe InGaAs–GaAs quantum-well lasers confined by AlAs native-oxide layers. AlAs native-oxide layers above and below waveguide region are employed for current and optical confinement. The low temperature (400 °C) selective wet oxidation technique is used to achieve native oxide layers. The devices demonstrate continuous wave threshold currents of 3.5 mA, external quantum efficiencies of 82%, and characteristic temperature of 133 K for 1.8 $\mu$m-wide aperture, 400 $\mu$m-long cavity. The threshold currents of 1.7 mA are obtained by applying HR coatings.

## Acknowledgment

The authors wish to thank F. Fang, K. Walker, M. Jansen, J. J. Yang for testing assistance, and K. Uppal for useful discussions.

## References

[1] H. Zhao, M. H. MacDougal, P. D. Dapkus, K. Uppal, Y. Cheng, and G. M. Yang, "Submilliampere threshold current InGaAs/GaAs/AlGaAs lasers and laser arrays grown on nonplanar substrates," *J. Select. Topics Quantum Electron.*, vol. 1, no. 2, pp. 196–202, June 1995.

[2] Y. K. Sin, H. Horikawa, Y. Matsui, and T. Kamijoh, "Ultralow laser threshold and high speed InGaAs–GaAs–InGaP buried heterostructure strained quantum well lasers for optical interconnects," *Electron. Lett.*, vol. 29, pp. 873–874, 1993.

[3] H. C. Casey, Jr. and M. B. Panish, *Heterostructure Lasers.* New York: Academic, 1978, pt. B, pp. 217–224.

[4] S. A. Maranowski, A. R. Sugg, E. I. Chen, and N. Holonyak, Jr., "Native oxide top- and bottom-confined narrow stripe p–n $Al_yGa_{1-y}As$–GaAs–$In_xGa_{1-x}As$ quantum well heterostructure laser," *Appl. Phys. Lett.*, vol. 63, pp. 1660–1662, 1993.

[5] S. J. Caracci, F. A. Kish, N. Holonyak, Jr., S. A. Maranowski, S. C. Smith, and R. D. Burnham, "High-performance planar native-oxide buried-mesa index-guided AlGaAs–GaAs quantum well heterostructure lasers," *Appl. Phys. Lett.*, vol. 61, pp. 321–323, 1992.

[6] M. H. MacDougal, P. D. Dapkus, V. Pudikov, H. Zhao, and G. M. Yang, "Ultralow threshold current vertical-cavity surface-emitting lasers with AlAs oxide-GaAs distributed Bragg reflectors," *IEEE, Photon. Technol. Lett.*, vol. 7, p. 229, 1995.

[7] D. L. Huffaker, D. G. Deppe, and K. Kumar, "Native-oxide defined ring contact for low threshold vertical-cavity lasers," *Appl. Phys. Lett.*, vol. 65, pp. 97–99, 1994.

[8] G. M. Yang, M. H. MacDougal, and P. D. Dapkus, "Ultralow threshold current vertical-cavity surface-emitting lasers obtained with selective oxidation," *Electron. Lett.*, vol. 31, no. 11, pp. 886–888, 1995.

[9] K. D. Choquette, R. P. Schneider, Jr., K. L. Lear, and K. M. Geib, "Low threshold voltage vertical-cavity lasers fabricated by selective oxidation," *Electron. Lett.*, vol. 30, pp. 2043–2044, 1994.

[10] F. A. Kish, S. A. Maranowski, G. E. Höfler, N. Holonyak, Jr., S. J. Caracci, J. M. Dallesasse, and K. C. Hsieh, "Dependence on doping type (p/n) of the water vapor oxidation of high-gap $Al_xGa_{1-x}As$," *Appl. Phys. Lett.*, vol. 60, pp. 3165–3167, 1994.

[11] K. D. Coquette, R. P. Schneider, Jr., K. L. Lear, M. Hagerott Crawford, K. M. Geib, J. J. Figiel, and R. Hull, "Robust and wavelength insensitive performance of selectively oxidized vertical cavity lasers," in *Talk TuD7-1 at OSA Conf. Semiconductor Lasers: Advance Devices and Applications*, Keystone, CO, Aug. 1995.

# Low-Threshold Native-Oxide Confined Narrow-Stripe Folded-Cavity Surface-Emitting InGaAs–GaAs Lasers

Yong Cheng, Gye Mo Yang, Michael H. MacDougal, and P. Daniel Dapkus, *Fellow, IEEE*

***Abstract*—Narrow-stripe folded-cavity surface-emitting InGaAs–GaAs lasers are demonstrated. AlAs native-oxide layers above and below waveguide region are employed for current and optical confinement to form narrow-stripe InGaAs–GaAs quantum-well lasers. A low-temperature (400 °C) selective wet-oxidation technique and an ion-beam-etching technique are used to fabricate insulator confined narrow-stripes and internal 45° deflectors, respectively. Continuous-wave threshold currents as low as 4.5 mA and 59% surface-emitting quantum efficiencies are achieved on the devices with a 2-$\mu$m-wide aperture and a 420-$\mu$m-long cavity.**

## I. Introduction

LOW-THRESHOLD and high-efficiency folded-cavity surface-emitting lasers (FCSEL's) are of great interest for application to optoelectronic integrated circuits (OEIC's) and free-space optical interconnects. FCSEL's employing dry-etched internal 45° deflectors to couple the light in the horizontal cavity toward the surface have the advantage of a much longer gain path. These devices are suitable for incorporation into three-terminal voltage-controlled device designs that are useful in OEIC's [1]. High-power GaAs–AlGaAs narrow-ridge waveguide [2] and broad-area [3] FCSEL's as well as high-power two-dimensional arrays of FCSEL's [4], [5] have been demonstrated. Threshold currents of 8 mA for InGaAs–GaAs FCSEL's incorporating high-reflectivity epitaxial Bragg reflectors, based on ridge waveguide structures [6] or nonplanar substrate structures [7], have been reported. Recently, we have demonstrated high-performance broad-area InGaAs–GaAs FCSEL's by using a novel folded-cavity design and a well-developed ion-beam-etching (IBE) technique [8]. In our FCSEL's design, the diffraction loss is reduced to result in low-threshold, high-efficiency lasers without employing Bragg reflectors [8], [9]. As a result, much less stringent requirements for growth control are obtained.

In this letter, we report the fabrication and characteristics of narrow-stripe folded-cavity surface-emitting InGaAs–GaAs lasers. Stripe formation in our devices is formed by selectively oxidizing buried AlAs layers to form a current constriction aperature similar to the work of S. A. Maranowski *et al.* [10]. Low-temperature (400 °C) selective wet oxidation and ion-beam-etching techniques are used to fabricate native-oxide confined narrow-stripes and internal 45° deflectors, respectively. Continuous-wave threshold currents as low as 4.5 mA and 59% surface-emitting quantum efficiencies are achieved on devices with a 2-$\mu$m-wide aperture and a 420-$\mu$m-long cavity.

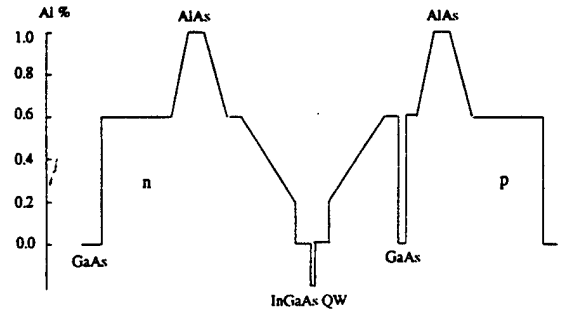


Fig. 1. The schematic of the conduction band of laser structurewith AlAs layers above and below the waveguide region for oxidation.

The laser structure, as shown in Fig. 1, is a single quantum well graded-index separate-confinement heterojunction with 60% Al confining layers and 20% Al barriers grown by metalorganic chemical vapor deposition. The structure also contains two 1000 Å AlAs layers to be partially oxidized as current constriction layers and a GaAs etch-stop layer. The AlAs layers are placed above and below the GaAs–InGaAs active region at a distance of 3000 Å and 2500 Å, respectively. These layers are also surrounded by 500-Å AlGaAs graded layers to reduce stress after oxidation. The GaAs etch-stop layer is designed as the output mirror for surface emission and is located 500 Å above the waveguide region.

50-$\mu$m-wide stripes to define the output mirrors are first patterned and etched down to the GaAs stop layer using GaAs (citric acid : $H_2O_2$/4 : 1) and AlGaAs (HF solution) selective etches. After coating with PECVD $Si_3N_4$, the sample is patterned with 20-$\mu$m-wide stripes and mesa etched to expose both AlAs layers for oxidation. The oxidation is performed in a furnace at 400 °C in which $H_2O$-vapor-saturated $N_2$ is flowing. Normally, the oxidation rate of $p$-type AlAs is faster than that of $n$-type AlAs [11]. An SEM picture of the oxidized mesa cross-section is shown in Fig. 2(a). The current aperture defined by top AlAs oxide layer is about 2 $\mu$m after 8 min oxidation. The top view of the mesa under optical

Manuscript received June 14, 1995; revised August 17, 1995. This work was supported in part by ARPA through the Ultra program, and by the Office of Naval Research.

The authors are with the National Center for Integrated Photonic Technology, Department of Electrical Engineering/Electrophysics, University of Southern California, Los Angeles, CA 90089-0483 USA.

IEEE Log Number 9415365.

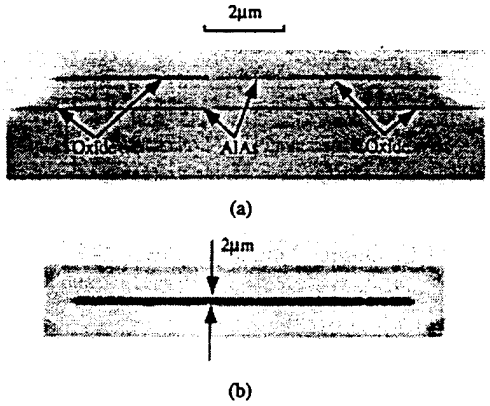


Fig. 2. (a) An SEM picture of the oxidized mesa cross-section. The aperture defined by the top AlAs oxide layer is about 2 $\mu$m. (b) The top view of the oxidized mesa under optical microscope.

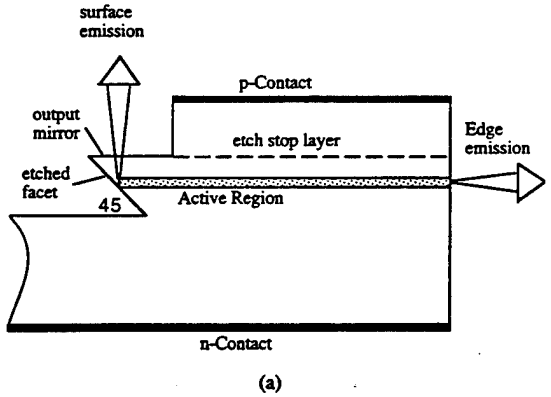


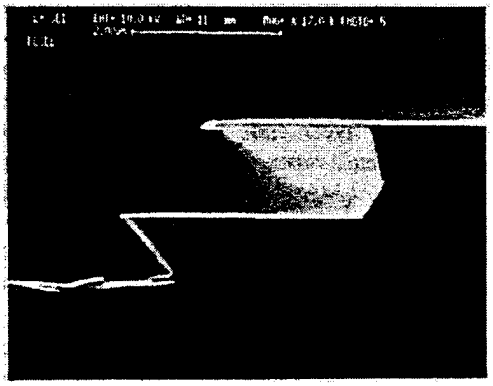


Fig. 3. (a) The schematic of a device for folded-cavity surface-emitting lasers. (b) An SEM picture of a FCSEL with wet-etched output mirror and ion beam-etched 45° deflector.

microscope is shown in Fig. 2(b). After oxidation, the sample is fully covered by $Si_3N_4$ using PECVD, 10-$\mu$m-wide stripes are opened on the mesa top, and Ti–Pt–Au contact pads are $e$-beam deposited as the p-contact. A single layer of photoresist is chosen as mask for IBE of the 45° deflecting mirrors. The IBE processing technique was described elsewhere [4]. After the sample is lapped down to about 100 $\mu$m, AuGe–Ni–Au is $e$-beam deposited on the bottom of the sample as $n$-contact. Finally, the sample is alloyed at 400 °C for 40 s. FCSEL's, consisting of a horizontal output mirror, an internal

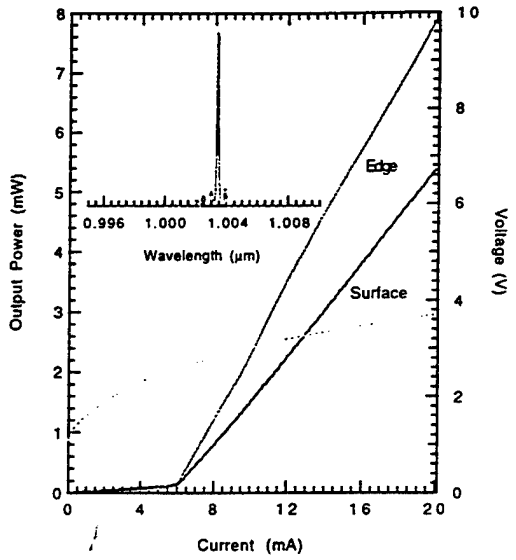


Fig. 4. The typical L-I and V-I curves for devices with a 2-$\mu$m-wide aperture and a 420-$\mu$m-long cavity. The inset shows a laser spectrum at 9 mA.

45° deflector, and a cleaved mirror, are schematically shown in Fig. 3(a). An SEM picture in Fig. 3(b) shows a wet-etched output mirror and an ion beam-etched 45° deflector.

The devices are tested under continuous wave (CW) operation at room temperature without a heat sink. The typical L-I and V-I curves for devices with 2-$\mu$m-wide apertures and 420-$\mu$m-long cavities are shown in Fig. 4. Threshold currents of 6 mA are obtained with external quantum efficiencies of 44% (0.55 W/A) and 31% (0.38 W/A) for edge emission and surface emission, respectively, which results in total quantum efficiency of 75%. A laser spectrum at 1.5 $I_{th}$ pumping current, as shown in the inset of Fig. 4, exhibits good single-mode operation. As shown in Fig. 4, the quantum efficiency for edge emission is higher than that for surface emission, which suggests that the effective reflectivity at the folded-cavity end is higher than that of cleaved facet ($R = 0.32$). This may result from an uncontrolled change in the reflectivity of the output mirror or from an interference effect between the oxide layer and the top surface at the folded cavity end of the structure. Also, the scattering losses due to roughness of etched facet at the folded-cavity end may cause less transmitted light for surface emission. The characteristic temperature ($T_0$) of FCSEL's is about 136 K in the temperature range from 0 °C to 50 °C at CW operation. For comparison, the native-oxide confined narrow-stripe edge-emitting lasers with two cleaved mirrors made from the same material have cw threshold currents of 6 mA and total quantum efficiencies of 82%. The pulsed (500-ns-width, 10-kHz repetition rate) threshold current density of broad-area lasers (100-$\mu$m-wide stripes) made from the same material is 70 A/cm$^2$ for a 1500-$\mu$m cavity length. The narrow-stripe cleaved lasers (~2.5-$\mu$m-wide aperture, 305-$\mu$m-long cavity) reported by S. A. Maranowski *et al.* [10] have CW threshold current of 8 mA and quantum efficiency of 61%. In native-oxide confined narrow-stripe laser structures, the active region width is thought to be wider than current aperture owing to current spreading.

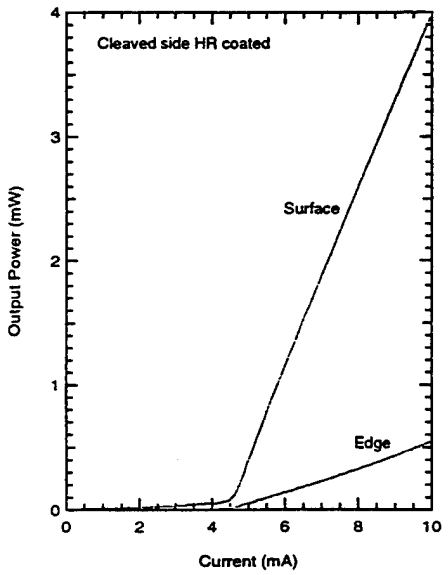


Fig. 5. The L-I curves for the FCSEL's with cleaved facet HR coated.

The far-field patterns (data not shown) for the devices with cleaved facets show the full width at half maximum (FWHM) of the beam perpendicular and parallel to the junction plane are 35° and 15°, respectively, independent of current above threshold. Far-field patterns for FCSEL's have not yet been measured but there is no particular reason to expect significant differences in the surface-emission far-field patterns from those of edge emission.

To date, 8 mA is the best reported threshold current for InGaAs–GaAs FCSEL's by C. P. Chao *et al.* [6] on ridge waveguide structure, and N. Frateschi *et al.* [7] in a buried structure on a nonplanar substrate, with surface-emitting quantum efficiencies of 22% and 10%, respectively. These two structures are essentially HR/AR or HR/HR coated devices because of their use of high-reflectivity epitaxial Bragg reflectors. The FCSEL's without Bragg reflectors we present here demonstrate threshold current of 6 mA with surface-emitting quantum efficiency of 31%. By applying 90% HR dielectric coating on the cleaved facet of the above devices, a threshold current of 4.5 mA with 59% surface-emitting quantum efficiency is obtained, as shown in Fig. 5. To our best knowledge, this is the lowest threshold current reported to date for FCSEL's.

In conclusion, we report here the fabrication and characteristics of the lowest threshold current folded-cavity surface-emitting InGaAs–GaAs lasers. Low-temperature (400 °C) selective wet oxidation of AlAs is used to fabricate narrow-stripe devices and ion-beam-etching is used to fabricate the internal 45° deflectors. Continuous-wave threshold currents as low as 6 mA and 31% surface-emitting quantum efficiencies are achieved on devices with one vertical emitting facet and with a 2-$\mu$m-wide aperture, and a 420-$\mu$m-long cavity. The characteristic temperature of 136 K is obtained for this kind of structure. With HR coatings on the cleaved facet, threshold currents of 4.5 mA and surface-emitting quantum efficiencies of 59% are achieved.

## REFERENCES

[1] N. C. Frateschi, H. Zhao, J. Elliot, S. Siala, M. Govindarajan, R. N. Nottenburg, and P. D. Dapkus, "Three-terminal bistable low-threshold strained InGaAs/GaAs laser grown on structured substrates for digital modulation," *IEEE Photon. Technol. Lett.*, vol. 5, pp. 275–278, 1993.

[2] F. R. Gfeller, P. Buchmann, K. Dätwyler, J. P. Reithmaier, P. Vettiger, and D. J. Webb, "50 mW CW operated single-mode surface-emitting AlGaAs lasers with 45° total reflection mirrors," *IEEE Photon. Technol. Lett.*, vol. 4, pp. 698–700, 1992.

[3] S. S. Ou, M. Jansen, J. J. Yang, and M. Sergant, "High-power cw operation of GaAs/AlGaAs surface-emitting lasers mounted in the junction-up configuration," *Appl. Phys. Lett.*, vol. 59, pp. 1037–1039, 1991.

[4] D. W. Nam, R. G. Waarts, D. F. Welch, and D. R. Scifres, "Operating characteristics of high continuous power (50 W) two-dimensional surface-emitting laser arrays," *IEEE Photon. Technol. Lett.*, vol. 5, pp. 281–284, 1993.

[5] J. P. Donnelly, W. D. Goodhue, C. A. Wang, R. J. Bailey, G. A. Lincoln, G. D. Johnson, L. J. Missaggia, and J. N. Walpole, "CW operation of monolithic arrays of surface-emitting folded-cavity InGaAs/AlGaAs diode lasers," *IEEE Photon. Technol. Lett.*, vol. 5, pp. 747–750, 1993.

[6] C. P. Chao, K. K. Law, and J. L. Merz, "Design and fabrication of ridge waveguide folded-cavity in-plane surface-emitting lasers," *IEEE Photon. Technol. Lett.*, vol. 4, pp. 223–227, 1992.

[7] N. C. Frateschi, P. D. Dapkus, S. S. Ou, J. J. Yang, and M. Jansen, "Low threshold InGaAs/GaAs 45° folded-cavity surface-emitting lasers grown on structured substrates," *IEEE Photon. Technol. Lett.*, vol. 5, pp. 741–743, 1993.

[8] Y. Cheng, G. M. Yang, and P. D. Dapkus, "Folded-cavity surface-emitting InGaAs/GaAs lasers with low threshold current density and high efficiency," *IEEE Photon. Technol. Lett.* in press.

[9] C. P. Chao, G. J. Shiau, and S. R. Forrest, "1.3 $\mu$m wavelength, InGaAsP-InP folded-cavity surface-emitting lasers grown by gas-source molecular-beam epitaxy," *IEEE Photon. Technol. Lett.*, vol. 6, pp. 1406–1408, 1994.

[10] S. A. Maranowski, A. R. Sugg, E. I. Chen, and N. Holonyak, Jr., "Native oxide top- and bottom-confined narrow stripe $p$-$n$ AlGaAs/GaAs/InGaAs quantum well heterostructure laser," *Appl. Phys. Lett.*, 63, pp. 1660–1662, 1993.

[11] F. A. Kish, S. A. Maranowski, G. E. Höfler, N. Holonyak, Jr., S. J. Caracci, J. M. Dallesasse, and K. C. Hsieh, "Dependence on doping type ($p/n$) of the water vapor oxidation of high-gap $Al_xGa_{1-x}As$," *Appl. Phys. Lett.*, vol. 60, pp. 3165–3167, 1994.

# Microcavity effects on the spontaneous emission from InGaAs/GaAs quantum wells

G. M. Yang, M. H. MacDougal, H. Zhao,[a] and P. D. Dapkus[b]
*Department of Electrical Engineering/Electrophysics, University of Southern California, Los Angeles, California 90089-0483*

(Received 1 November 1994; accepted for publication 13 June 1994)

The spontaneous emission from an InGaAs/GaAs single-quantum well surrounded by AlAs/GaAs distributed Bragg reflectors (DBR) under the near-resonance condition between the exciton level and the confined optical mode is investigated. Under such conditions, on-axis spontaneous emission enhancement at the cavity resonant wavelength is clearly identified. The strength and character of the interaction of the exciton with the confined optical mode is determined by the dependence of photoluminescence spectra on the reflectivity of the DBR. Temperature dependence of the enhanced spontaneous emission shows the cavity resonant wavelength shifts at 0.85 Å/°C around room temperature. An increase of emission intensity at the cavity resonant wavelength with increasing temperature is also observed, which can be related to the increase of the interaction between excitonic emission and cavity mode. 

## I. INTRODUCTION

Quantum wells (QWs) embedded in microcavities have recently been employed to investigate both fundamental and applied aspects of photonics.[1–6] In a semiconductor microcavity, a high intensity optical field is confined by distributed Bragg reflectors (DBRs) composed of λ/4 multilayers. Reduction in the available photon modes in a direction perpendicular to the cavity results in an increase in the emission into allowed cavity modes. Experimental studies on the alteration of spontaneous emission characteristics in various systems have been carried out.[7–13] Much attention has been concentrated on making use of the microcavity effect in semiconductor optical devices to improve device performance in several respects, such as an extreme reduction of a threshold current for the onset of lasing, the suppression of noise, and low divergence of output beams. However, little attention has been given to the reflectivity dependence of spontaneous emission.

The thermal characteristics of vertical-cavity surface-emitting lasers (VCSELs) are uniquely determined by the relative spectral positions of the cavity resonance and laser gain. The lasing wavelength for a VCSEL is determined by the optical properties of the mirrors and the cavity. Both the gain spectrum and the cavity resonance shift to longer wavelengths, but at different rates with increasing temperature.[14–17] The temperature dependence of the cavity resonance is determined by the temperature dependence of the refractive indices, while the gain spectrum has the temperature dependence of the energy band gap. An understanding of the relationship between the gain spectrum and the cavity resonance is important in order to achieve low room-temperature thresholds, to minimize thermal quenching, and to improve high-temperature performance.

In this work, we report systematic experimental results on the reflectivity dependence of the spontaneous emission enhancement through the continuous tuning of the reflectivity, under a near resonance condition between the exciton level and the confined optical mode. This is similar to the detuning condition of a VCSEL taking into account the difference of the temperature dependence of the cavity mode and QW exciton level.[3] We also detune the interaction between the excitonic emission and cavity resonance mode by changing the temperature, which makes the emission intensity of the cavity resonance mode increase with increasing temperature. The thermal changes of the cavity resonant wavelength and the QW wavelength are determined at the same time by observing the peaks in the photoluminescence (PL) spectra.

## II. EXPERIMENTS

The vertical microcavity structure is grown by metalorganic chemical vapor deposition. The top and bottom DBRs consist of 15 pairs and 16 pairs of λ/4 AlAs/GaAs alternating layers, respectively. The 1-λ cavity consists of GaAs spacers and an 80 Å $In_{0.17}Ga_{0.83}As$ single QW at the center of the cavity. *In situ* laser reflectometry is used for thickness control of the AlAs and GaAs layers used in this structure.[18] The calculated reflectivities of bottom and top DBRs seen from the QW side are 99.1% and 99.4%, respectively. The wavelength of cavity mode is about 100 Å longer than the QW wavelength at room temperature. Because the wavelengths are distinguishable from each other, this system is ideal for measuring the temperature dependence of the QW wavelength and cavity resonant wavelength simultaneously.

In order to study DBR effects on the QW spontaneous emission clearly, the reflectivity of top DBR is continuously tuned using the selective etching of the quarter-wave stacks

[a]Present address: SDL, Inc., 80 Rose Orchard Way, San Jose, CA 95134-1365.
[b]Electronic mail: dapkus@mizar.usc.edu

 0021-8979/95/78(6)/3605/5/$6.00 

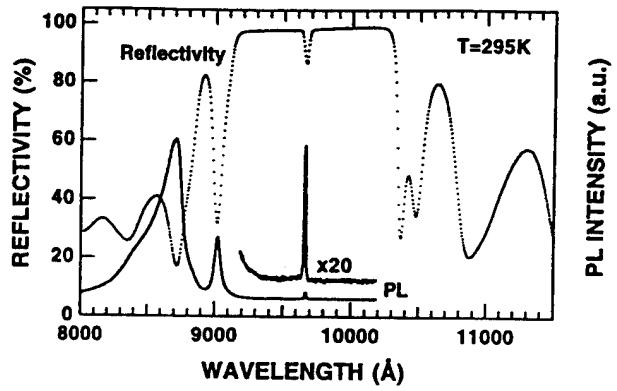


FIG. 1. Reflectivity and spontaneous emission spectra of the as-grown sample measured at room temperature. Photoluminescence was recorded with a solid angle of $\sim 3\times10^{-2}\,\pi$ measured from the normal to the epitaxial surface.

of the upper DBR. The GaAs and AlAs in DBR stacks are selectively etched using a 4:1 solution of citric acid/$H_2O_2$ and a buffered oxide etchant, respectively. After each pair is etched, the structure is characterized using PL and reflectivity measurements. Reflectivity measurements are performed using a Cary 2300 spectrophotometer in the reflection mode. The PL perpendicular to the sample surface is recorded with an acceptance solid angle of $\sim 3\times10^{-2}\pi$. The PL spectra are excited with $Ar^+$ laser through the top mirror. Since the high-reflectivity zone is away from the wavelength of the incident light, the pump laser is only slightly reflected by the top DBR mirror.

## III. RESULTS AND DISCUSSION

### A. Reflectivity-dependent spontaneous emission

Figure 1 shows the measured reflectivity and the spontaneous emission spectra of the as-grown sample at room temperature. A strong influence of the DBR reflectivity on the PL is observed. At a wavelength of 9666 Å, a dip in the reflectivity is observed, indicating the resonance mode of the cavity. $\delta$-functionlike emission spectra with a linewidth of 15 Å occurs at the cavity resonant wavelength, with the spontaneous linewidth determined by a cavity quality factor, $Q$, of about 280. It is also interesting to note the influence of the cavity resonances on the spontaneous emission of carriers excited in the GaAs layers. The PL spectrum shows peaks which coincide with the cavity transmission peaks.

The measured PL spectra at room temperature corresponding to different numbers of top DBR pairs are shown in Fig. 2. Since GaAs layers in the DBR absorb the excitation light, the spectral intensities for each condition cannot be compared with one another in an absolute sense. The spectral shapes do not change when the excitation intensity is varied from 50 (the detection limit) to 350 W/cm$^2$. The PL intensity increased linearly with the excitation intensity in this range, indicating that spontaneous emission is the dominant recombination process and stimulated emission is negligibly small. In the case of a top DBR with 15 pairs, a very sharp PL peak at 9666 Å is observed. As the number of top DBR pairs is decreased, another broad PL peak at a wavelength of 9565 Å

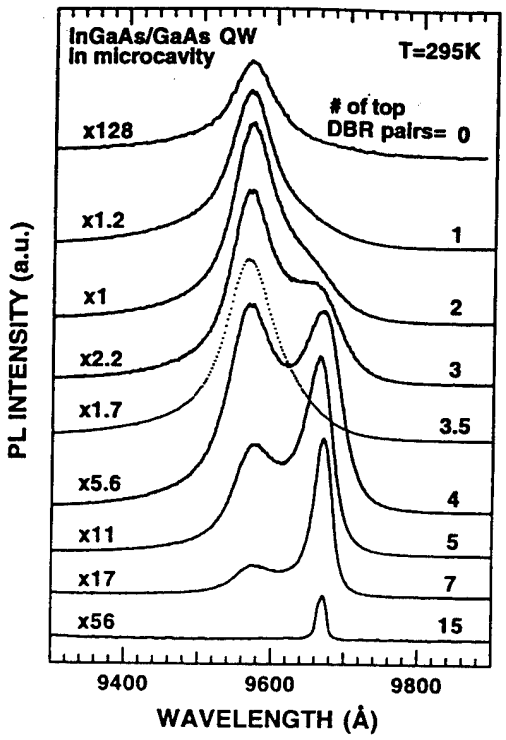


FIG. 2. Photoluminescence spectra measured at room temperature of microcavity corresponding to different numbers of top DBR pairs. The QW emission peak at 9565 Å and cavity resonance peak at 9666 Å are observed. In the case of 3.5 pairs DBR, AlAs is the topmost layer and phase matching condition is destroyed.

appears and becomes dominant. Finally, only the 9565 Å peak is seen in the structure without a cavity. This broad peak is the PL spontaneous emission of the InGaAs QW active layer without cavity resonance effects. The 9666 Å peak is related to the enhancement of the spontaneous emission of the InGaAs QW at the resonant wavelength of the cavity.

Figure 3 shows the measured reflectivity at room temperature corresponding to different numbers of top DBR pairs. Besides the resonance mode at 9666 Å, we observed an absorption-induced reflectance dip at 9565 Å due to the InGaAs QW, whose position is the same as that of its emission (see Fig. 2).[19] In particular, two dips occur in the reflectivity curve at room temperature in the structure with four pairs in the top DBR. In the structures with two or three pairs in the top DBR, the two dips cannot be resolved. However, with one pair in the top DBR, the broad and shallow dip centered at the resonant wavelength of the cavity is distinct from the QW absorption-related dip at 9565 Å. The dip at 9565 Å is still dominant in the structure without any top DBR, which consists of a bottom DBR and an active region. As the number of top DBR pairs decreases, the absorption-induced dip increases in strength in the reflectivity curve in the range of 7–3 pairs, and then weakens in the range of 2–0 pairs due to the decrease of cavity effect on QW absorption. Although the InGaAs active region is thin, optical absorption is enhanced, because of multiple reflection caused by the two DBR mirrors forming the vertical cavity. The cavity resonance dip becomes weak and broad as the number of top

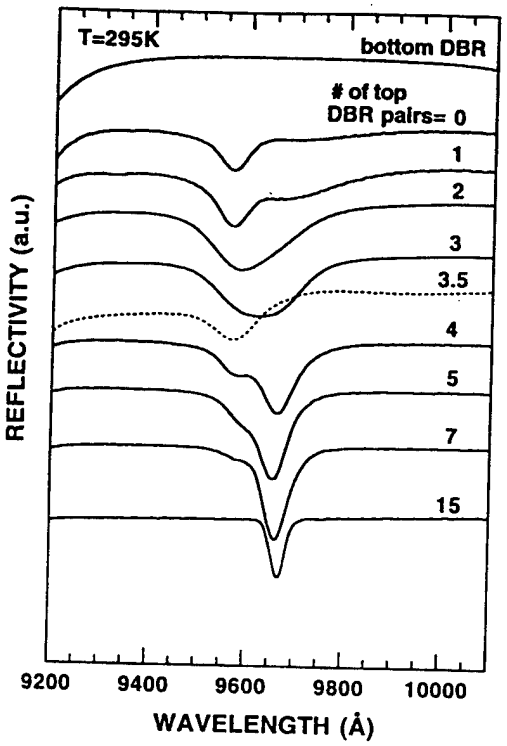


FIG. 3. Measured reflectivity spectra at room temperature of microcavity with different numbers of top DBR pairs when the wavelength detuning between QW wavelength and cavity mode wavelength is about 100 Å. In the case of 3.5 pairs DBR, AlAs is the topmost layer and phase matching condition is destroyed. The spectra are offset for clarity.

DBR pairs decreases, which is in a good agreement with theoretical results. This effect signifies that the 9565 Å dip is related to the interaction between the excitonic emission of InGaAs QW and cavity mode. Finally, the typical reflectivity curve of a DBR is observed after removing the cavity region below the top DBR.

To remove the cavity effects on InGaAs QW emission, the phase matching condition is intentionally destroyed by selective etching the GaAs layer on the top DBR. Thus, the topmost layer is AlAs. For proper phase matching, the phase of the final reflection should be equal to the phase of the previous reflection at the AlAs/GaAs interface (modulo $2\pi$). The dotted curves in Fig. 2 and Fig. 3 show the results of the structure with 3.5 pairs top DBR. In this structure, the photons reflected from the AlAs topmost layer/air interface and from the previous GaAs/AlAs interface are not phase-matched (modulo $\sim\pi/2$). Being exposed to $H_2O$ and air, the top AlAs layer is oxidized. Taking into account its refractive index of 1.55,[20] the oxidized AlAs has an optical thickness of $\sim\lambda/8$. The effect of the cavity has disappeared in PL spectrum as well as the reflectance spectrum. Only the QW spontaneous emission and absorption are observed in these curves.

In Fig. 4, we plot the experimentally determined enhancement factor in PL at the resonant wavelength as a function of the number of top DBR pairs, together with theoretical results. The modified vacuum field intensity $E^2$ in the resonance antinode position is calculated by simply assum-

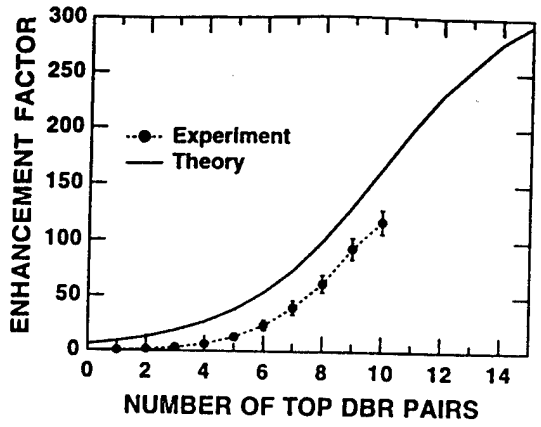


FIG. 4. Experimentally and theoretically determined spontaneous emission enhancement factor at the cavity resonant wavelength as a function of the number of top DBR pairs. The solid line is the theoretical fit and the dotted line is used as a guide for eyes.

ing two lumped reflectors with a one wavelength thickness separation based on Ref. 21 and 22

$$\frac{E^2}{E_0^2}(\theta)=\frac{(1-R)[1+R+2\sqrt{R}\cos(2\pi\cos\theta)]}{(1-R)^2+4R\sin^2(2\pi\cos\theta)}, \tag{1}$$

$$\frac{E^2}{E_0^2}(\theta=0)=\frac{[1+\sqrt{R}]^2}{1-R}, \tag{2}$$

where it is assumed that the emission wavelength is coincident with the cavity resonant wavelength. $E_0^2$ is vacuum field intensity, $\theta$ is the angle in the cavity measured from the normal direction, and $R$ is the power reflectivity of DBRs. The on-axis emission ($\theta\approx0$) is expected to exhibit a strong enhancement as $R\rightarrow1$. The theoretically calculated curve is obtained by spatially integrating the spontaneous emission over the solid angle in the microcavity relative to free-space emission for each value of $R$. The variation of emission lifetime due to the cavity is not taken into account. The experimentally obtained enhancement factor is determined by fitting the line shape of QW emission and subtracting it from the measured on-axis PL spectrum to obtain the spectrum of cavity resonance emission. All spectra are first normalized to give the same QW emission intensity. Then, the ratio of resonance emission intensity to the QW emission intensity at the cavity resonant wavelength is plotted. Since most of excitation power is absorbed in the top mirror, QW emission cannot be detected in the structure when more than ten pairs are present in the top DBR, and the enhancement factor cannot be determined. The experimental data show that the resonant coupling of the excitonic emission with the cavity mode results in an enhancement of the oscillator strength of the spontaneous emission at the resonant wavelength by more than a factor of 100 when the top mirror has ten AlAs/GaAs pairs (which has an calculated reflectivity of $R\sim96.7\%$). The expected enhancement with additional pairs results from a significant reduction in the number of available cavity modes and an increasing tendency to emit spontaneous emission into these modes. The experimental enhancement factor is

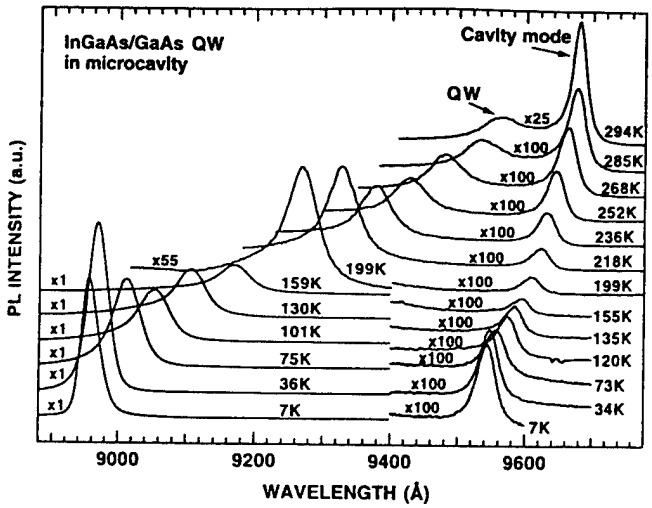


FIG. 5. Photoluminescence spectra of the cavity structure with 7 pairs in the top DBR as a function of temperature. Both the QW peak and the cavity mode peak are observed.

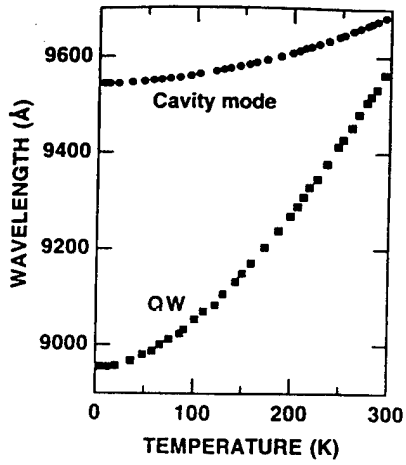


FIG. 6. Peak wavelengths of two photoluminescence emissions are plotted as a function of temperature. In the case of the QW peak, the exciton binding energy is not considered.

smaller than the calculated one, possibly due to the detuning of the emission wavelength from the cavity wavelength.[11]

### B. Influence of temperature on the enhanced spontaneous emission

Figure 5 shows the PL spectra of the cavity structure with seven pairs in the top DBR as a function of temperature. Both the QW peak and the cavity mode peak are observed. Both peaks shift to longer wavelengths with increasing temperature. However, the QW peak shifts faster than the cavity mode peak and, in fact, approaches the cavity mode peak. The QW peak broadens, and its intensity decreases abruptly with increasing temperature, which is due to the well-known phenomena of thermal broadening and thermal quenching. Meanwhile, the PL intensity of the cavity mode peak increases with increasing temperature above 150 K. This emission enhancement at the resonant wavelength is due to increased interaction between the excitonic emission and the cavity mode, which, in turn, is caused by the differing wavelength shifts with temperature. In the temperature range of 7–150 K, however, the PL intensity of the cavity mode peak decreases with increasing temperature. This phenomenon is not understood at present. The possibility of QW emission enhancement is low in this temperature range, since the QW peak wavelength is over 500 Å from the cavity mode wavelength on the shorter wavelength side.

In Fig. 6, the peak wavelengths of two PL emissions are plotted as a function of temperature. In the case of the QW peak, the exciton binding energy is not considered. The thermal variation of QW wavelength is ~3.3 Å/°C around room temperature, which is in good agreement with that of the lasing wavelength of edge-emitting lasers.[16] Meanwhile, the cavity mode wavelength shifts at 0.85 Å/°C around room temperature, which is in good agreement with the result determined using a thermally controlled reflectivity measurement in the cavity structure with a central layer of GaAs.[23] Also, this value agrees with the 0.84 Å/°C temperature coefficient measured from the temperature dependence of the lasing wavelength of InGaAs VCSEL with carrier confinement layers of $Al_{0.2}Ga_{0.8}As$.[24] But this shift is about 30% larger than the reported data of 0.6~0.65 Å/°C measured from the temperature dependence of the lasing wavelengths of GaAs VCSELs[15–17] and of InGaAs VCSELs with carrier confinement layers of $Al_{0.5}Ga_{0.5}As$.[3]

The difference in thermal variation of the cavity wavelength may originate from the different thermal variations of the refractive indices of the constituents in each structure. As well, the measurement of laser wavelength versus temperature is affected by local heating in the device.[15–17] There is inevitable error in measuring the device temperature by measuring the temperature of the device holder because excessive heating is produced in VCSELs by the high series resistance of the heterostructure DBRs and by the higher current densities at which VCSELs operate. The heat density is high and causes a large temperature gradient to build up. Lasing also occurs at high densities ($\sigma > 10^{12}$ cm$^{-2}$) of carriers in the QWs leading to enhanced many-body effects. The many-body effects can assist the lasing process by aligning spectral gain with longitudinal mode energy. As a consequence, the lasing threshold and wavelength are influenced by the many-body exchange correlation.[25] In this study, many-body effects and the temperature variation of sample due to the PL excitation light are negligible since the excitation intensity for PL is low (~100 W/cm$^2$ on the surface of sample).

## IV. CONCLUSIONS

We have studied microcavity effects on the spontaneous emission enhancement through the continuous tuning of the reflectivity. Quantum well absorption modulates PL emission and reflectivity even in the case of near resonance between the QW luminescence and mode energy (wavelength detuning $\Delta\lambda \approx 100$ Å from the cavity resonant wavelength at room temperature). The spontaneous emission enhancement factor is determined systematically by PL measurements. The room-temperature PL intensity of the on axis emission is 1–2 orders of magnitude higher for phase-matched cavity structure as compared to the structure without phase matching.

We also detune the interaction between the excitonic emission and cavity resonance mode by changing the temperature, which makes the emission intensity of the cavity resonance mode increase with increasing temperature. The optical mode shift with temperature was determined of 0.85 Å/°C by observing the temperature-dependence enhanced spontaneous emission at the cavity resonant wavelength instead of thermally controlled reflectivity measurement.

The work presented here quantifies the effects of a resonant cavity on the emission from a quantum well. The data clearly show that as the $Q$ of the cavity increases, the spontaneous emission normal to the surface is preferentially emitted in the allowed cavity mode. These data support the concepts that lead to the possibility of the "thresholdless" laser.[2]

## ACKNOWLEDGMENTS

One of the authors (G.M. Yang) is grateful for project sponsorship by Professor Byung-Doo Choe, Professor Hyung Jae Lee, and Professor Weon Guk Jeong. This work was partly supported by the Ministry of Science and Technology of Korea through SPRC at Jeonbuk National University and by the U. S. Office of Naval Research.

[1] C. Weisbuch, M. Nishioka, A. Ishikawa, and Y. Arakawa, Phys. Rev. Lett. **69**, 3314 (1992).
[2] Y. Yamamoto, F. Matinaga, S. Machida, A. Karlsson, J. Jacobson, G. Björk, and T. Mukai, J. Physique IV **3**, 39 (1993).
[3] D. B. Young, J. W. Scott, F. H. Peters, M. G. Peters, M. L. Majewski, B. J. Thibeault, S. W. Corzine, and L. A. Coldren, IEEE J. Quantum Electron. **29**, 2013 (1993).
[4] G. Shtengel, H. Temkin, T. Uchida, M. Kim, P. Brusenbach, and C. Parsons, Appl. Phys. Lett. **64**, 1062 (1994).
[5] D. G. Deppe and C. Lei, J. Appl. Phys. **70**, 3443 (1991).
[6] T. Baba, T. Hamano, F. Koyama, and K. Iga, IEEE J. Quantum Electron. **27**, 1347 (1991).
[7] K. Nishioka, K. Tanaka, T. Nakamura, Y. Lee, and M. Yamanishi, Appl. Phys. Lett. **63**, 2944 (1993).
[8] T. Yamauchi, Y. Arakawa, and M. Nishioka, Appl. Phys. Lett. **58**, 2339 (1991).
[9] E. F. Schubert, A. M. Vredenberg, N. E. J. Hunt, Y. H. Wong, P. C. Becker, J. M. Poate, D. C. Jacobson, L. C. Feldman, and G. J. Zydzik, Appl. Phys. Lett. **61**, 1381 (1992).
[10] A. M. Vredenberg, N. E. J. Hunt, E. F. Schubert, D. C. Jacobson, J. M. Poate, and G. J. Zydzik, Phys. Rev. Lett. **71**, 517 (1993).
[11] Y. Yamanoto, S. Machida, Y. Horikoshi, K. Igeta, and G. Björk, Opt. Commun. **80**, 337 (1991).
[12] N. E. Hunt, E. F Schubert, R. F. Kopf, D. L. Sivco, A. Y. Cho, and G. J. Zydzik, Appl. Phys. Lett. **63**, 2600 (1993).
[13] H. Cao, J. Jacobson, G. Björk, S. Pau, and Y. Yamamoto, Appl. Phys. Lett. **66**, 1107 (1995).
[14] B. Lu, P. Zhou, J. Cheng, K. J. Malloy, and J. C. Zolper, Appl. Phys. Lett. **65**, 1337 (1994).
[15] B. Tell, K. F. Brown-Goebeler, and R. E. Leibenguth, IEEE Photon. Tech. Lett. **5**, 637 (1993).
[16] B. Tell, K. F. Brown-Goebeler, R. E. Leibenguth, F. M. Baez, and Y. H. Lee, Appl. Phys. Lett. **60**, 683 (1992).
[17] G. Hasnain, K. Tai, L. Yang, Y. H. Wang, G. J. Fischer, J. D. Wynn, B. Weir, N. K. Dutta, and A. Y. Cho, IEEE J Quantum Electron. **27**, 1377 (1991).
[18] N. Frateschi, S. G. Hummel, and P. D. Dapkus, Electron. Lett. **27**, 155 (1991).
[19] A. Frey, G. Junk, and R. Hey, Appl. Phys. Lett. **64**, 2214 (1994).
[20] M. H. MacDougal, H. Zhao, P. D. Dapkus, M. Ziari, and W. H. Steier, Electron. Lett. **30**, 1147 (1994).
[21] K. H. Drexhage, in *Progress in Optics*, edited by E. Wolf (North-Holland, New York, 1974), Vol. 12, Chap. 4, p. 163.
[22] R. R. Chance, A. Prock, and R. Silbey, in *Advances in Chemical Physics*, edited by I. Prigogine and S. A. Rice (Wiley, New York, 1978), Vol. 37, Chap. 1, p. 1.
[23] J. Talgahader and J. S. Smith, Appl. Phys. Lett. **66**, 335 (1995).
[24] R. S. Geels, B. J. Thibeault, S. W. Corzine, J. W. Scott, and L. A. Coldren, IEEE J. Quantum Electron. **29**, 2977 (1993).
[25] P. L. Gourley, S. K. Lyo, T. M. Brennan, B. E. Hammons, C. F. Schaus, and S. Sun, Appl. Phys. Lett. **55**, 2698 (1989).

# Ultralow threshold current vertical-cavity surface-emitting lasers obtained with selective oxidation

G.M. Yang, M.H. MacDougal and P.D. Dapkus

*Indexing terms: Vertical cavity surface emitting lasers, Oxidation*

The authors report InGaAs single quantum well vertical-cavity surface-emitting lasers with an intracavity *p*-contact fabricated by selective oxidation of AlAs and distributed Bragg reflectors composed of binary materials (AlAs/GaAs). Record low threshold currents of 8.7μA in ~3μm square devices and 140μA in 10μm square devices with maximum output powers over 1.2mW are achieved.

Vertical-cavity surface-emitting lasers (VCSELs) are promising for various applications in optical systems. VCSELs fabricated by selective oxidation [1, 2] can achieve ultralow threshold currents [2 - 6]. Oxidised Al(Ga)As has been used as a current aperture under a top distributed Bragg reflector (DBR) mirror rather than proton implantation or pillar etching. The low refractive index (~1.55 [7]) of the wet thermal oxide films has also motivated their use in high refractive index contrast multilayer mirrors [7] and surface-emitting lasers based on such mirrors [4, 8]. Continuous-wave (CW) room temperature threshold currents as low as 91μA have been reported using the oxidised AlAs as a current aperture under a top dielectric DBR mirror [3]. However, low maximum output power and short lifetime of the order of minutes were observed in these structures due to the stress induced by the native-oxide layer [3]. Also, there are demonstrations of VCSELs with oxidised AlGaAs as a buried current aperture within all-semiconductor monolithic structures [5, 6], which exhibit thresholds as low as 350 μA with very high power conversion efficiency [6]. In this Letter, we report ultralow threshold single quantum-well (QW) VCSELs fabricated by selective oxidation from an all epitaxial structure with intracavity *p*-contact layers grown by metal organic chemical vapour deposition. 10μm square devices show threshold currents of 140μA with maximum output powers over 1.2mW. Approximately 3μm square devices show a threshold current of 8.7μA and a corresponding threshold current density of ~97A/cm². This threshold is the lowest reported to date for a semiconductor laser.

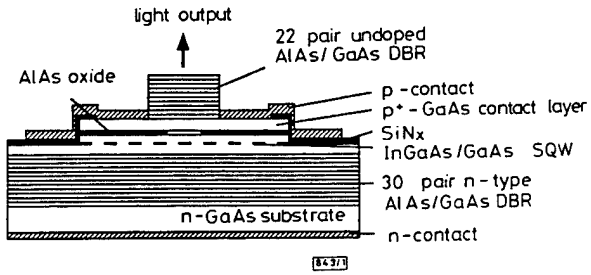


**Fig. 1** *Schematic cross-section of VCSEL with native-oxide constriction layer and binary material DBRs*

The design of this structure is optimised for low thermal resistance by using DBRs composed completely of binary materials. Since the top DBR would produce a very high resistance and substantial Joule heating due to the abrupt interfaces, it is bypassed by using an intracavity *p*-contact. Fig. 1 shows a schematic cross-section of the fabricated VCSELs. The epitaxial structure is grown on an $n^+$-GaAs (100) substrate and consists of a 30-pair *n*-doped AlAs/GaAs quarter-wave DBR, an AlGaAs/GaAs/InGaAs resonant cavity, *p*-doped contact layers, and a 22-pair undoped AlAs/GaAs quarter-wave DBR. The active region contains a single $In_{0.2}Ga_{0.8}As$ QW of thickness 80Å with adjacent GaAs barriers of thickness 150Å. The cladding layers are $Al_{0.22}Ga_{0.78}As$ whose thicknesses are adjusted to bring the total cavity thickness to one wavelength. The *p*-doped contact layers are formed from a 0.25λ AlAs current constriction layer and a 0.75λ GaAs intracavity contact layer. Two intermediate layers of heavily *p*-doped 150Å $Al_{0.7}Ga_{0.3}As$/ 150Å $Al_{0.22}Ga_{0.78}As$ are used between them, which is effective in reducing the electrical series resistance and the stress induced by oxidised AlAs current constriction layer.

After growth, the top DBR is selectively wet etched into both 14 and 5μm square mesas down to the *p*-type GaAs contact layer. Then, 50μm square mesas, whose centres coincide with the centres of the 14 and 5μm mesas, are formed by wet chemical etching, stopping just below the active region to expose the AlAs so that it may be oxidised. Thick $SiN_x$ is deposited on the top DBR sidewalls to protect the AlAs layers in the top mirror during oxidation of the current apertures. Current flow apertures of 10 and ~3μm squares are formed below the 14 and 5μm square top mirrors, respectively, by selective oxidation as described previously [1, 2, 4, 7]. The refractive index is 1.55 in the oxidised region of the current constriction layer and 2.96 in the unoxidised region of the current constriction layer, and this lateral index step provides index guiding in the cavity. Ti/Au is the *p*-type contact, and AuSn is the *n*-type contact.

The characteristics of all VCSELs were constant, showing no burn-in effects during testing. The CW room temperature laser characteristics in Figs. 2 and 3 show extremely low threshold currents of 140 and 8.7μA for 10 and ~3μm square devices, respectively, measured without a heatsink. The threshold current density of <100A/cm² for the 3μm square device is slightly lower than of 140A/cm² for the 10μm square device, since the lasing wavelength of 980.37nm for the 3μm square device (see inset in Fig. 3) is closer to the QW photoluminescence wavelength (977.5nm) than that of 992.34nm for the 10 μm square device (see inset in Fig. 2). This variation in cavity resonant wavelength is caused by nonuniformity of deposition rates in our growth chamber. The device with 10μm square active region shows a maximum output power over 1.2mW, a slope efficiency of 25%, and a maximum power conversion efficiency of 10% at 0.5mA. The threshold voltages are 1.75 and 6.2V for 10 and 3μm square devices, respectively. We expect improvements in device performance with further processing optimisation. The 10 μm square laser operates in a single mode with 20dB of transverse mode suppression up to 3 times threshold.

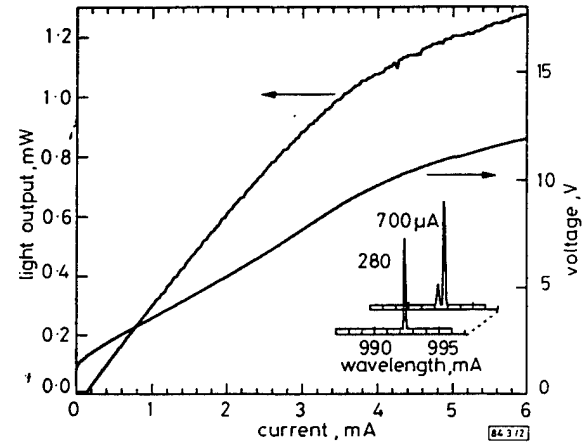


**Fig. 2** *Light output and voltage against current characteristics for 10μm square VCSEL*

Inset: lasing spectra at 280 and 700μA

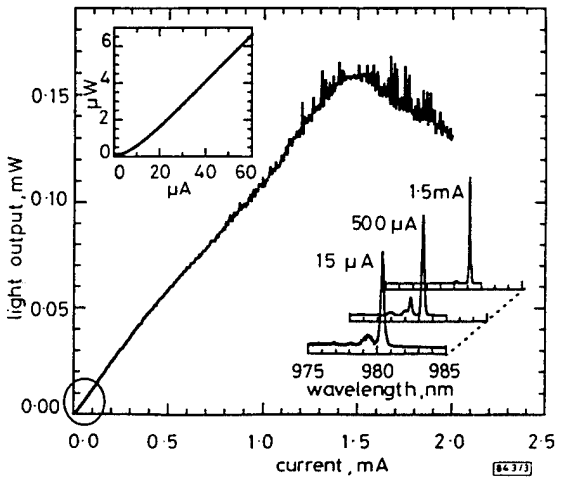


**Fig. 3** *Light output against current characteristic for ~3μm square VCSEL*

Reprinted from ELECTRONICS LETTERS 25th May 1995 Vol. 31 No. 11 pp. 886-887

The yield of the 3μm square devices was low but a few of these devices produced threshold currents below 18μA. The lowest threshold observed is 8.7μA (see Fig. 3). This device operates with a slope efficiency of 10% and produces a maximum output power of 160μW. The spectral emission from this device shows a continuous increase in the side mode suppression ratio. At 160μW output power, the side mode suppression ratio is 18dB. The continuous variation of characteristics is typical of the behaviour expected for microcavity lasers in which there is efficient coupling of the spontaneous emission into the cavity mode [9 – 11].

In conclusion, we have demonstrated VCSELs with a record low threshold current of 8.7μA, fabricated from an all epitaxial structure based on selective oxidation. In addition, we have obtained output power greater than 1mW in devices with threshold currents as low as 140μA.

*Acknowledgments:* G.M. Yang is grateful to Byung-Doo Choe, Hyung Jae Lee, and Weon Guk Jeong for their continuous encouragement. This work was supported by the Office of Naval Research and the Ministry of Science and Technology of Korea through SPRC at Jeonbuk National University.


*4 April 1995*
*Electronics Letters Online No: 19950610*

G.M. Yang, M.H. MacDougal and P.D. Dapkus (*Department of Electrical Engineering/Electrophysics, University of Southern California, Los Angeles, CA 90089-0483, USA*)

## References

1 DALLESASSE, J.M., HOLONYAK, N. Jr., SUGG, A.R., RICHARD, T.A., and EL-ZEIN, N.: 'Hydrolyzation oxidation of $Al_xGa_{1-x}As$-AlAs-GaAs quantum well heterostructures and superlattices', *Appl. Phys. Lett.*, 1990, **57**, (26), pp. 2844–2846

2 HUFFAKER, D.L., DEPPE, D.G., and KUMAR, K.: 'Native-oxide defined ring contact for low threshold vertical-cavity lasers', *Appl. Phys. Lett.*, 1994, **65**, (1), pp. 97–99

3 HUFFAKER, D.L., SHIN, J., and DEPPE, D.G.: 'Low threshold half-wave vertical-cavity lasers', *Electron. Lett.*, 1994, **30**, (23), pp. 1946–1947

4 MACDOUGAL, M.H., DAPKUS, P.D., PUDIKOV, V., ZHAO, H., and YANG, G.M.: 'Ultralow threshold current vertical-cavity surface-emitting lasers with AlAs oxide/GaAs distributed Bragg reflectors', *IEEE Photonics Technol. Lett.*, 1995, **7**, (3), pp. 229–231

5 CHOQUETTE, K.D., SCHNEIDER, R.P. Jr., LEAR, K.L., and GEIB, K.M.: 'Low threshold voltage vertical-cavity lasers fabricated by selective oxidation', *Electron. Lett.*, 1994, **30**, (24), pp. 2043–2044

6 LEAR, K.L., CHOQUETTE, K.D., SCHNEIDER, R.P., KILCOYNE, S.P., and GEIB, K.M.: 'Selectively oxidised vertical cavity surface emitting lasers with 50% power conversion efficiency', *Electron. Lett.*, 1995, **31**, (3), pp. 208–209

7 MACDOUGAL, M.H., ZHAO, H., DAPKUS, P.D., ZIARI, M., and STEIER, W.H.: 'Wide-bandwidth distributed Bragg reflectors using oxide/GaAs multilayers', *Electron. Lett.*, 1994, **30**, (14), pp. 1147–1149

8 RIES, M.J., RICHARD, T.A., MARANOWSKI, S.A., HOLONYAK, N. Jr., and CHEN, E.I.: 'Photopumped room-temperature edge- and vertical-cavity operation of AlGaAs-GaAs-InGaAs quantum-well heterostructure lasers utilizing native oxide mirrors', *Appl. Phys. Lett.*, 1994, **65**, (6), pp. 740–742

9 YAMAMOTO, Y., MACHIDA, S., and BJÖRK, G.: 'Micro-cavity semiconductor lasers with controlled spontaneous emission', *Opt. Quantum Electron.*, 1992, **24**, pp. S215–S243

10 YOKOYAMA, H., NISHI, K., ANAN, T., NAMBU, Y., BRORSON, S.D., IPPEN, E.P., and SUZUKI, M.: 'Controlling spontaneous emission and threshold-less laser oscillation with optical microcavities', *Opt. Quantum Electron.*, 1992, **24**, pp. S245–S272

11 SHTENGEL, G., TEMKIN, H., UCHIDA, T., KIM, M., BRUSENBACH, P., and PARSONS, C.: 'Spontaneous emission factor and its scaling in vertical cavity surface emitting lasers', *Appl. Phys. Lett.*, 1994, **64**, (9), pp. 1062–1064

# Influence of Mirror Reflectivity on Laser Performance of Very-Low-Threshold Vertical-Cavity Surface-Emitting Lasers

Gye Mo Yang, Michael H. MacDougal, Vasily Pudikov, and P. Daniel Dapkus, *Fellow, IEEE*

*Abstract*— **The influence of mirror reflectivity on laser performance of InGaAs–GaAs vertical-cavity surface-emitting lasers fabricated by selective oxidation is investigated by the stepwise change of the number of pairs in top mirror stack after device fabrication. Devices with 18-pair stacks in the top mirror, which is the optimized number of pairs in this structure, show an output power over 1.9 mW and a slope efficiency of 55% while maintaining a low threshold current of 212 $\mu$A. The analysis of the threshold current and differential efficiency related to mirror reflectivity shows an internal quantum efficiency of 95%, an internal round-trip loss of 0.07%, and a transparency current density of 71 A/cm$^2$.**

## I. Introduction

VERTICAL-CAVITY surface-emitting lasers (VCSEL's) fabricated by selective oxidation are attractive to achieve ultralow threshold current and/or high external efficiency [1]–[4]. Oxidized Al(Ga)As has been used as a current aperture under a top DBR mirror or as a component of high refractive index contrast multilayers mirrors. Recently, there has also been an interest in measurements of some of the basic laser parameters needed for realistic modeling of VCSEL's [5], [6]. It is, thus, useful to vary the reflectivity of at least one mirror in order to determine the internal parameters of VCSEL [6]. In this paper, we report experimental results on the reflectivity dependence of the laser light-current characteristics for InGaAs single quantum well (SQW) VCSEL fabricated by selective oxidation from all epitaxial structure. By employing an intracavity contact to the p-layer, we are able to vary mirror losses by directly changing the number of pairs in distributed Bragg reflector (DBR) mirror in a low-threshold VCSEL.

A schematic cross-section of the fabricated VCSEL's is shown in Fig. 1. The epitaxial structure grown by metalorganic chemical vapor deposition (MOCVD) consists of a 30-pair $n$-doped AlAs–GaAs quarter-wave DBR, an $Al_{0.22}Ga_{0.78}As$–GaAs–$In_{0.2}Ga_{0.8}As$ resonant $\lambda$-cavity, $p$-doped contact layers, and a 22-pair undoped AlAs–GaAs quarter-wave DBR. The $p$-doped contact layers are formed from a 0.25 $\lambda$ AlAs current constriction layer and a 0.75 $\lambda$ GaAs intracavity contact layer. After growth, the top DBR is selectively wet etched into 14 $\mu$m square mesas down to the $p$-type GaAs contact layer. Then, 50 $\mu$m square mesas, whose centers coincide with the centers of the 14 $\mu$m mesas, are formed by wet chemical etching. Current flow apertures of $10 \times 10$ $\mu$m$^2$ are formed below the 14-$\mu$m-square top mirrors by selective oxidation [1]–[3].

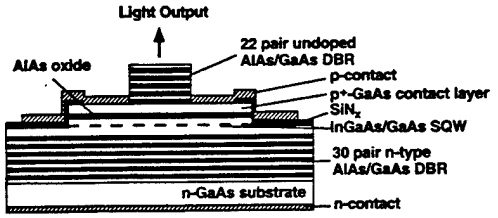


Fig. 1. Schematic cross section of VCSEL with a native-oxide constriction layer and binary material DBR's.

This is a good device structure for studying the reflectivity-dependent laser characteristics because the top DBR is composed of binary materials (AlAs–GaAs) with abrupt interfaces and can be selectively removed one pair at a time. There are also no changes in the current-voltage characteristics caused by reducing the number of top pairs owing to the use an intracavity $p$-contact. After photoresist is applied to open a window on the top mirror, the GaAs and AlAs in the DBR stack are selectively etched using 4:1 solution of citric acid–$H_2O_2$ and 1:7 Buffered HF, respectively. After each pair is etched, the continuous-wave light-current curves of VCSEL are taken at room temperature. The threshold current and the light output slope efficiency through the top mirror are obtained for each value of the reflectivity of top mirror.

Fig. 2 shows the light-current curves for different numbers of pairs in the top DBR. The threshold current for 22-pair DBR is as low as 143 $\mu$A with a corresponding threshold current density of 143 A/cm$^2$. As the mirror reflectivity is reduced, the output coupling from the cavity is increased, resulting in a higher external quantum efficiency. However, reducing the reflectivity also increases the total loss in the cavity tending to increase the threshold current. For very high mirror reflectivities, when the number of pairs in the top DBR is in the range of 18–22, the internal loss is dominant, so a decrease in mirror reflectivity results in very little change in the threshold current. The device with 18-pair stacks in the mirror shows an output power over 1.9 mW while maintaining a low

Manuscript received June 21, 1995; revised July 26, 1995. Supported in part by the Office of Naval Research, the Advanced Projects Research Agency through the National Center for Integrated Photonic Technology, and the Ministry of Science and Technology of Korea through SPRC at Jeonbuk National University.

The authors are with the Department of Electrical Engineering/Electrophysics, University of Southern California, Los Angeles, CA 90089-0483 USA.

IEEE Log Number 9414929.

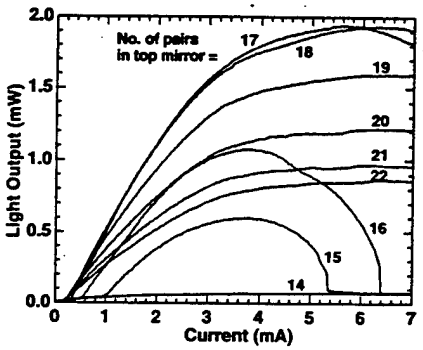


Fig. 2. Continuous-wave room-temperature light output against current characteristics for different numbers of pairs in the top mirror.

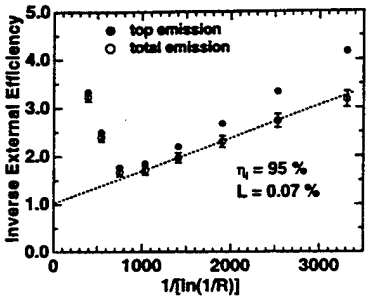


Fig. 3. Inverse external efficiency as a function of $1/\ln(1/R)$, where $R$ is the mean power reflectivity. To obtain the external efficiency for total emission, the top emission external efficiency is corrected by the power emitted through the bottom Bragg mirror taking into error in layer thicknesses.

threshold current of 212 $\mu$A. A slope efficiency of 55% and a maximum power conversion efficiency of 16% are achieved in this device. A further decrease in reflectivity (in the case of 16 and 15 pairs) results in an increase in threshold current and a decrease in differential efficiency. Increased drive current causes a temperature rise that shifts the gain peak causing a mismatch between the gain peak and the cavity mode. The temperature rise also lowers the carrier confinement in the QW. Finally, the device no longer lases because the mirror loss is too high and the gain at the cavity mode is too low to support laser operation.

We have measured the effect of temperature change on the threshold in a device with 22 pairs in the top DBR and found that a minimum threshold occurs around room temperature where the cavity mode matches the gain peak. Also the emission wavelength increases quadratically with injection current. The change of wavelength up to 500 $\mu$A is approximately 0.04 nm, indicating that the thermal effects due to electrical resistance are quite small in this range.

In Fig. 3, we plot the inverse external efficiency as a function of $1/\ln(1/R)$, where $R = (R_t R_b)^{1/2}$ is the mean power reflectivity. $R_t$ and $R_b$ is the top and bottom mirror reflectivities, respectively. The external quantum efficiency for light coming out the top mirror, $\eta_d^t$, is measured just above the threshold current in each curve shown in Fig. 2 and the reflectivity for each structure is calculated using the transfer matrix method [7]. To obtain the external efficiency for total emission, $\eta_d$, $\eta_d^t$ is corrected by the power emitted through the bottom Bragg mirror using the following relation;

$$\eta_d^t = \eta_d \frac{(1-R_t)}{(1-R_t)+(1-R_b)\sqrt{\frac{R_t}{R_b}}} \tag{1}$$

The reflectivity of the bottom mirror including 30 pairs DBR and calibration layers is about 99.986% in the presence of the bottom metal contact. Layer thicknesses are determined to an accuracy of better than 2% using *in situ* laser reflectometry as a growth monitoring tool in our MOCVD reactor [8]. This error in layer thicknesses results in a very small change of DBR reflectivity of approximately 0.02% at the lasing wavelength. For each mirror reflectivity, the threshold gain, $g$th, is determined via [5]

$$\Gamma L_g g_{\rm th} \xi = L + \ln(1/R) \tag{2}$$

where $\Gamma$ is the lateral confinement factor, $L_g$ is the total gain thickness, $\xi$ is the gain enhancement factor due to the presence of the electric field standing wave in the cavity [9], and $L$ is the round-trip loss. In the VCSEL, the light wave is traveling in an anisotropic region containing many different layers with various doping concentrations and penetrates a finite length into the DBR mirror region where further scattering losses, diffraction losses, and absorption losses may occur. Therefore, the total loss is bundled into the term $L$. Then, the external quantum efficiency can be calculated using

$$\eta_d = \eta_i \frac{\ln(1/R)}{L+\ln(1/R)} \tag{3}$$

where $\eta_i$ is the internal quantum efficiency.

We fit the data in Fig. 3 with $\eta_i = 0.95$ and $L = 0.0007$ in the range of 18–22 pairs in the top DBR to eliminate thermal effects on the efficiency, as discussed above. Approximately, we can write $L$ as $L_{\rm eff}\alpha_i$, where $L_{\rm eff}$ is the effective cavity length, equal to the physical length of resonant cavity plus penetration depth into bottom and top mirrors and $\alpha_i$ is the internal loss. Using the relations obtained in [10], we calculate $L_{\rm eff} = 1.294$ $\mu$m for our device. Thus, $L_{\rm eff}$ is nearly independent of the number of pairs in the top mirror in this range. It should be noted that $\alpha_i$ as determined here includes the usual intracavity losses and also losses in the DBR mirrors. The low value of $\alpha_i \sim 5.5$ cm$^{-1}$ obtained here results, we believe, from the use of the oxide current constriction to reduce edge scattering losses and the use of an undoped $p$-mirror to reduce free carrier losses.

Threshold current densities, $J_{\rm th}$, of the VCSEL's with various reflectivities are shown in Fig. 4. Here, a plot of $\log(J_{\rm th})$ versus $\ln(1/R)$ is presented. When $J_{\rm th}$ is low enough that laser operation on the second quantized state does not occur, the gain and current density can be related by a semilogarithic function $g = g_0 \ln(\eta_i J/n_w J_{\rm tr})$, where $g_0$ is the gain parameter, $J_{\rm tr}$ is the transparency current density, and $n_w$ is the number of wells [11]. This relation does not take into account variation of gain with wavelength, which can have a large effect in VCSEL's. Thus, to be correct for VCSEL's, the gain peak and cavity resonance must be in perfect alignment for this equation to adequately describe the relationship of threshold current and threshold gain in VCSEL's, as we have achieved in the structure described here. Then, we can relate

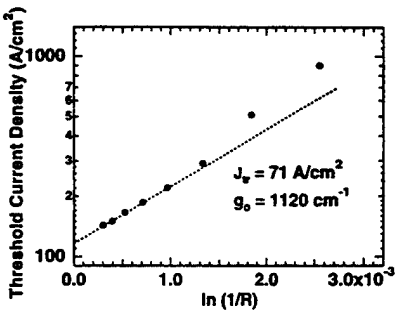


Fig. 4. Threshold current density of the VCSEL's with various reflectivities. Here, a plot of $\log(J_{\rm th})$ versus $\ln(1/R)$ is being presented.

the reflectivity and loss to the threshold current

$$J_{\rm th} = \frac{n_w J_{\rm tr}}{\eta_i} \exp\left[\frac{L + \ln\left(\frac{1}{R}\right)}{\Gamma L_g g_0 \xi}\right] \quad (4)$$

$$\ln(J_{\rm th}) = \ln\left(\frac{n_w J_{\rm tr}}{\eta_i}\right) + \frac{L}{\Gamma L_g g_0 \xi} + \frac{1}{\Gamma L_g g_0 \xi} \ln\left(\frac{1}{R}\right) \quad (5)$$

Equation (5) says that $\ln(J_{\rm th})$ is linearly depends on $\ln(1/R)$, which is confirmed in Fig. 4 in the range of $R$ for which thermal effects are negligible. At high values of $\ln(1/R)$, a deviation of the data in Fig. 4 from linear dependence likely results from a shift of the gain peak caused by thermal effects. We fit the data in Fig. 4 with (5) using the measured values of $\eta_i$ and $L$ to determine the values of $J_{\rm tr}$ and $g_0$. We obtain $J_{\rm tr} = 71$ A/cm$^2$ and $1/(\Gamma L_g g_0 \xi) = 558$. If $\Gamma = 1$, $\xi = 2$, and $L_g = 8$ nm, then we obtain $g_0 = 1120$ cm$^{-1}$. Earlier experiments on InGaAs edge-emitting ultralow threshold lasers in our research group [12] have produced comparable material parameters for comparable structures ($J_{\rm tr} = 44.5$ A/cm$^2$, $g_0 = 1132$ cm$^{-1}$, and $\eta_i = 0.98$). Thus, the parameters of our VCSEL are consistent with these high quality structures.

## II. Conclusion

We have fabricated VCSEL's by using oxide current constriction, intracavity $p$-contact, and binary semiconductor DBR structures. The cavity reflectivity is tuned by changing the number of pairs in the top DBR, which is useful to determine the internal parameters of VCSEL's. The device with an 18-pair stack in the top mirror, which gives the highest output power in this structure, shows an output power over 1.9 mW and a high slope efficiency of 55% while maintaining a very low threshold current of 212 $\mu$A.

## Acknowledgment

One of the authors, G. M. Yang, is grateful to B.-D. Choe, H. J. Lee, and W. G. Jeong for their continuous encouragement.

## References

[1] D. L. Huffaker, J. Shin, and D. G. Deppe, "Low threshold half-wave vertical-cavity lasers," *Electron. Lett.*, vol. 30, no. 23, pp. 1946–1947, 1994.

[2] K. L. Lear, K. D. Choquette, R. P. Schneider, Jr., S. P. Kilcoyne, and K. M. Geib, "Selectively oxidised vertical cavity surface emitting lasers with 50% power conversion efficiency," *Electron. Lett.*, vol. 31, no. 3, pp. 208–209, 1995.

[3] M. H. MacDougal, P. D. Dapkus, V. Pudikov, H. Zhao, and G. M. Yang, "Ultralow threshold current vertical-cavity surface-emitting lasers with AlAs oxide-GaAs distributed Bragg reflectors," *IEEE Photon. Technol. Lett.*, vol. 7, no. 3, pp. 229–231, 1995.

[4] G. M. Yang, M. H. MacDougal, and P. D. Dapkus, "Ultralow threshold VCSEL's fabricated by selective oxidation from all epitaxial structure," in *Conf. Lasers Electro-Optics (CLEO)*, Bultimore, MD, May 22–26, 1995, postdeadline paper CPD4.

[5] J. W. Scott, R. S. Geels, S. W. Corzine, and L. A. Coldren, "Modeling temperature effects and spatial hole burning to optimize vertical-cavity surface-emitting laser performance," *IEEE J. Quantum Electron.*, vol. 29, no. 5, pp. 1295–1308, 1993.

[6] D. V. Kuksenkov, H. Temkin, and S. Swirhun, "Measurement of internal quantum efficiency and losses in vertical cavity surface emitting lasers," *Appl. Phys. Lett.*, vol. 66, no. 14, pp. 1720–1722, 1995.

[7] M. Born and E. Wolf, *Principles of Optics*. Oxford: Pergamon, 1994.

[8] N. C. Frateschi, S. G. Hummel, and P. D. Dapkus, "In situ laser reflectometry applied to the growth of $Al_xGa_{1-x}As$ Bragg reflectors by metalorganic chemical vapor deposition," *Electron. Lett.*, vol. 27, no. 2, pp. 155–157, 1991.

[9] S. W. Corzine, R. S. Geels, J. W. Scott, R. H. Yan, and L. A. Coldren, "Design of Fabry–Perot surface-emitting lasers with a periodic gain structure," *IEEE J. Quantum Electron.*, vol. 25, no. 6, pp. 1513–1524, 1989.

[10] D. I. Babic and S. W. Corzine, "Analytic expressions for the reflection delay, penetration depth, and absorptance of quarter-wave dielectric mirrors," *IEEE J. Quantum Electron.*, vol. 28, no. 2, pp. 514–524, 1992.

[11] T. A. DeTemple and C. M. Herzinger, "On the semiconductor laser logarithimic gain-current density relation," *IEEE J. Quantum Electron.*, vol. 29, no. 5, pp. 1246–1252, 1993.

[12] H. Zhao, "The development of low threshold laser arrays and their applications in parallel optical datalinks," Ph.D. Dissertation, University of Southern California, 1994.

# Wide-bandwidth distributed Bragg reflectors using oxide/GaAs multilayers

M. H. MacDougal, H. Zhao, P. D. Dapkus, M. Ziari and W. H. Steier

*Indexing terms: Distributed Bragg reflector lasers, Vertical cavity surface emitting lasers*

The authors have designed and fabricated a wide bandwidth high reflectivity distributed Bragg reflector (DBR) using the native oxide of AlAs as the low refractive index layer and GaAs as the high refractive index layer. Results show that the refractive index of the native oxide is 1.55±0.01, the peak reflectivity of the DBR is over 99%, and the reflectivity bandwidth is ~460nm.

Distributed Bragg reflectors (DBRs) are used in a wide variety of optoelectronic devices, including vertical cavity surface emitting lasers (VCSELs) [1] and resonant cavity devices [2]. Because of the low refractive index ratio of 3.5/3.0 for typical epitaxial materials, many pairs of the constituent materials must be grown to achieve a reflectivity of greater than 99%, and the band for which the reflectivity is greater than 90% is only around 110nm. Furthermore, the reflectivity and spectral bandwidth are very sensitive to the thickness and thickness uniformity of the layers. To relax this constraint as well as increase the spectral bandwidth, the use of two materials that have a much larger refractive index difference is necessary. In this Letter, we describe the fabrication of epitaxially grown wide bandwidth high reflectivity DBRs using the native oxide of AlAs [3–5] as the low refractive index layer and GaAs as the high refractive index layer so that the refractive index ratio is increased from 1.2in GaAs/AlAs to 2.3in GaAs/AlAs oxide. We and others have previously demonstrated the highest index ratio mirrors possible by fabricating GaAs/air Bragg reflectors [6, 7]. In these structures, the AlAs is etched away and replaced either with air or acrylic resin. This approach requires great care to keep the DBR from collapsing and requires supports on the side to hold up the GaAs layers. In contrast, the AlAs oxide/GaAs DBR structure we report here is a robust, self-supporting structure. In addition to its physical robustness, the oxide/GaAs structure will exhibit a wide bandwidth and wide angular acceptance. These attributes are expected to show benefits in broadband devices such as light emitting diodes (LEDs) and solar cells by increasing the angular spectrum of light that is reflected.

To design and simulate the DBR, the refractive index and thickness of each layer must be known. The thickness of the AlAs and GaAs epitaxial layers used in this structure is controlled by laser reflectometry [8, 9] and the refractive indices for these materials are well known [10, 11]. Our structure uses the native oxide of AlAs [4] as one of the reflector layers, but little data are available about its optical properties. Sugg and co-workers have measured the refractive index of the native oxide of $Al_{0.8}Ga_{0.2}As$ to be 1.63 [12]. Using ellipsometry, we have measured the refractive index of the native oxide of AlAs to be between 1.5 and 1.56, depending on oxidation conditions. The thickness of the oxide layer is also a variable because AlGaAs has been observed to contract in thickness by 60–70% when oxidised [4]. Owing to the limited data available on the native oxide, we designed the layer thicknesses for the Bragg reflector under the assumption that the oxide index of refraction is 1.54 and that there is no contraction in the thickness. The centre wavelength of the DBR is designed to be at 1μm.

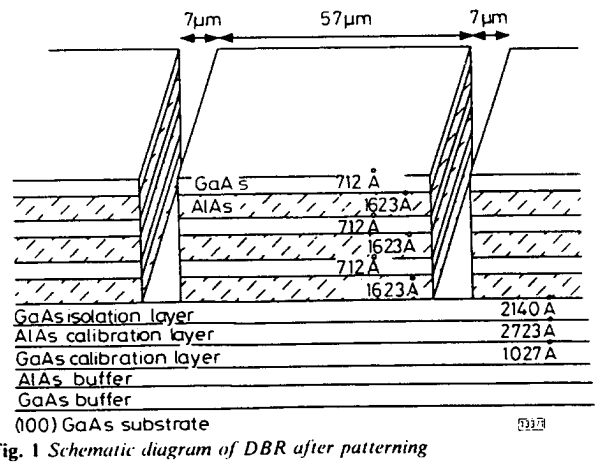


**Fig. 1** *Schematic diagram of DBR after patterning*

The designed structure, shown in Fig. 1, is grown by MOCVD. After growth, the wafer is coated with $SiN_x$, photolithographically patterned, and etched through the top three DBR pairs to expose edges of the AlAs for oxidation. The native oxide of AlAs is formed by flowing $N_2$, bubbled through $H_2O$ at 90°C, over the sample at 425°C [3, 5]. The oxidation of the AlAs starts at the sides of the mesa, as shown in Fig. 2, and moves toward the middle, until the whole AlAs layer is oxidised. The growth rate calibration layers are not exposed and thus left unoxidised. For our mesa width of 57μm, the oxidation time required for all three AlAs layers to oxidise completely is 45 min.

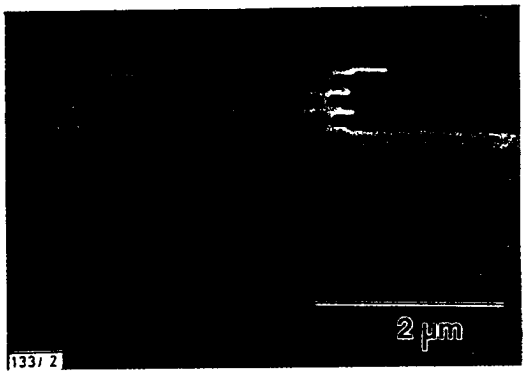


**Fig. 2** *SEM of one side of DBR mesa after oxidation*

The reflectivity of the DBR, shown in Fig. 3, is measured by a Cary spectrophotometer in reflection mode. Because the refractive index and the thickness of the oxide are unknowns, these variables have been varied in the simulation to match the measured spectrum. To achieve optimal matching in the simulation, the oxide index of refraction is 1.55, and the oxide thickness is 1427Å or 87.9% of the original intended AlAs thickness. When the layers at the bottom of the vias were added into the simulation in proportion to their aerial coverage, they drastically changed the shape of the simulated spectrum, and the simulation could not be made to fit the measured spectrum. Presumably, these layers do not contribute to the measured spectrum because the etched surface does not reflect the light specularly. The reflectance is measured at one wavelength ($\lambda$ = 1.064μm) on the DBR and an Au film of known reflectivity using a microscope objective to focus the light on each to obtain the absolute reflectance of the DBR at this wavelength. The ratio between this absolute reflectance and the reflectance measured by the spectrophotometer at the same wavelength is

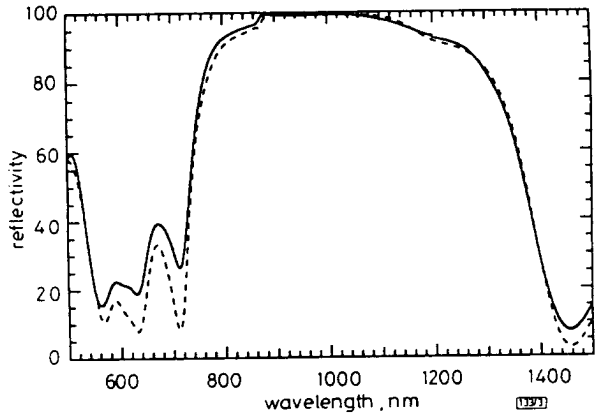


**Fig. 3** *Measured and simulated reflectivity of AlAs oxide/GaAs DBR*

Structure in Fig. 1 is used for reflectivity simulation

——— measured
- - - - simulated

multiplied with the rest of the measured spectrum to obtain the absolute reflectivity for the other wavelengths. The peak reflectivity is ~960nm and is greater than 99%. The bandwidth, the range of wavelengths for which the reflectivity is greater than 90%, is 460nm. By comparison, a DBR with 16 pairs of AlAs/GaAs gives a reflectivity of 99.5% and a bandwidth of only 110nm. The fact that a high reflectivity is achieved, even when the oxide layer thickness is more than 10% off its designed thickness, demonstrates the thickness insensitivity of this type of DBR. In addition to the advantages of our DBR mentioned above, it achieves high reflectivity with only three pairs and a total epitaxial thickness of ~7000Å. When simulating four pairs, the reflectivity increases to 99.7%, which is suitable for use in VCSELs. The large bandwidth of this structure makes it an ideal candidate as a broadband reflector. Because it can be grown under the active region unlike delectric reflectors such as ZnS and $SiO_2$, it could be placed beneath an LED and increase its power efficiency. Of course, its use will also complicate the contacting geometry because the oxide layers are insulating.

In this Letter, we have presented the design and fabrication of a wide bandwidth, high reflectivity distributed Bragg reflector. The DBR makes use of the large refractive index ratio between GaAs and the native oxide of AlAs to achieve these advantages.


*12 May 1994*
*Electronics Letters Online No: 19940754*

M. H. MacDougal, H. Zhao, P. D. Dapkus, M. Ziari and W. H. Steier (*Department of Electrical Engineering/Electrophysics University of Southern California, Los Angeles, CA 90089-0483, USA*)

## References

1 SAKAGUCHI, T., KOYAMA, F., and IGA, K.: 'Vertical cavity surface-emitting laser with an AlGaAs/AlAs Bragg reflector', *Electron. Lett.*, 1988, 24, (15), pp. 928–929

2 DODABALAPUR, A., and CHANG, T. Y.: 'Resonant-cavity InGaAlAs/InGaAs/InAlAs phototransistors with high gain for 1.3–1.6μm', *Appl. Phys. Lett.*, 1992, 60, (8), pp. 929–931

3 DALLESASSE, J. M., HOLONYAK, N., SUGG, A. R., RICHARD, T. A., and EL-ZEIN, N.: 'Hydrolyzation oxidation of $Al_xGa_{1-x}As$-AlAs-GaAs quantum well heterostructures and superlattices', *Appl. Phys. Lett.*, 1990, 57, (26), pp. 2844–2846

4 SUGG, A. R., HOLONYAK, N., BAKER, J. E., KISH, F. A., and DALLESASSE, J. M.: 'Native oxide stabilization of AlAs-GaAs heterostructures', *Appl. Phys. Lett.*, 1991, 58, (11), pp. 1199–1201

5 SUGG, A. R., CHEN, E .I., RICHARD, T. A., HOLONYAK, N., and HSIEH, K. C.: 'Native oxide-embedded $Al_yGa_{1-y}As$-GaAs-$In_xGa_{1-x}As$ quantum well heterostructure lasers', *Appl. Phys. Lett.*, 1993, 62, (11), pp. 1259–1261

6 HO, S.-T., MCCALL, S. L., SLUSHER, R. E., PFEIFFER, L. N., WEST, K. W., LEVI, A. F. J., BLONDER, G. E., and JEWELL, J. L.: 'High index contrast mirrors for optical microcavities', *Appl. Phys. Lett.*, 1990, 57, (14), pp. 1387–1389

7 BEYLER, C. A., HUMMEL, S. G., FRATESCHI, N., and DAPKUS, P. D.: 'Small dimension Bragg reflectors formed by air-isolated GaAs layers', *Electron. Lett.*, 1991, 27, (7), pp. 588–589

8 FRATESCHI, N., HUMMEL, S. G., and DAPKUS, P. D.: 'In situ laser reflectometry applied to the growth of $Al_xGa_{1-x}As$ Bragg reflectors by metalorganic chemical vapour deposition', *Electron. Lett.*, 1991, 27, (2), pp. 155–156

9 HUMMEL, S.G.: 'The growth and characterisation of multilayer structure by metal-organic chemical vapor deposition'. PhD Dissertation, University of Southern California, 1993

10 ASPNES, D. E., and STUDNA, A. A.: 'Dielectric functions and optical parameters of Si, Ga, GaP, GaAs, GaSb, InP, InAs, and InSb from 1.5 to 6.0eV', *Phys. Rev. B*, 1983, 27, (2), pp. 985–1009

11 FERN, R. E., and ORTON, A.: 'Refractive index of AlAs', *J. Appl. Phys.*, 1971, 42, (9), pp. 3499–3500

12 SUGG, A. R., CHEN, E. I., HOLONYAK, N., HSIEH, K. C., BAKER, J. E., and FINNEGAN, N.: 'Effects of low-temperature annealing on the native oxide of $Al_xGa_{1-x}As$', *J. Appl. Phys.*, 1993, 74, (6), pp. 3880–3885

# Epitaxial (Al,Ga)InP–Oxide Distributed Bragg Reflectors for Use in Visible-Wavelength Optical Devices

Michael H. MacDougal, *Student Member, IEEE*, Steven G. Hummel, *Member, IEEE*, P. Daniel Dapkus, *Fellow, IEEE*, Hanmin Zhao, and Yong Cheng

***Abstract*— Epitaxially-grown distributed Bragg reflectors (DBR's) employing thermally oxidized AlAs as the low refractive index constituent and (Al,Ga)InP as the high index constituent are fabricated. The 4.5-pair $Ga_{0.5}In_{0.5}P$–oxide and $Al_{0.5}In_{0.5}P$–oxide DBR's exhibit high reflectivity (>90%) over a range of 635–967 nm and 470–676 nm, respectively. The (Al,Ga)InP–oxide DBR's are shown to require less material to produce high reflectivity and to have significantly wider bandwidth than all-semiconductor DBR's used in the visible spectrum.**

## I. Introduction

DISTRIBUTED Bragg reflectors (DBR's) are used in a wide variety of optoelectronic devices, including vertical-cavity surface-emitting lasers (VCSEL's) and asymmetric Fabry–Perot light modulators. These multilayer structures are also used to enhance the performance of light emitting diodes (LED's) by reflecting light away from an absorbing substrate [1], [2]. DBR's employed in cavity-based, visible wavelength devices pose many challenges by requiring high reflectivity at specific wavelengths, which is problematic due to the small index difference available between the constituent materials [3]. In this letter, we present epitaxially-grown DBR's employing thermally oxidized AlAs as the low refractive index constituent and $(Al,Ga)_{0.5}In_{0.5}P$ as the high index constituent. The large refractive index ratio (~2) between these materials leads to DBR's possessing reflectivities greater than 90% and wide spectral bandwidths greater than 200 nm. Furthermore, since these DBR's are epitaxially grown, they can be freely located within a device structure and not limited to the surface as is the case for deposited dielectric mirrors.

AlAs is converted from a high index ($n \sim 3.0$) material to a low index ($n \sim 1.55$) material by wet thermal oxidation. Dallesasse and coworkers demonstrated that applying this technique results in a robust oxide unlike the poor quality oxide generated by the oxidation of AlAs at room temperature [4]. Sugg and coworkers reported that AlAs could be laterally oxidized while adjacent GaAs layers remain unoxidized [5]. This property has been utilized to create high reflectivity, wide-bandwidth DBR's centered at 960 nm by using AlAs oxide–GaAs pairs [6] and, recently, to demonstrate low threshold VCSEL's at 950 nm using these mirrors [7].

Manuscript received November 11, 1994; revised December 6, 1994. This work was supported in part by the the Office of Naval Research, the Army Research Office, the Advanced Research Projects Agency, and the Ballistic Missile Defense Organization.

M. H. MacDougal, P. D. Dapkus, H. Zhao, and Y. Cheng are with the University of Southern California, National Center for Integrated Photonic Technology, Department of Electrical Engineering/Electrophysics, Los Angeles, CA 90089-0483 USA.

S. G. Hummel is with Hewlett-Packard Laboratories, Palo Alto, CA 94303-0867 USA.

IEEE Log Number 9409033.

## II. Fabrication

The use of GaAs as one of the constituent materials in a DBR operating in the visible wavelength region will limit available reflectivity due to absorbing characterics below 860 nm. In this work, AlAs oxide is paired with $Ga_{0.5}In_{0.5}P$ and $Al_{0.5}In_{0.5}P$, whose absorption cutoffs of 650 nm and 500 nm, respectively, permit high reflectivity in most of the visible region. The 4.5-period DBR structures contain five layers of AlAs and four layers of $(Al,Ga)_{0.5}In_{0.5}P$ and are grown by low-pressure metalorganic chemical vapor deposition (MOCVD) on (100) $n^+$-doped GaAs substrates. In the $Ga_{0.5}In_{0.5}P$-based structure, each period consists of 540 Å of $Ga_{0.5}In_{0.5}P$ and 1330 Å of AlAs to achieve a center reflectance wavelength of 740 nm after thermal oxidation. In the $Al_{0.5}In_{0.5}P$-based structure, each period consists of 390 Å of $Al_{0.5}In_{0.5}P$ and 970 Å of AlAs to achieve a center wavelength of 540 nm.

The samples are processed and oxidized identically. The thermal oxidation process requires that the edges of the layers first be exposed. $SiN_x$ is deposited on the sample to protect the surface from any oxidation affects, and subsequently 3-$\mu$m-wide trenches are defined by photolithography so that they are spaced 55 $\mu$m apart. Ion beam etching (IBE) is then used to isotropically etch the trenches and expose the AlAs edges. The photoresist is removed by chemical stripping.

At this point the samples are ready for oxidation. The native oxide of AlAs is formed by first flowing $N_2$ through $H_2O$ at 90 °C, and then passing the wet mixture over the sample at 425 °C. An oxidation time of 45 minutes ensures that all AlAs layers are fully transformed. Since the $Ga_{0.5}In_{0.5}P$ layers do not contain any Al, they are left unaffected by the oxidation. Although the $Al_{0.5}In_{0.5}P$ contains Al, its oxidation rate at this temperature is much lower than that of the AlAs [8]. $Al_{0.5}In_{0.5}P$ begins to oxidize appreciably at 500 °C, and even then at only a small rate, whereas AlAs oxidizes rapidly at

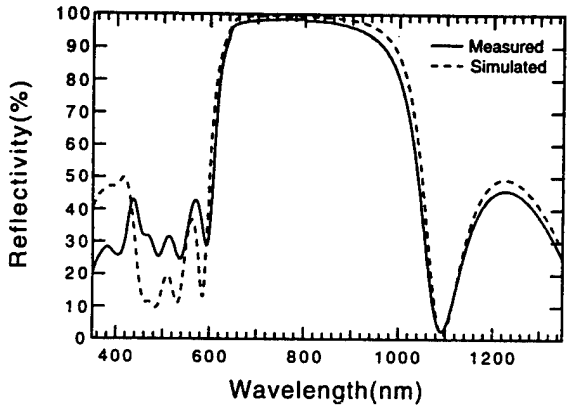


Fig. 1. Reflectance spectra for the 4.5-pair $Ga_{0.5}In_{0.5}P$–oxide DBR.

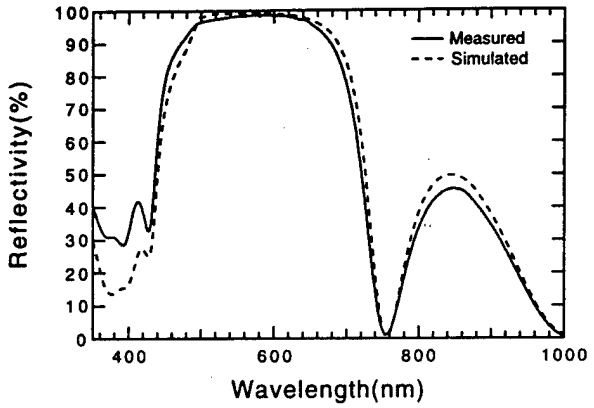


Fig. 2. Reflectance spectra for the 4.5-pair $Al_{0.5}In_{0.5}P$–oxide DBR.

400 °C. No evidence of $Al_{0.5}In_{0.5}P$ oxidation is observed in these samples under the optical microscope.

## III. Optical Characterization

The resulting reflectance vs. wavelength behavior for the 4.5 pair $Ga_{0.5}In_{0.5}P$–oxide and $Al_{0.5}In_{0.5}P$–oxide DBR's are shown in Figs. 1 and 2, respectively. These measurements are performed with a spectrophotometer in the reflectance mode. Although the 3 $\mu$m wide trenches are within the illuminated area, they are quite small compared with the mirror area and do not specularly reflect due to rough etching. As a result, they do not contribute to the shape of the reflectivity spectrum. To establish the absolute reflectance of the mirrors, monochromatic light is focussed down to a 15-$\mu$m spot away from the trenches, and the reflected light intensity is measured and compared to the reflected intensity off a calibrated reflector. A Ti-sapphire laser at 791 nm is used for the InGaP-oxide DBR, and a He-Ne laser at 594 nm is used to for the $Al_{0.5}In_{0.5}P$–oxide DBR. The $Ga_{0.5}In_{0.5}P$–oxide DBR has a reflectance bandwidth ($\Delta\lambda_{90}$), defined here as the wavelength range for which reflectance is greater than 90%, of 332 nm with the stop band extending slightly beyond the absorption cutoff to 640 nm. The $Al_{0.5}In_{0.5}P$–oxide reflector demonstrates a bandwidth of 206 nm with reflectance greater than 90% extending to 470 nm. Since one of the objectives of this study is to determine the shortest wavelength at which high reflectivity is attained, these bandwidths are limited by the absorption cutoff on the short wavelength side. However, the bandwidth would be wider if the center wavelength were moved farther away from the absorption cutoff. The peak reflectivity of both DBR's is greater than 98.5%. No degradation in reflectivity with time has been observed, suggesting good structural reliability. However, aging tests that include thermal stress cycling have yet to be performed.

## IV. Discussion

In an earlier study of GaAs–oxide DBR's [6], the index of refraction of AlAs oxide was found to be 1.55 and the oxide layer thickness was found to be approximately 88% of the original AlAs layer thickness. Subsequently, we have determined that the index varies from run to run within a range of 1.53 to 1.57, and the shrinkage varies within a range of 88% to 91%. The source of these variations is not fully understood, but are believed to be related to process steps that can be better controlled. It is important to note that the determination of these variations is also influenced by the limited precision of layer thickness measurement. We suspect that slight internal strain is generated at the interface because of this layer shrinkage, but its deleterious effects may be suppressed by the amorphous nature of the oxide. Using these numbers ($n$ = 1.55, shrinkage = 88%) along with predicted indices [9] for the $(Al,Ga)_{0.5}In_{0.5}P$ layers to simulate the reflectivity spectrum of the grown structure, a close match is found with the measured data as shown in Figs. 1 and 2. This match suggests that the oxide does not extend beyond the interface of the $(Al,Ga)_{0.5}In_{0.5}P$–AlAs layers and verifies that the previously determined oxide characteristics are also applicable when used with this material system.

Having verified that the refractive index and thickness change for the oxide is accurate when used with this material system, we can calculate the reflectivity of the oxide-based DBR's at other center wavelengths and compare it to the reflectivity of all-semiconductor DBR's. The beneficial impact of (Al,Ga)InP–oxide DBR's becomes more apparent at shorter wavelengths. Thus, a comparison is made using DBR's centered at 650 nm since that is near the shortest wavelength at which current state-of-the-art VCSEL's are fabricated [10]. The DBR pair that is normally used in visible VCSEL's is composed of $Al_{0.5}Ga_{0.5}As$ and AlAs whose refractive indices are well known [11]. Fig. 3(a) shows the difference between a 5-pair $Al_{0.5}In_{0.5}P$–oxide DBR and a 35-pair $Al_{0.5}Ga_{0.5}As$–AlAs DBR, which both exhibit peak reflectivities of 99.93%. However, the oxide semiconductor DBR requires less than one quarter of the material thickness and many fewer pairs than an all-semiconductor DBR of the same reflectivity. The advantages of thinner DBR's include shorter epitaxial growth times and reductions in absorption, scattering, and diffraction losses. Furthermore, the bandwidth of the oxide-based DBR is 302 nm, over seven times larger than the 41 nm bandwidth of all-semiconductor DBR. A major benefit that follows from the wide bandwidth of the oxide-based DBR is the flatter phase response on reflection, which relaxes the precise growth targets normally required

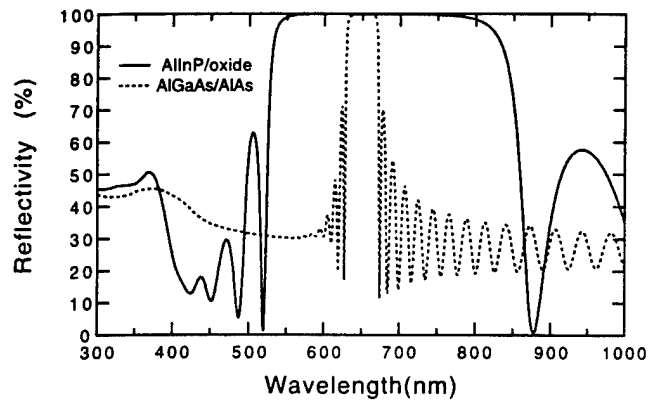


(a)

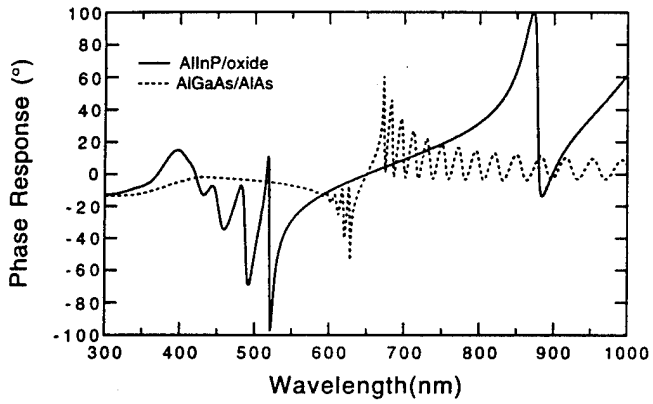


(b)

Fig. 3. Comparison of reflection characteristics between a 5-pair $Al_{0.5}In_{0.5}P$–oxide DBR and a 35-pair $Al_{0.5}Ga_{0.5}As$–AlAs DBR. (a) Calculated reflectance spectra where the peak reflectivities for both spectra are 99.93%. (b) Calculated phase response on reflection.

to obtain high reflectivity in resonant cavity devices such as VCSEL's. The calculated phase responses for the two different types of DBR's are shown in Fig. 3(b), and near the center of the stopband where the phase response is approximately linear, the rate of change of phase response per change in wavelength is 0.18°/nm for the $Al_{0.5}In_{0.5}P$–oxide DBR while the rate of change for the $Al_{0.5}Ga_{0.5}As$–AlAs DBR is five times greater at 0.95°/nm. For a cavity surrounded by $Al_{0.5}In_{0.5}P$–oxide DBR's, the flatter phase response causes the resonant wavelength of the cavity to be less sensitive to thickness deviation within the DBR's, and, consequently, makes it easier to align the cavity resonance with the gain peak than for a cavity surrounded by $Al_{0.5}Ga_{0.5}As$–AlAs DBR's. However, to gain these advantages in optoelectronic devices, the contacting geometries become more complex due to the insulating nature of the oxide layers.

## V. Conclusion

In conclusion, we have demonstrated DBR's possessing extremely wide bandwidth and high reflectivity across the visible wavelength region. These performance features, combined with the ability to be epitaxially integrated below or above an active region, suggests the use of such DBR structu+res in VCSEL and LED devices emitting at visible wavelengths. The performance of the oxide-based DBR's has been compared with all-semiconductor DBR's and shown to be superior in reflectivity bandwidth while reducing the amount of material required for high reflectivity. The wide bandwidth properties can be advantageously applied through relaxation of the extreme growth precision required for VCSEL structures, as well as through an increase in angular capture of available photons in visible LED's. The $Ga_{0.5}In_{0.5}P$–oxide combination would be preferable in the red region due to the higher electrical conductivity of $Ga_{0.5}In_{0.5}P$ and absence of Al in the semiconductor region. The $Al_{0.5}In_{0.5}P$–oxide combination would provide higher reflectance in the yellow, orange and green regions due to decreased absorption.

## Acknowledgment

The authors would like to thank M. Ziari for assistance with absolute reflectance measurements.

## References

[1] M. G. Craford and F. M. Steranka, "Light emitting diodes," in *Encyclopedia Applied Physics*, G. Trigg, Ed. New York: VCH, 1994.

[2] H. Sugawara, A. Itaya, H. Nozaki, and G. Hatakoshi, "High-brightness InGaAlP green light-emitting diodes," *Appl. Physics Lett.*, 1992, vol. 61, pp. 1775–1777.

[3] R. P. Schneider, Jr., R. P. Bryan, J. A. Lott, E. D. Jones, and G. R. Olbright, "MOVPE growth of InAlGaP-based visible vertical-cavity surface-emitting lasers," *J. Crystal Growth*, 1992, vol. 124, pp. 763–771.

[4] J. M. Dallesasse, N. Holonyak, Jr., A. R. Sugg, T. A. Richard, and N. El-Zein, "Hydrolyzation oxidation of $Al_xGa_{1-x}As$-AlAs-GaAs quantum well heterostructures and superlattices," *Appl. Physics Lett.*, 1990, vol. 57, pp. 2844–2846.

[5] A. R. Sugg, E. I. Chen, T. A. Richard, N. Holonyak, Jr., and K. C. Hsieh, "Native oxide-embedded $Al_yGa_{1-y}As$-GaAs-$In_xGa_{1-x}As$ quantum well heterostructure lasers," *Appl. Physics Lett.*, 1993, vol. 62, pp. 1259–1261.

[6] M. H. MacDougal, H. Zhao, P. D. Dapkus, M. Ziari, and W. H. Steier, "Wide-bandwidth distributed Bragg reflectors using oxide/GaAs multilayers," *Electron. Lett.*, 1994, vol. 30, pp. 1147–1149.

[7] M. H. MacDougal, P. D. Dapkus, V. Pudikov, H. Zhao, and G. M. Yang, "Ultralow threshold current vertical-cavity surface-emitting lasers with AlAs oxide/GaAs distributed Bragg reflectors," to be published in *IEEE Photon. Technol. Lett.*

[8] F. A. Kish, S. J. Caracci, N. Holonyak, Jr., K. C. Hsieh, J. E. Baker, S. A. Maranowski, A. R. Sugg, and J. M. Dallesasse, "Properties and use of $In_{0.5}(Al_xGa_{1-x})_{0.5}P$ and $Al_xGa_{1-x}As$ native oxides in heterostructure lasers," *J. Electron. Materials*, 1992, vol. 21, pp. 1133–1139.

[9] H. Tanaka, Y. Kawamura, and H. Asahi, "Refractive indices of $In_{0.49}Ga_{0.51-x}Al_xP$ lattice matched to GaAs," *J. Appl. Physics*, 1986, vol. 59, pp. 985–986.

[10] R. P. Schneider, Jr. and J. A. Lott, "Cavity design for improved electrical injection in InAlGaP/AlGaAs visible (639–661 nm) vertical-cavity surface-emitting laser diodes," *Appl. Physics Lett.*, 1993, vol. 63, pp. 917–919.

[11] D. E. Aspnes, S. M. Kelso, R. A. Logan, and R. Bhat, "Optical properties of $Al_xGa_{1-x}As$," *J. Appl. Physics*, 1986, vol. 60, pp. 754–767.

# Ultralow Threshold Current Vertical-Cavity Surface-Emitting Lasers with AlAs Oxide–GaAs Distributed Bragg Reflectors

Michael H. MacDougal, P. Daniel Dapkus, *Fellow, IEEE*, Vasily Pudikov, Hanmin Zhao, and Gye Mo Yang

***Abstract*— An electrically-pumped, vertical-cavity, surface-emitting laser (VCSEL) using an AlAs oxide–GaAs DBR above the AlGaAs–GaAs–InGaAs gain region and a conventional AlAs–GaAs DBR below is described. By selective oxidation, devices with current flow apertures of different areas are fabricated, and in 8-$\mu$m-square devices, threshold currents as low as 0.22 mA are achieved. Being the first electrically-pumped VCSEL to utilize the oxide-based DBR, it demonstrates that the oxide-based DBR is of sufficient quality to realize submilliampere threshold currents.**

## I. Introduction

VERTICAL-CAVITY surface-emitting lasers (VCSEL's) are promising candidates as light sources in optical systems. They are inherently integrable into arrays, can be coupled efficiently into fibers, and are amenable to on-wafer testing. These advantages must be weighed against the stringent epitaxial layer thickness control required in their fabrication. In VCSEL's, very high reflectivity mirrors are required on each side of the resonant cavity since the gain region is small, especially compared with that of edge-emitting lasers. Epitaxial semiconductor distributed Bragg reflectors (DBR's) can be placed above and below the active region allowing the VCSEL to be grown in one step; however, the requirements on thickness precision are high and the DBR pairs must be repeated many times (>20) to achieve high reflectivity (>99%). The difference in index of refraction between the DBR pairs is small (3.5–3.0 for GaAs–AlAs), resulting in a narrow stop band and a strong variation of the reflection phase change within the stop band. These factors place stringent requirements on the layer thickness precision (±1%) to ensure that the cavity resonance is aligned with the gain peak. Single-wafer, *in situ* thickness measurement techniques are used to achieve the high degree of control needed to reproducibly grow these structures [1], [2].

In contrast to semiconductor DBR's, dielectric mirrors which have been used in VCSEL's have a high index difference (2.98–1.37 for $Sb_2S_3$–$MgF_2$), a wide stop band, and high reflectivity using relatively few layers. As a result, the alignment of the cavity resonance with the gain peak is not as difficult as in semiconductor DBR's. In addition, Huffaker *et al.* have suggested that the use of high refractive index contrast mirrors on both sides of the active region reduces the fundamental lateral spread of the cavity mode and allows extremely low threshold currents to be achieved [3]. It is difficult, however, to fabricate VCSEL's with deposited dielectric mirrors on both sides of the active region.

To take advantage of the favorable properties of each type of DBR, we recently fabricated an epitaxially-grown, 3-pair DBR with high reflectivity and a wide stop band, using the combination of AlAs oxide–GaAs [4]. The refractive index difference of this pair is high (1.55–3.5), and the AlAs–GaAs pair can be epitaxially grown and later oxidized. Holonyak and coworkers have pioneered the technique of wet oxidation of AlGaAs [5], [6] and have shown that AlAs can be oxidized without significantly affecting the GaAs [7]. In fact, they have recently used the AlAs oxide–GaAs DBR to make a photopumped laser which emits through the sides as well as vertically [8]. In this paper, we present an electrically-pumped VCSEL using an AlAs oxide–GaAs DBR above the gain region and a conventional AlAs–GaAs DBR below and show that the oxide DBR is of sufficient quality to realize submilliampere threshold currents.

## II. Design, Growth, and Fabrication

The basic structure, shown in Fig. 1, consists of a 30-pair $n$-doped quarter-wave AlAs–GaAs DBR stack, an AlGaAs–GaAs–InGaAs resonant cavity, $p$-doped contact layers and a 4-pair, undoped, quarter-wave AlAs oxide–GaAs DBR. The AlAs–GaAs DBR is doped $n$-type with a doping level of $\sim 2 \times 10^{18}$ cm$^{-3}$ and has a calculated reflectivity of 99.992%. The undoped active region contains three 60 Å $In_{0.15}Ga_{0.85}As$ quantum-wells (QW's) separated by 100 Å GaAs barriers. On either side are 100 Å GaAs layers to separate the QW's from the $Al_{0.5}Ga_{0.5}As$ confinement layers. The doped $Al_{0.5}Ga_{0.5}As$ layers are used to center the active region on the electric field standing wave peak in a one-wavelength cavity and to provide carrier confinement. The top DBR does not conduct current when oxidized so one additional doped Bragg pair, whose constituent layers are multiples of quarter wavelengths and are placed between the top DBR and the cavity. These $p$-doped layers provide an electrical path for the current to reach the active region. A 0.25$\lambda$ $p$-type AlAs layer borders the cavity followed by a 1.75$\lambda$ $p^+$ GaAs layer. The AlAs

Manuscript received October 10, 1994; revised November 2, 1994. This work was supported by the Office of Naval Research, the Army Research Office, the Ballistic Missile Defence Organization, and ARPA.

The authors are with the Department of Electrical Engineering–Electrophysics, University of Southern California, Los Angeles, CA 90089-0483 USA.

IEEE Log Number 9408440.

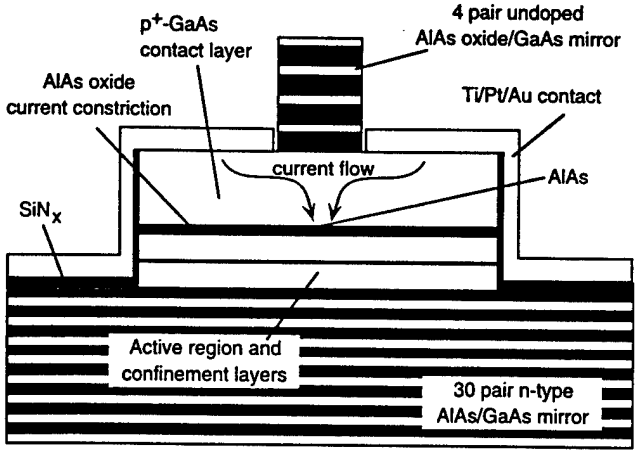


Fig. 1. Schematic of VCSEL utilizing native oxide constriction layer and an AlAs oxide–GaAs DBR.

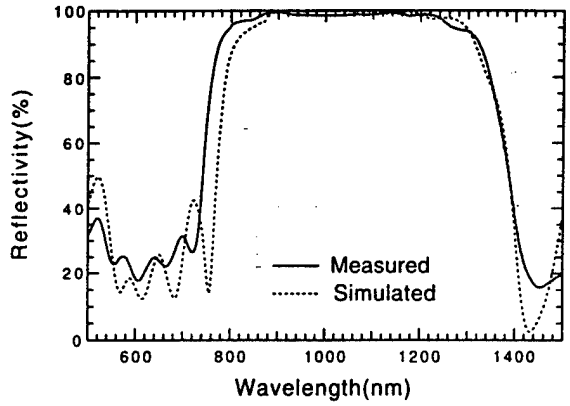


Fig. 2. Reflectivity of four-pair quarter-wavelength AlAs oxide–GaAs DBR stack.

is nonintentionally doped and has a doping level of $\sim 10^{17}$ $cm^{-3}$, and the GaAs has a doping level of $\sim 4 \times 10^{18}$ $cm^{-3}$. The AlAs serves a dual function as a current constriction as well as a quarter-wave Bragg layer. An insulating current constriction, created by laterally oxidizing the AlAs until the oxide front is underneath the top DBR [9], forces the current path and gain region into the optical mode. This current constriction layer allows the top DBR to be wider than the current injection layer thereby decreasing leakage of the optical mode from the waveguide [10]. The refractive index is 1.55 in the oxidized region of the current constriction layer and 2.96 in the unoxidized region of the current constriction layer, and this index step provides a measure of index guiding in the cavity. Together, these qualities contribute to low threshold currents when matched with high reflectivity mirrors. The top DBR is made up of four AlAs–GaAs pairs before processing. From previous studies [4], we have determined the refractive index of AlAs oxide to be 1.55 and the thickness of the oxide to be 90% of the original AlAs thickness. After processing, it becomes a quarter wave AlAs oxide–GaAs DBR. The reflectivity spectrum of a typical 4-pair oxide DBR is shown in Fig. 2. It has a peak reflectivity of 99.8% (calculated) and a stop band of 540 nm. Output power is limited by the very high reflectivity of these mirrors, but the original intent of this study was to demonstrate that the reflectivity of the native oxide DBR was sufficient to obtain lasing in a vertical cavity. Across the wafer, the gain peak varies from 940–950 nm as determined by photoluminescence measurements and the cavity peak varies from 920–950 nm as determined by laser spectra. This variation is caused by inadvertent nonuniformity of deposition rates in our growth chamber.

The VCSEL's are grown by atmospheric-pressure metal-organic chemical vapor deposition (MOCVD). *In situ* laser reflectometry is used to monitor the thickness at the center of the wafer [1], [11]. The sources are trimethylgallium, trimethylaluminum, trimethylindium, and arsine. The dopants are disilane and diethylzinc. After growth, 15-$\mu$m–square mesas are wet-etched through the top DBR down to the GaAs contact layer. The exposed AlAs is oxidized at 425 °C for 10 minutes. The selectivity of this process transforms the AlAs to AlAs oxide while leaving the GaAs unaffected. Then, 50-$\mu$m–square mesas, whose centers coincide with the centers of the 15-$\mu$m mesas, are defined, and the $p$-type GaAs contact layer and AlAs current constriction layer are selectively etched to expose the AlAs so that it may be oxidized. Current flow apertures of 15 $\mu$m and 8 $\mu$m are created by oxidizing the AlAs at 425 °C for 8 min and 10 min, respectively. $SiN_x$ is deposited outside and on the edges of the 50-$\mu$m square to isolate the $p$-type metal from the active region The $p$ contact is made with Ti–Pt–Au and the $n$ contact is made with AuSn.

## III. Results

Devices were tested with no temperature control under cw excitation. No heat sinking was present other than the contact with the metal test stage to the bottom of the chip. Laser characteristics for the 15 $\mu$m square and 8 $\mu$m square devices are shown in Figs. 3 and 4. The 15 $\mu$m and 8 $\mu$m devices have minimum threshold currents of 1.55 mA and 0.22 mA, respectively. These low numbers demonstrate that the oxide DBR is a viable mirror option in electrically-pumped VCSEL's and can be used to achieve very low threshold currents. The threshold current density for the 15 $\mu$m device (667 A/$cm^2$) is higher than that for the smaller 8-$\mu$m device (344 A/$cm^2$) because the current aperture is equal to or greater than the top mirror mesa. This causes reduced reflectivity and increases scattering. These effects are reflected in both the higher threshold current density and lower efficiency of the 15-$\mu$m–aperture laser. In addition, the higher current density causes the 15-$\mu$m device to have a higher threshold voltage drop of 3.56 V as compared to a 2.55-V drop for the 8-$\mu$m device. The emission wavelengths of the 15 $\mu$m and 8 $\mu$m device are 949 nm and 936 nm, respectively. The difference in wavelength is due to the different growth rates across the wafer causing the bottom reflector stop band to vary. As expected, the best devices occurred when the QW emission wavelength and the cavity resonance wavelength were close to one another. The 8-$\mu$m device emits in a single mode and has a next order transverse mode suppression of 35 dBm. The 15-$\mu$m device has a smaller mode suppression due to the appearance of transverse modes in the wide aperture oxide-defined device as noted by Huffaker *et al.* [12] These first generation devices

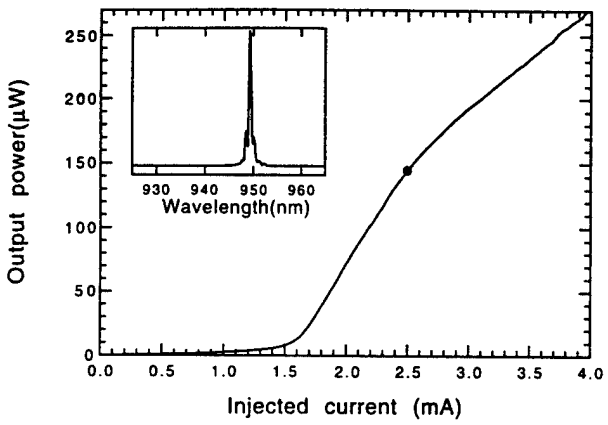


Fig. 3. Light versus current curve for VCSEL with 15 $\mu$m square current aperture measured under cw excitation at room temperature. The inset shows laser spectra when operated at 2.5 mA, cw.

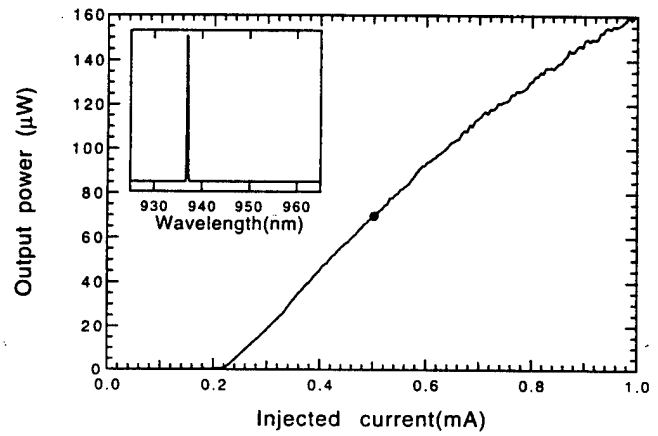


Fig. 4. Light versus current curve for VCSEL with 8 $\mu$m square current aperture measured under cw excitation at room temperature. The inset shows laser spectra when operated at 0.5 mA, cw.

exhibit low threshold currents and good modal quality using an 8-$\mu$m–square current aperture and, with further optimization, should have higher power output.

## IV. Summary

In conclusion, we have demonstrated the use of AlAs oxide–GaAs DBR's in electrically-pumped VCSEL's. The top mirror is a 4-pair quarter-wave stack with peak reflectance of 99.8% (calculated) and a stop band of 540 nm. Employing an oxide DBR above the active region and a semiconductor below, VCSEL's achieve submilliampere thresholds, which suggests that little scattering or absorption occurs in the oxide DBR's. These high-contrast DBR's have a short, effective penetration depth which may lead to extremely low threshold currents ($<10\,\mu$A) when placed on both sides of the active region. The device presented here indicates that such an extremely low threshold device is feasible.

## Acknowledgment

The authors would like to thank S. Hummel (Hewlett-Packard Labs) and R. Schneider (Sandia National Labs) for useful discussions and comments, and S. Dubovitsky for assistance with laser measurements.

## References

[1] N. C. Frateschi, S. G. Hummel, and P. D. Dapkus, "In situ laser reflectometry applied to the growth of $Al_xGa_{1-x}As$ Bragg reflectors by metalorganic chemical vapor deposition," *Electron. Lett.*, vol. 27, no. 2, pp. 155–156, 1991.

[2] S. A. Chalmers and K. P. Killeen, "Method for accurate growth of vertical-cavity surface-emitting lasers," *Appl. Phys. Lett.*, vol. 62, no. 11, pp. 1182–1184, 1993.

[3] D. L. Huffaker, C. C. Lin, D. G. Deppe, B. G. Streetman, and T. J. Rogers, "Mode dependence on mirror contrast in Fabry–Perot microcavity lasers," *IEEE Photon. Technol. Lett.*, vol. 6, no. 2, pp. 135–138, 1994.

[4] M. H. MacDougal, H. Zhao, P. D. Dapkus, M. Ziari, and W. H. Steier, "Wide-bandwidth distributed Bragg reflectors using oxide/GaAs multilayers," *Electron. Lett.*, vol. 30, pp. 1147–1149, 1994.

[5] J. M. Dallesasse, N. Holonyak Jr., A. R. Sugg, T. A. Richard, and N. El-Zein, "Hydrolyzation oxidation of $Al_xGa_{1-x}As$–AlAs–GaAs quantum well heterostructures and superlattices," *Appl. Phys. Lett.*, vol. 57, no. 26, pp. 2844–2846, 1990.

[6] A. R. Sugg, N. Holonyak Jr., J. E. Baker, F. A. Kish, and J. M. Dallesasse, "Native oxide stabilization of AlAs—GaAs heterostructures," *Appl. Phys. Lett.*, vol. 58, no. 11, pp. 1199–1201, 1991.

[7] A. R. Sugg, E. I. Chen, T. A. Richard, N. Holonyak Jr., and K. C. Hsieh, "Native oxide-embedded $Al_yGa_{1-y}As$-GaAs-$In_xGa_{1-x}As$ quantum- well heterostructure lasers," *Appl. Phys. Lett.*, vol. 62, no. 11, pp. 1259–1261, 1993.

[8] M. J. Ries, T. A. Richard, S. A. Maranowski, N. Holonyak Jr., and E. I. Chen, "Photopumped room-temperature edge- and vertical-cavity operation of AlGaAs–GaAs–InGaAs quantum-well heterostructure lasers utilizing native oxide mirrors," *Appl. Phys. Lett.*, vol. 65, no. 6, pp. 740–742, 1994.

[9] D. L. Huffaker, D. G. Deppe, K. Kumar, and T. J. Rogers, "Native-oxide defined ring contact for low threshold vertical-cavity lasers," *Appl. Phys. Lett.*, vol. 65, no. 1, pp. 97–99, 1994.

[10] J. W. Scott, R. S. Geels, S. W. Corzine, and L. A. Coldren, "Modeling temperature effects and spatial hole burning to optimize vertical-cavity surface-emitting laser performance," *IEEE J. Quantum Electron.*, vol. 29, no. 5, pp. 1295–1308, 1993.

[11] S. G. Hummel and P. D. Dapkus, 1993, (unpublished).

[12] D. L. Huffaker, D. G. Deppe, and T. J. Rogers, "Transverse mode behavior in native-oxide-defined low threshold vertical-cavity lasers," *App. Phys. Lett.*, vol. 65, no. 13, pp. 1611–1613, 1994.